INTEGRATED MICROVALVES FOR CORTICAL DRUG-DELIVERY AT THE CELLULAR LEVEL

by

Kyusuk Baek

A dissertation submitted in partial fulfillment
of the requirements for the degree of
Doctor of Philosophy
(Electrical Engineering)
in The University of Michigan
2009

Doctoral Committee:

Professor Kensall D. Wise, Chair
Professor Shuichi Takayama
Professor Zhaohui Zhong
Research Associate Professor Sanford C. Bledsoe

To GOD, for his love.

ACKNOWLEDGMENTS

I would deeply like to thank Professor Kensall Wise. Without his continuous full support, patience and encouragement throughout my graduate study at the University of Michigan, I would not be able to make this thesis. I learned from him not only knowledge, but more important, his professional attitude and personal integrity. He is the "best" advisor in my eyes, for raising my interest and expectation into the BioMEMS world.

I also thank my dissertation committee, Professor Shuichi Takayama, Professor Sanford and Professor Zhaohui Zhong, for their support and feedback.

This work would not have been finished without help from Ms. Ning Gulari. As my mentor in the clean room, she gave me invaluable advice from her experience, and much of the fabrication work presented in this thesis was supported by her. I also deeply benefited from her sharing with me her professional development experience.

I would also like to thank Mr. Brendan Casey, Mr. Robert Gordenker for valuable help with my experiment setup, to Ms. Katherine Beach for additional processing support. I want to acknowledge my colleagues, Dr.Gayatri Perlin, Sister Mary Elizabeth Merriam, Mr. Razi Haque and Ms. Angelique Johnson, and all friends at the University of Michigan WIMS ERC. Thanks will not be complete without acknowledgement to the entire MNF and WIMS ERC staff for making this research possible. I learned remarkably

from this environment during the time I spent here. Finally, thanks to my wife, Sehee Jung, for her continuous love and support through the years.

TABLE OF CONTENTS

LIST OF TABLES

LIST OF FIGURES

ABSTRACT

INTEGRATED MICROVALVES FOR CORTICAL DRUG-DELIVERY AT THE CELLULAR LEVEL

by

Kyusuk Baek

Chair: Kensall D. Wise

Microelectrode arrays now allow the simultaneous electrical recording and stimulation of large numbers of neurons in the central nervous system, providing a basis for major advances in neuroscience and in prosthetic devices for disorders such as epilepsy, deafness, and Parkinson's disease. However, the neuronal system is chemical as well as electrical, and for many of these applications, the development of miniature drug-delivery systems for in-vivo use is essential. This research has developed microvalves that can be integrated into these arrays to provide control over the chemical environment at the cellular level.

Microchannels for drug delivery are formed in the body of a multi-electrode probe by undercutting a selectively-etched boron-doped silicon and/or dielectric masking structure. The mask openings are then sealed using deposited dielectrics. In order to control fluid flow in these channels, integrated microvalves have been developed that require only two extra masks beyond the normal probe process. The normally-open valve structure uses pressure to deflect a corrugated circular diaphragm against a seat, blocking the flow path as needed.

Using stress-compensated silicon dioxide and silicon nitride corrugated diaphragms 400μm in diameter and 1-2μm thick, two different on-probe pneumatically-actuated valve structures were demonstrated. Two sacrificial 5μm-thick polysilicon layers sandwiched between dielectric layers were used to form the two chambers of the microvalves. Both valve types provide an open flow rate greater than 500pL/sec at an applied input pressure of 10kPa and meet the design target of a leak rate less than 25pL/sec at an actuation pressure of 35kPa.

Prototype thermopneumatically-actuated microvalves were also designed and fabricated. Simulations show that using the phase-change of a low-boiling-point liquid (42°C, cyclopentane), less than 10mW is required to generate a drive pressure of 35kPa, closing the valve in less than 20msec. The temperature rise in the surrounding tissue should be less than 2°C, making the valve safe for use in-vivo. This is the first reported microvalve suitable for on-probe use in a cellular drug-delivery system, and as a low-voltage low-power structure capable of high actuation pressure and throw, it should have many other applications as well.

CHAPTER 1

INTRODUCTION

Silicon microelectrode arrays have become widely used in neurophysiological research over the past decade. Microelectrode arrays capable of stimulating or recording in the nervous system are one of the principal tools used today for studying the central nervous system at the cellular level. They are also the basis for a number of neuroprosthetic devices being developed to address neurological disorders such deafness, blindness, epilepsy, paralysis and Parkinson's disease. Thousands of neural probes have been supplied to researchers worldwide from the University of Michigan and have resulted in over 300 publications to date in the neuroscience literature [1, 2]. The probes are fabricated using a high-yield single-sided bulk-micromachined process [3]. The probe can include on-chip circuitry for signal processing [4-8] and can be microassembled in three-dimensional arrays [9, 10] with telemetry interfaces [11].

1.1 Need for Acute Drug Delivery Systems for Neuropharmacology

Determining the electrical response of a neural network to electrical, acoustical or other types of stimulation has been a topic of great interest [3], but monitoring the electrical activity in biological neural networks gives only partial insight into what is really an electrochemical system. For example, to fully explore neuronal pathways and the conditions determining their activity requires the use of equipment capable of

controlling doses of activating or inhibiting chemicals as needed. To obtain a more complete understanding of cell function, the use of a chemical delivery system at the cellular level is essential. The brain is mechanically protected by a rigid skull and is chemically and physically isolated by the blood-brain barrier. These features increase the difficulty of controlling the local chemical environment of the brain, and they need to be addressed in the development of any acute microfluidic drug delivery system intended for a neural use. A first step toward controlling the chemical environment was the integration of drug-delivery capabilities into electrical recording/stimulating neural probes [12, 13]. This approach breaks the blood-brain barrier by inserting a drug-delivery system into the region of interest. The injection of drugs or other chemicals through the delivery system changes the chemical environment of the neurons and can give important new insights into the workings of the nervous system.

1.2 Conventional Instrumentation for Neuropharmacology

The most common method used by neuropharmacologists to record, stimulate, and deliver chemicals to neurons has involved the use of micropipettes. They are easily fabricated in small numbers using only simple equipment (Figure 1.1(a)). The manufacturing process for them begins with a cylindrical glass tube, which is clamped into a machine containing a heating coil that surrounds a portion of the tube and a weight pulling at the bottom. Current flowing through the heating coil increases its temperature, heating the glass tube. When the temperature of the glass approaches its melting point, it begins to soften. The weight clamped on the bottom of the tube then induces necking in its diameter. The tube continues to neck down until it ultimately breaks. The pipette can be filled with either an electrolyte or a drug, depending on its intended use. The former is

used for electrical stimulation or recording of neural activity. For this case, a wire is inserted in the back end of the micropipette to transport the signal from the pipette to the outside world. The electrolyte is responsible for passing any signal between the tip and the wire. The use of the micropipette as a chemical delivery device is even simpler. The desired chemical is added to the pipette, and a tube is connected from the back of the pipette to a pressure-driven delivery system. To deliver the chemical, pressure is applied to the back end of the probe, which causes a pressure gradient along the channel. The fluid naturally moves in a manner that will equalize the pressure, resulting in a net movement of chemical out of the pipette.

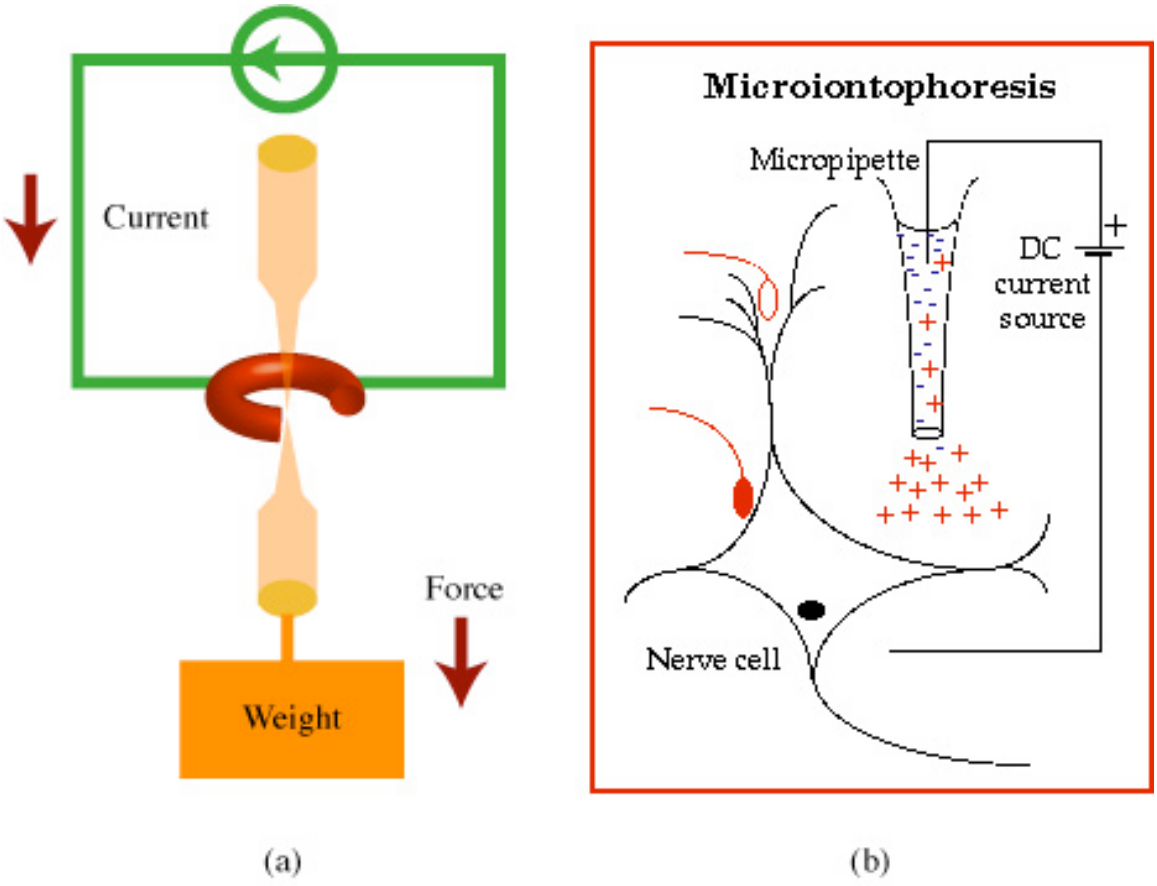

Figure 1.1: (a) Micropipettes are made from a glass tube with a portion of it placed inside a wire coil and the bottom attached to a weight. (b) Microiontophoretic ejection is accomplished by applying a voltage across the micropipette (electrode), causing it to become polarized.

A second method of delivering chemicals is iontophoresis (Figure 1.1(b)). This technique utilizes the charge in a fluid, created by either the inherent ionic nature of the fluid or the addition of dissolved salts, to force movement through the application of an electric field. For example, when used in an organism, a positively charged chemical is delivered by applying a positive bias in the pipette filled with the solution and a negative bias to some other point on the body. The natural tendency for like charges to repel creates a net movement of solution out of the pipette and into the organism [14-16].

Pressure or iontophoretic actuation, however, do not permit the integration of electrical stimulation or recording with chemical delivery nor do they permit the accurate placement of electrodes and chemical delivery sites in relation to each other when the number of desired sites is greater than two. Therefore, the integration of drug-delivery capabilities into neural probes that can overcome these shortcomings is essential.

1.3 Past Work in Integrated Drug Delivery Probes

In the past three decades, a solution to many of the problems associated with multibarrel micropipettes using pressure or iontophoretic actuation has emerged. Neural probes made using batch silicon wafer processing technology provide an inexpensive alternative for multi-site recording, stimulation, and chemical delivery. They also permit dimensional control on the order of a micron and site placements that remain fixed in position relative to each other. In addition, this higher spatial control can be accomplished with less externally-mounted equipment and less tissue displacement.

Wise, et al., first reported this type of probe in 1969 [17, 18]. These probes used metal electrode lines which ran along the length of the probe, insulated on either side by silicon dioxide. The size of the probe was determined by an etch-back from the backside

of the wafer with the remaining wafer thickness becoming the probe substrate. Because a back-side etch was required, the accuracy of probe dimensions was primarily controlled by lithography and by the reproducibility of the isotropic etchants used to shape the silicon. Other probes mimicked the overall form of these probes by using similar technology. One such case was reported by Prohaska *et al* [19] in which metal lines were patterned over a glass substrate and insulated with a 1μm thick evaporated silicon dioxide layer. The probe was then diamond scribed into a needle shape. In 1979, a glass substrate was also used by Pochay *et al* where metal electrodes were patterned on the outside of a glass pipette using electron-beam lithography [20]. As a result, the volumetric displacement of the tissue was reduced, minimizing the intrusiveness and damage to the neural system. These basic techniques are all extensions of microwire technology, which use single wires with one end implanted in the region of interest and the other end connected to readout electronics.

With the development of silicon micromachining technology, the substrate thickness was reduced by using anisotropic silicon etchants together with a highly-doped boron region to define the probe shape [21-23]. Due to a drastic reduction in the number of free carriers, electrons in the silicon induced by the high levels of boron [24], this portion of the substrate remains after the wafer is dissolved in hot ethylenediamene pyrocatechol (EDP). The electrode interconnect material was also changed from metal to polysilicon, which permits the use of high processing temperatures for dielectric deposition after the electrode interconnects are defined. Through the development of circuitry on the probe by Najafi [25] and further refinements of this technology by Ji [26], recording probes have increased the signal quality and number of available sites with the

integration of on-chip amplifiers and multiplexers [27, 28]. From there, the technology has added iridium oxide sites for high-charge-capacity stimulation [29] and on-chip circuitry to allow access to 16 [30], 64 [31], or more sites [32]. Moreover, this technology has not only allowed a higher site density, but also the expansion from one-dimensional arrays to two-dimensional [29] and now three-dimensional [33] structures, thereby permitting more flexibility and accuracy in the mapping of the neural activity.

Additionally, the use of semiconductor processing facilitates the further development of this technology to meet any particular need. This technology has grown over the past decades to become the method of choice for neural recording and stimulating probes. Its versatility has lead to the development of long probes designed for insertion deep within the cochlea [34], multi-shank probes [30], and three-dimensional probes with circuitry to allow access to hundreds of recording and stimulating sites for more accurate mapping and triangulation of neurons [35].

The functionality of the silicon neural probe has also been extended from the electrical domain into the chemical domain. Chen and Wise [32] added buried channels to the neural probes, which are totally compatible with the formation of active and passive electrodes arrays for electrical recording and stimulation on the same chip. With only one more mask, the buried channels were added to the probes to allow chemical delivery to specific locations with respect to stimulating or recording sites without altering the rest of the processing steps. This feature allows the probes to be used in neuropharmacological experiments in which the chemical environment of neurons can be altered while monitoring and/or stimulating them electrically. The Michigan drug delivery probe has already been applied *in vitro* and *in vivo* successfully and has shown it is an effective

means of collecting extracellular data from neurons.

Over the years, many different microchannel structures in addition to the Michigan probes have been reported based on lithography [36-39]. They have been formed primarily by electroplating or by the chemical-vapor-deposition (CVD) of a wall material over a sacrificial layer (Figure 1.2), although they have also been fabricated using lamination. In the first method (Figure 1.2 left), the channel length, width and height are defined using a sacrificial material (usually either photoresist or silicon dioxide). Then the channel walls are formed by depositing some other material over it. When photoresist is used as the sacrificial layer, this material is usually electroplated metal [38]. Some of the most recent work using this approach has been done at the University of Utah and the Unversity of California at Berkeley. At Utah, sacrificial photoresist is patterned on top of an electroplated metal layer. Then, the sidewalls and top are electroplated. Next, the sacrificial layer is removed in an acetone soak. This method requires only simple processing and works well when only drug delivery is desired. However, this approach is not compatible with the formation of on-chip high performance electrical recording and stimulation sites.

For channels defined by a silicon dioxide sacrificial layer (Figure 1.2 right), CVD polysilicon or silicon nitride is usually the material of choice for the channel wall as was done at Berkeley by Pisano and Lin [37]. If the channel length is long, holes are typically added along the sides of the channel to allow the etchant to access the sacrificial material from more locations. Without these holes, the etch process has been seen to slow down and even stop all together beyond a certain length.

Another approach also uses etch selectivity to define the channel, but with the

sealing done later either by refill [39] or full wafer bonding [40] (Figure 1.3). For example, if the channels are formed in glass, a polysilicon mask defines the channel length. Then, by placing the wafer in buffered hydrofluoric acid, the channels form as the glass is isotropically etched, undercutting the mask. Following this step, the channels are sealed by refilling the gap in the masking layer.

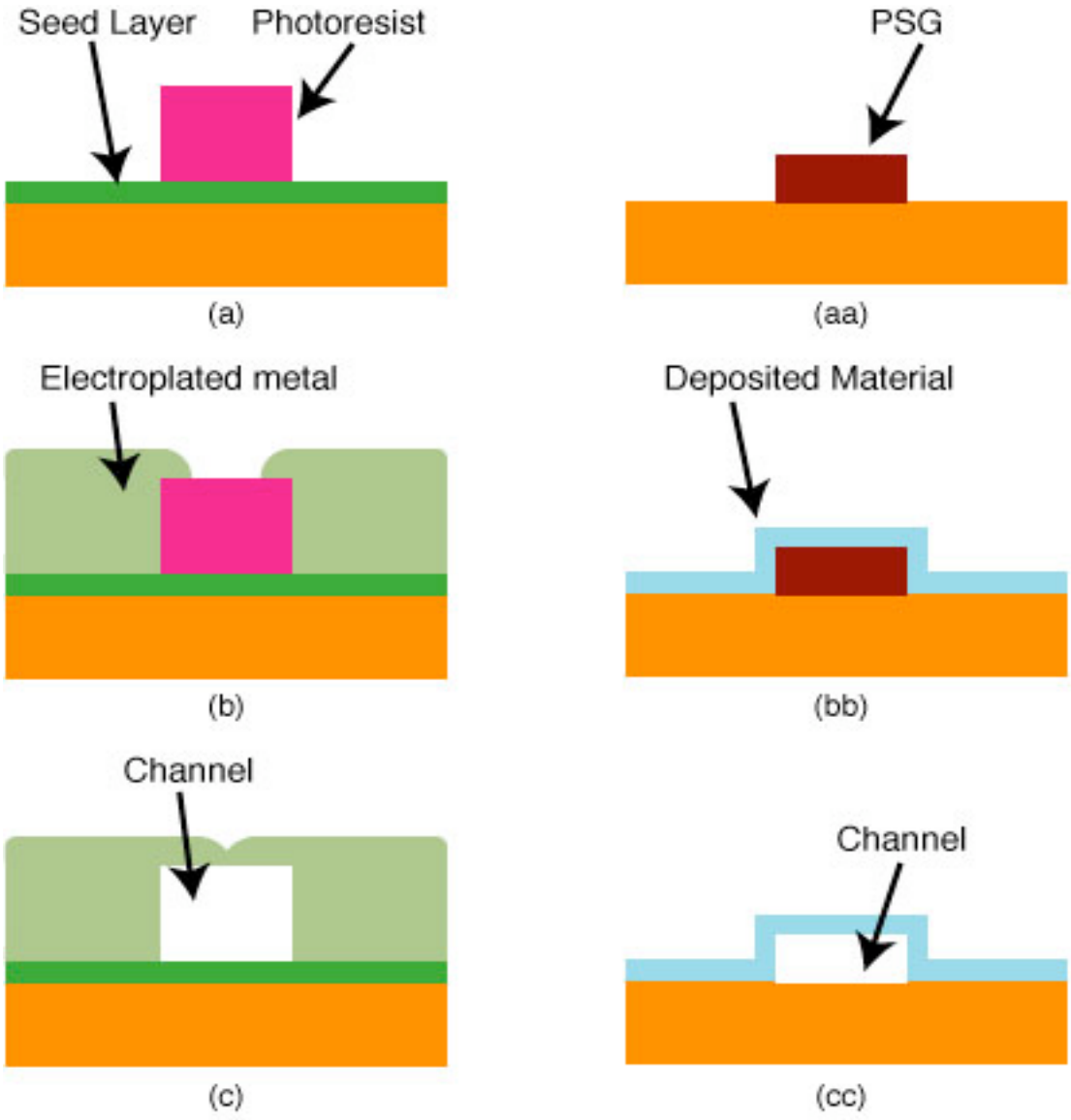

Figure 1.2: Sacrificial channel methods. The left side shows the process for forming a channel using photoresist and electroplating. In the other method shown on the right, the sacrificial material is phosphosilicate glass encapsulated by deposited nitride.

The lamination technique also uses a glass wafer, but only as a substrate to work from [41]. Channels are created through the addition of resists. First, a layer of either SU8 or Riston negative photoresist is placed on the substrate through spin-on or lamination, respectively. The channels are defined photolithographically with this layer. Then, a layer of Riston is laminated on top, sealing the channel.

Three more techniques have become available with the development of deep reactive ion etching (RIE) machines [42-44]. The two techniques developed at Georgia Tech by Allen [42] both begin with identical processing steps. Circular regions are formed using silicon dioxide and act to protect the underlying areas from the following step. The wafer is then etched anisotropically using RIE. Although it is an anisotropic etching technique, a finite amount of lateral etching does occur. Therefore, as the length of the needle increases, the circular regions are also increasingly undercut on all sides at the top. Since the amount of undercut is naturally dependent on the duration of the etch, the resulting structure is narrower at the top of the wafer and progressively widens to the dimensions of the patterned area at the bottom. The exact profile of the needle is controlled through the use different etch recipes for different degrees of anisotropy. The next steps differentiate the fabrication process. In the first method, holes are etched through the needles using deep RIE to form chemical delivery channels. The other method uses a molding technique. After the needles have been formed, UV light sensitive epoxy is poured over the needles and cured. The needles are then removed from the epoxy leaving behind a mold. Next, by electroplating the epoxy, the surfaces are covered by metal. Finally, dissolving the epoxy away leaves behind arrays of hollow core metal microneedles. A third technique is polymer/parylene-based process. Microprobes with

embedded microelectrodes and microfluidic channels were fabricated with polyimide [28, 45, 46] (Figure 1.4, Figure 1.5). On-chip CMOS circuitry is not compatible with this technique.

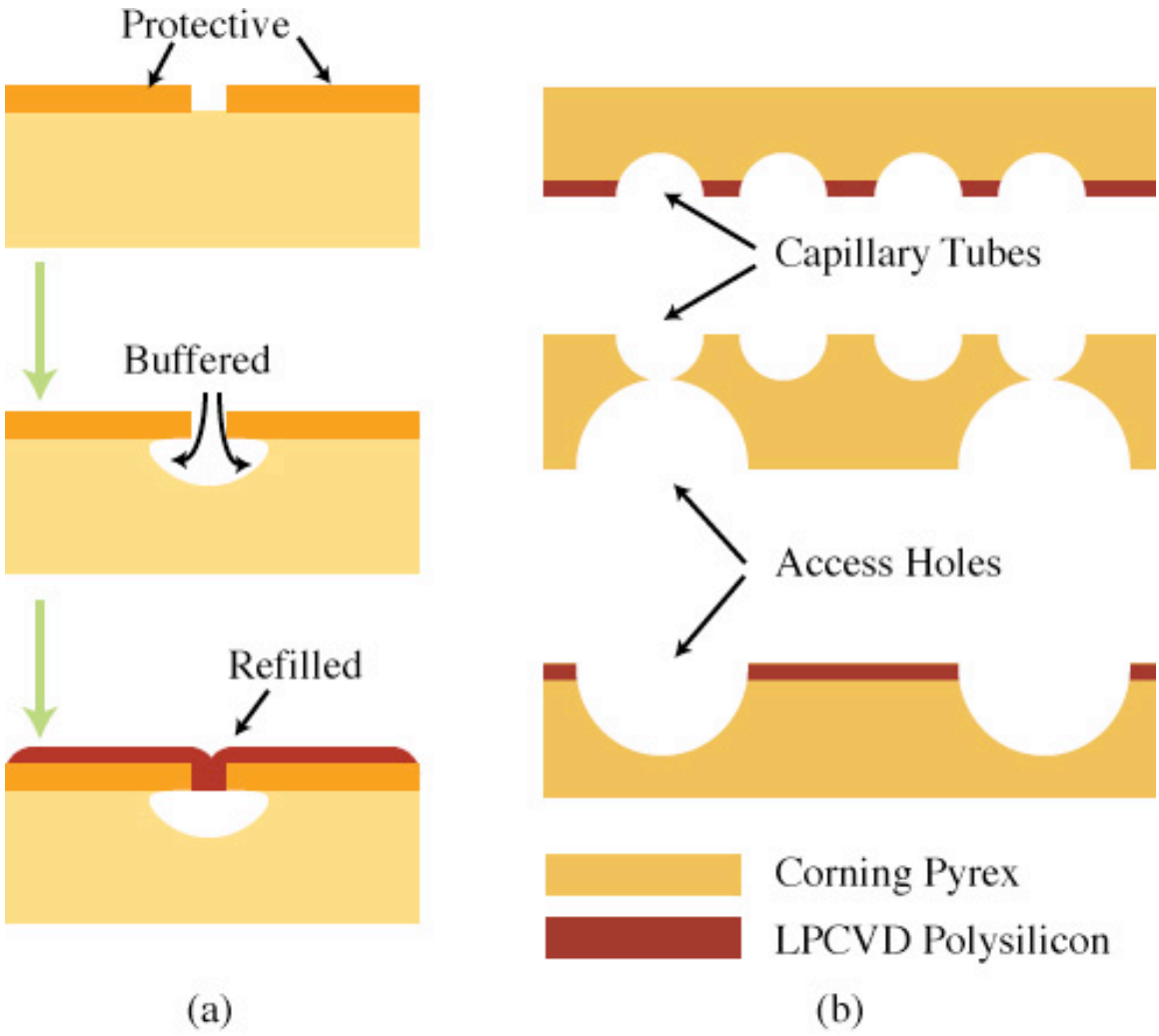

Figure 1.3: (a) Refilled channel process. First a protective layer (i.e. polysilicon) is placed over a glass substrate and patterned in the areas where the channel will be formed. A buffered HF dip isotropically etches the glass, undercutting the protective layer, and forming a cavity underneath it. The completed channel is then formed by refilling the gaps in the protective layer, sealing the channel. (b) Cross-section of capillary tubes [40].

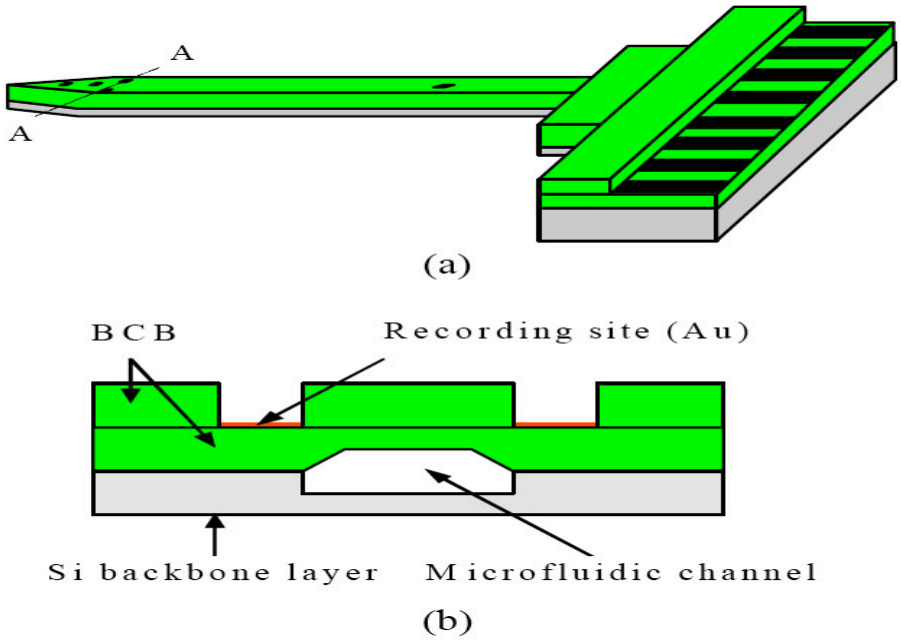

Figure 1.4: Simple schematic diagram of the biocompatible benzocyclobutene (BCB)-based drug delivery probe developed at Arizona State University in 2004: (a) top view and (b) cross-sectional view of A-A. The micro-fluidic channel was embedded in the middle of the silicon backbone layer [45].

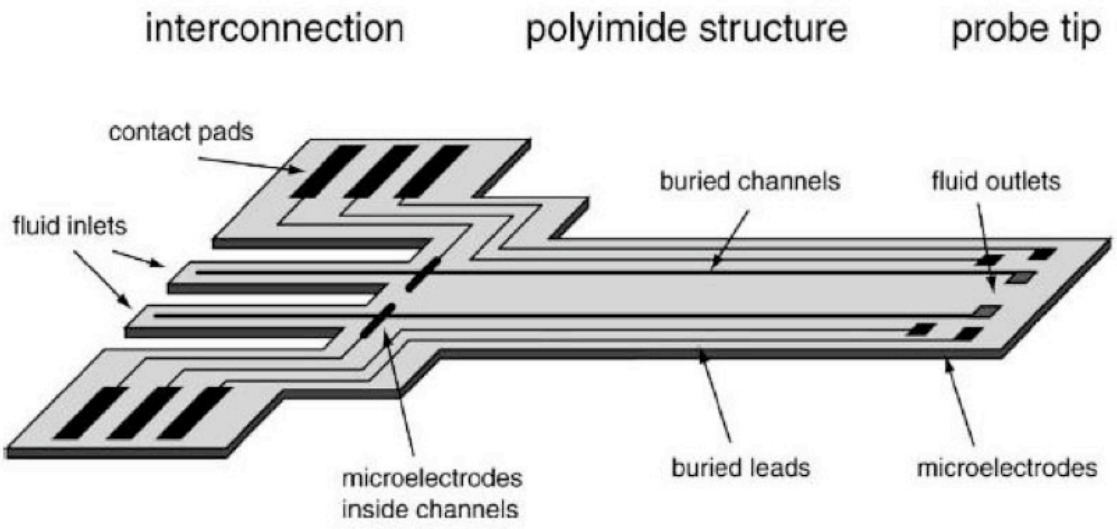

Figure 1.5: Illustration of the implantable, flexible polyimide probe with microelectrodes and microfluidic channels developed at the Central Medical University, Switzerland, in 2004. At the tip of the device microelectrodes and channel outlets are located adjacent to each other for simultaneous electric and fluidic interfacing with tissue. Contact pads and fluid inlets are provided at the other end of the microstructure for interconnection to the external setup. Additional, microelectrodes may be integrated at the bottom of the microchannels for fluid flow measurements and chemical detection [28, 46].

The channels formed by the various methods mentioned above are good for transporting chemicals; however, they are not very compatible with the University of Michigan's neural probe process. But the addition of chemical delivery capabilities must complement extracellular electrical recording, stimulating sites and on-chip circuitry. As a result, the chemical delivery channel must still permit high-performance electrical recording and stimulation while not creating overly complicated processes.

1.4 Needs of Chronic Drug Delivery Systems for Neural Prosthetics

Neural prosthetic devices are artificial extensions to the body that restore or supplement functions of the nervous system lost due to disease or injury [47]. Neural prosthetics are devices that are used to allow disabled individuals the ability to control their own bodies and lead more productive lives. Neural prostheses have already provided substantive benefits to individuals. For example, success has been realized in the development of cochlear prostheses [48], which bypass damaged hair cells in the auditory system by direct electrical stimulation of the auditory nerve, and deep brain electrical stimulation [49], which has been useful for some patients in reducing the tremors associated with Parkinson's disease. Clearly, individuals living with Parkinson's disease and some classes of deafness have been positively impacted by neural prosthetics.

But the fact that many neurological disorders and injuries are a result of chemical imbalances in the brain limits effectiveness of electrical stimulation in repairing or replenishing functions of the impaired nervous system. One potential treatment for these imbalances is the direct delivery of therapeutic agents into the brain using a miniaturized chronically implantable chemical delivery system. A chronic drug delivery system capable of precise and timely delivery of therapeutic drugs to local areas of brain tissue

can be expected to give effective therapy as a neuroprosthesis when paired with a full understanding of how impaired neurons behave in response to the delivered agent.

1.4.1 Epilepsy

One possible neurological disorder that might be managed using a chronic drug system is epilepsy. Epilepsy (sometimes referred to as a seizure disorder) is a common chronic neurological disorder that is characterized by recurrent unprovoked seizures [50]. (A seizure is a change in sensation, awareness, or behavior brought about by abnormal discharges in groups of neurons in the brain [51]). These seizures are transient signs and/or symptoms due to abnormal, excessive or synchronous neuronal activity in the brain [51]. Normally, neurons carrying electrical impulses form a network allowing communication between the brain and the rest of the body. Neurons fire electrical impulses toward surrounding cells, stimulating neighboring cells to fire. In people with epilepsy, too many neurons fire at one time, causing an electrical stroke within the brain [50]. Epilepsy is usually controlled, but not cured, with medication, although surgery may be considered in difficult cases. Not all epilepsy syndromes are lifelong – some forms are confined to particular stages of childhood. Epilepsy should not be understood as a single disorder, but rather as a group of syndromes with vastly divergent symptoms but all involving episodic abnormal electrical activity in the brain.

About 2.7 million people in the United States have epilepsy, and every 3 minutes a new case is diagnosed. There are 800,000 Americans with uncontrolled seizures, and there are 360,00 children, under the age of fifteen, affected with epilepsy. Some 25,000 to 50,000 people die of seizure related causes each year in the USA [50].

1.4.1.1 Conventional Drug Therapy for Epilepsy

Oral Medication: Many options currently exist for oral medication to treat epilepsy, but none are ideal because current oral epilepsy therapy distributes the medication throughout the body, including many areas where it is not used to stop seizures and may produce adverse effects [52]. When patients have acute seizures, oral medication is not an option and establishing intravenous access involves significant delays [53].

Rectal/Nasal Medication: Currently, only the rectal administration of medication for epilepsy is approved in the United States [54]. Administration to the nasal mucosa can be more practical and convenient than is delivery to rectal mucosa [54] but has yet to be approved. Nasal sprays to deliver epilepsy drugs do not run the risk of the aspiration, pneumonia, or bite injuries associated with oral medication during a seizure.

Skin Medication: Skin presents the most accessible path for administering medications, if they are applied to penetrate the epidermis and enter into the blood-rich dermal layer [55]. Many medications, such as hormones, scopolamine for nausea, nitroglycerin, and others are delivered dermally. One study has looked at the efficacy of dermally delivered lidocaine for seizures. In 19 patients suffering seizures, the application of lidocaine tape to the skin caused rapid remission of recurrent seizures in 13 seizure events, but it also produced adverse effects [56].

Inhalation Medication: It is possible for antiepileptic medications to be delivered by the pulmonary route, but technical problems associated with delivering the drug by inhalation will require further development since respirations can be shallow and irregular during a seizure.

1.4.1.2 Direct Drug Delivery Methods to the Central Nervous System for Epilepsy

Direct delivery of Anti Epileptic Drugs (AEDs) to the central nervous system (CNS) theoretically provides for the possibility of a therapeutic-toxic ratio [52] greater than can be found in systemic drug delivery. Unintended adverse reactions, such as kidney stones, liver toxicity, or skin rashes would not occur with direct delivery to the CNS [53]. Side effects resulting from toxicity within the CNS might still remain, but also could be limited by localized distribution in the brain.

Delivery to the Cerebrospinal Fluid (CSF): CSF delivery can be within the system of ventricles in the brain (Intraventricular) or the space under the arachnoid membrane of the brain (Intrathecal) [57]. Those routes are relatively easy and safe, since the medication can be injected into the CSF without any surgical trauma to the brain. However, an unresolved question of delivery to CSF is the degree of drug penetration into brain tissue itself, especially where needed.

Implanted Drug-Eluting Wafers: A drug wafer is a polymer matrix with interwoven drug. As a polymer dissolves, it slowly releases medication over a period of time, typically weeks, months or even a few years. Drug-releasing wafers have become well known to neurologists and neurosurgeons form the BCNU(carmustine)-containing wafer, which is left in the bed of tumor resection. Potential disadvantages of therapy with polymer wafers include the low solubility of most current antiepileptic drugs as well as their low strength, which would require a large wafer size [58]. As the polymer dissolves in-vivo, release of the drug becomes considerably nonlinear.

Local Perfusion by CNS Catheter: Local perfusion is the delivery of a medication through an implanted catheter attached to a pump [59]. The pump can be programmed to infuse medication at a constant or a variable rate. In some experiments, antiepileptic

medication, such as adenosine, was infused in order to see whether it could prevent seizures [60]. But excess drug produced toxic local effects or spread to portions of the brain involved in control of respiration and blood pressure.

Seizure-Activated Drugs: In this approach, an inactivated precursor drug is activated by a substance released at the seizure focus. This results in a highly specific concentration of drug at the seizure focus, which causes little effect at other brain locations. One drug utilizing this approach is DP-VPA [61], which is an analog of valproic acid. With the phospono group attached, the drug is without effect. When a seizure occurs, elevated activity of the enzyme phospolipase-A2 cleaves the phosphono part and generates locally high concentrations of valproic acid [61]. Unresolved questions of the intrinsic characteristics of the drug itself, which determine its utility in real clinical situations, still remain.

Liposomes-Polysomes: A liposome is a fatty bubble, filled with a medication of interest. More precisely, liposomes are colloidal particles composed of phospholipid molecules assembled in a cell membrane-like bilayer or multilayer. Polysomes use artificial polymers, such as polysorbate, used to package the drug [62]. Chemists can change the characteristics of the membranes and the preparation medium in order to produce a variety of different types of liposomes or polysomes. The goal usually is to produce delivery vehicles that are able to steadily release the drug regionally over a period of days-to-weeks. A problem that the preparation must be able to penetrate the blood-brain barrier has made this delivery difficult to achieve in real life.

1.4.1.3 System Components for Integrated Chronic Drug Delivery Systems for Epilepsy

Current oral and other conventional epilepsy therapies [52] distribute the medication throughout body. Other routes [53] of administration still have problems; however, an integrated drug delivery system based on MEMS technology could be very attractive. First, electrical stimulation of the nervous system is an attractive possible therapy for epilepsy [63]. Not only stimulation of the vagus nerve has been proven and accepted as therapy in this area, but also other varieties of stimulation therapy for seizures presently are involved in clinical trials [52]. Second, targeted drug delivery is another possible therapy by delivering high concentrations of drug where it is really needed. For epileptic patients, seizures begin with the rhythmic firing of neurons in a highly localized area of the brain. Surrounding neurons are assimilated into the patterned firing as the seizure develops. While the area is small, the onset of the seizure is still invisible to the person. As a larger portion of the brain becomes involved, the seizure becomes noticeable and evolves into a serious event. If a drug-delivery system is capable of electrical recording, stimulating and controlling drug delivery in terms of time and quantity (Figure 1.6), the seizure could likely be stopped in its early stages. A drug-delivery system properly located near the neurons where the seizure is initiated (the epileptic focus) could detect the firing patterns associated with the beginnings of a seizure. Circuitry placed on the rear area of the system (Figure 1.6) could analyze the signals and identify them as symptomatic of a seizure. Once identified, pumps could send inhibiting drugs down the appropriate chemical delivery channel closest to the target area. The injection of the fluid can be controlled using microvalves to open or block channels. For a multi-site system, having a separate line and pump from the drug reservoir to each site is impractical. Large amounts of space could be saved and the complexity of the

system layout could be greatly reduced by using microvalves to form a fluidic multiplexer. Flowmeters placed within the channels would monitor the dose being delivered, and closed-loop circuitry could then stop the injection of drugs using microvalves when the appropriate level had been reached. Microchannels and flowmeters have been reported [3-5], so that valves are the only component still needed for the realization of integrated drug delivery systems.

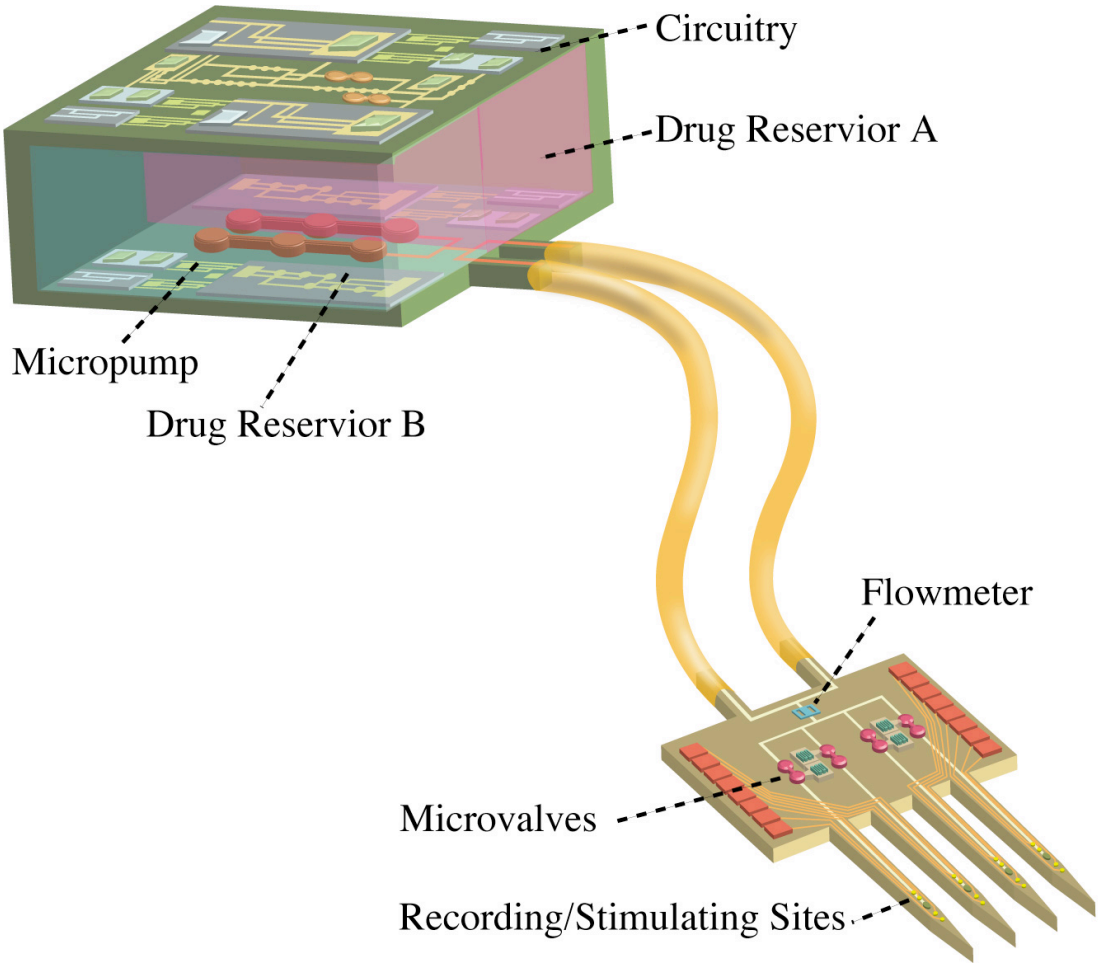

Figure 1.6: Illustration of a closed-loop drug delivery system with implantable microprobe with chronically recording/stimulating sites, microvalves, and a flowmeter.

1.5 Microvalve Metrics and Previously Reported Work on Microvalves

The components mentioned in the previous section are all important parts of any

chemical delivery system that is to be chronically implanted. However, for multi-site, multi-chemical injection, there must be a way to select the desired chemical and route it to the proper site in order to minimize the fluidic lead count. In this way, if two chemicals are to be used, only three lines are needed for the implant: the first chemical, the second chemical, and perhaps a saline flushing solution. By being able to direct the fluid flow, any of the chemicals can be routed down any number of channels to the respective sites. Without these capabilities, only the chemical in a particular line can be injected down that line to the single associated site. A separate line would be needed for each individual site, making multi-delivery-site devices excessively tethered by the external microchannel tubes coming off the back end. The solution to this situation requires on-chip fluidic multiplexers, which are an integral part of every chemical delivery system in the macro world [12, 64].

1.5.1 Metrics

Pressure ejection is the method used on the Michigan drug delivery probe. In operation, nitrogen pressure is applied to the fluidic drug reservoir, and the fluid in the channel moves along the direction of the pressure gradient. The flow rate is determined by the liquid properties (viscosity), applied pressure, and channel cross-sectional area. A typical cortical neuron can be recorded electrically over a distance of roughly 50-100μm. In order to effectively alter the neuronal environment, the minimum amount of injected chemical can arbitrarily be taken at about 10% of a 100μm-diameter sphere, which is equivalent to about 50pL. This amount of chemical is generally injected into the tissue in 100 mSec, which results in a typical flow rate of 500pL/Sec, or 30nL/min. Drugs were previously delivered by 1-2 psi pressure pulses having duration of 100msec [65].

Recently, it has been observed that fast chemical injection can mechanically damage or even kill some cells, so the trend is to deliver drugs over longer pulse-durations (5nl for 10Sec) or to deliver smaller volumes with higher concentrations of drugs [66].

The integrated microvalves on a neural probe must be compatible with current probe fabrication technology without adding too much process complexity. They should also be robust and compatible with chronic use in-vivo. Therefore, high actuation voltages (>10V) and high temperatures are precluded in order to avoid damaging the neural system. Moreover, the entire delivery system must be kept small enough to avoid excessive tissue displacement and disruption of the cellular system. The temperature rise in the tissue must be no more than 2°C to avoid neural damage.

Robustness: This characteristic concerns microvalve lifetime and the ability to tolerate a harsh environment. Operating frequency, pressure overstress, and temperature cycling patterns [67] may all shorten the life of a microvalve. Even if a valve does not fail catastrophically, long-term fatigue can steadily degrade valve performance. Due to the difficulty of replacing a chronic device, any such device needs long-term reliability (>5 years) and packaging to withstand the extracellular environment.

Low actuation-voltage: The use of high voltages within any organism is not attractive due to the risk of electrical leakage and shock. In order to avoid damaging the neural system, a low actuation voltage (< 10V) is required.

Low operating temperature: The operating temperature of the microvalve is an essential factor to be considered because of the unique in-vivo operating environment. The microvalve should not produce a temperature rise of more than $2^{o}C$ in the surrounding tissue. The temperature rise of the valve depends strongly on the material

and its actuation mechanism.

Fabrication compatibility: This may be the most critical design metric and varies greatly among valve structures. The formation of the valve structure should not complicate the probe process or require any steps that are not compatible with the standard probe process. Because simply-structured devices tend to be more cost-effective and allow for higher overall system density, integrated microvalves should be fabricated with a minimum number of additional masks to the standard probe process.

Low leak rate: The leak rate of a microvalve depends on a number of factors including actuation force, sealing surface geometry and topology, differential pressure applied to the valve, and any particulates on the valve sealing surfaces. The minimum acceptable leak rate would vary greatly among target applications. As mentioned earlier, a typical cortical neuron can be recorded electrically over a distance of roughly 100μm. The negligible amount of injected chemical can arbitrarily be taken at about 0.5% of this 100μm-diameter sphere, which is equivalent to about 2.5pL. For example, for a 100mSec delivery pulse duration, the leak rate should be less than 25pL/Sec.

1.5.2 Actuation Methods for Chronic Drug-Delivery

1.5.2.1 Thermomechanical Valves

Bimetallic: Bimetallic actuation uses the difference in thermal coefficients of expansion of two bonded solids. This is often called thermal bimorph actuation. The heater is usually integrated between the two solid materials or on one side of the bimorph. Bimetallic actuators offer an almost linear deflection dependence on heating power. There are a number of different bimetal combinations possible for the structure, but one pair that is attractive is aluminum and silicon. The force and deflection are maximized for

pairs which have a large difference in thermal expansion coefficients. It is often desirable to use materials with low thermal conductivities to limit power loss through conduction. Unfortunately both silicon and aluminum have high thermal conductivities, resulting in relatively large power dissipation when these materials are used with thick diaphragms. Reported bimetallic valves (Figure 1.7) often have high operating temperatures (>180^{o}C) and high power consumption (1030mW) with a 200μm × 200μm valve opening [68, 69].

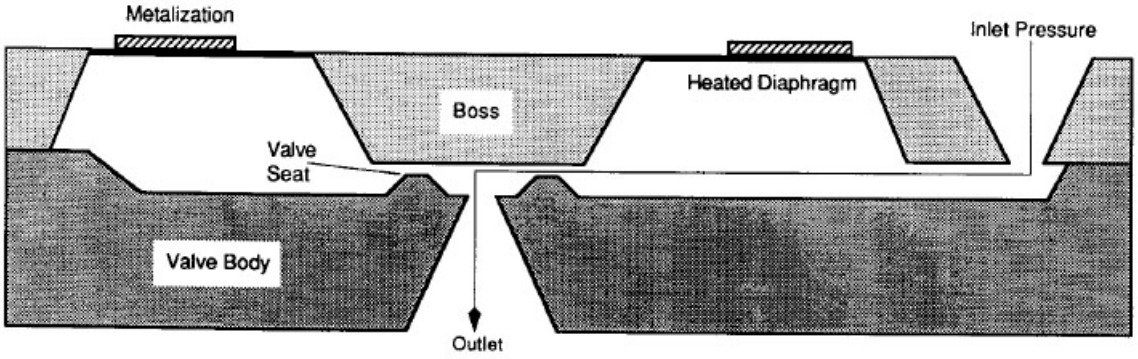

Figure 1.7: Cross section of a micromachined, bimetallically-actuated diaphragm valve [68].

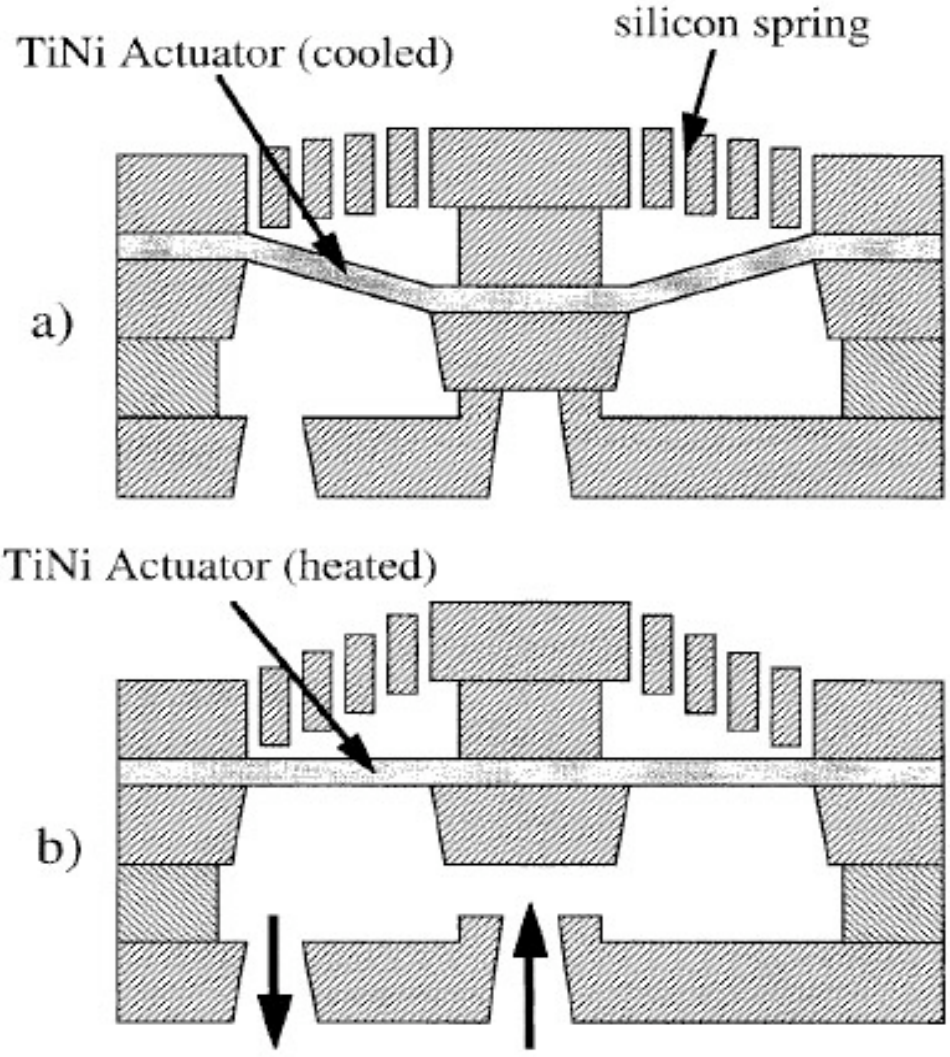

Figure 1.8: Schematic cross-sectional drawings of a TiNi-actuated microvalve in the (a) closed and (b) open positions [70].

Shape memory alloy: Shape memory alloys (SMAs) are materials such as titanium/nickel alloy which, once mechanically deformed, return to their original undeformed shape on a change of temperature. SMAs transform their phase from a "soft" state at low temperatures to a "hard" state at higher temperatures. For example, Ti-Ni Alloy's microvalve is quite fast (25mS), has useful flow and pressure ranges, but SMAs tend to lose their force if overstressed (Figure 1.8). Robustness and fabrication complexity could be an obstacle [70]. The advantages of SMA actuators are high force

and large stroke. However typical transformation temperatures range from -190 ^{o}C to 180 ^{o}C, which is substantially lower or higher than permitted for use in the body [71].

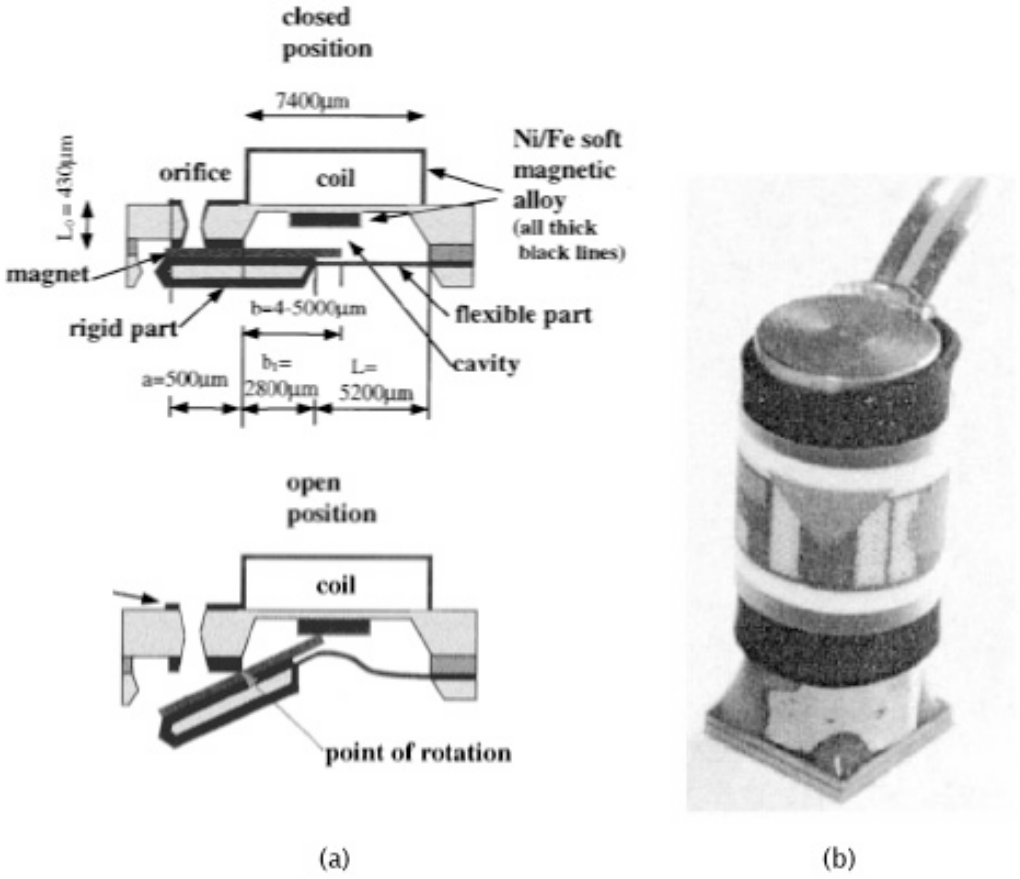

Figure 1.9: (a) Schematic cross-sectional drawings of a micromachined electromagnetically actuated microvalve (b) the realized device [72].

1.5.2.2 Electromagnetic Valves

Electromagnetic devices have come to dominate actuation in the macroworld. Magnetic fields are largely actuator-volume dependent, and thus actuation force is simply increased by using larger (or denser) windings and/or larger, stronger permanent magnets. But the unfavorable scaling of forces for small devices makes electromagnetics a difficult approach to microactuation and difficult to use in-vivo (Figure 1.9). The fabrication of integrated coils with low resistance continues to be a challenge and makes it difficult to

develop a low-power actuator. Moreover, the difficulty of integrating this structure into the probe process and structure makes it impossible to utilize in this research application [72].

1.5.2.3 Electrostatic Valves

The most widely explored actuation scheme for microdevices of all types is that of electrostatics (Figure 1.10). Unlike the volume dependence of electromagnetic forces, electrostatic forces are surface-area dependent (due to stored surface charge), and thus are more compatible with scaling. This actuation scheme is simple to fabricate, and exhibits very fast response times (<13mS) [73]. Being a charge-storage phenomenon, electrostatic actuation also has the distinct advantage of zero static power consumption. However, this method cannot be used here because electrostatic actuators generate a limited actuation force, in spite of scaling gains, show chronic particulate contamination problems, and require high voltages (tens or hundreds of volts) for actuation over significant distances [73, 74].

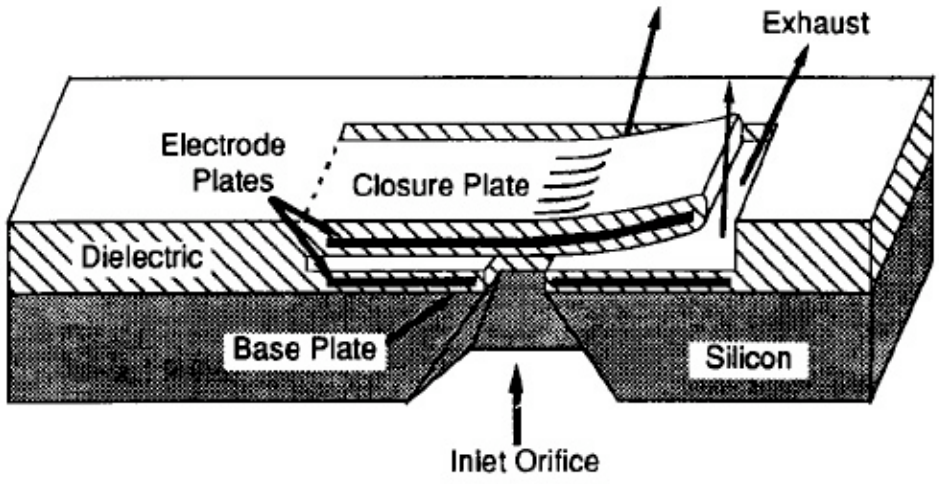

Figure 1.10: Perspective view of electrostatically actuated microvalve cross section [73].

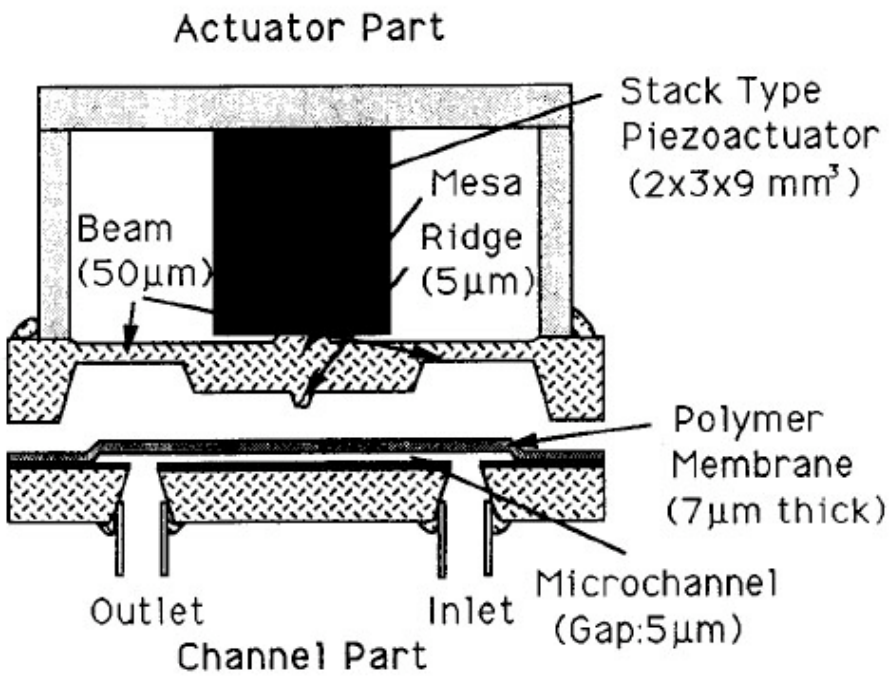

Figure 1.11: Perspective view of piezoelectric microvalve using a rubber membrane [75].

1.5.2.4 Piezoelectric Valves

Piezoelectric actuation initially is a very attractive method for generating motion. Piezoelectricity is a reversible effect in which a mechanical stress on a material generates electrical charge and an applied electric field generates a mechanical strain in the material (Figure 1.11). Piezoelectric actuators generally generate small strain (usually less than 0.1%) and high stresses (several Mpa). Therefore, they are suitable for applications which require large forces but small displacements [75]. However, this method cannot be used here due to the integration problems on the probe and high operating voltages. Piezoelectric actuators require a separately assembled stack of individual piezo elements to generate useful displacement [75]. Furthermore, this stack is usually glued onto the valve body, thus resulting in a hybrid structure that severely limits any sort of batch

processing or easy integration into a complete microsystem. Also piezoelectric elements may require high drive voltages to operate, as much as 150V in some cases [76].

1.5.2.5 Thermopneumatic Valves

Thermopneumatic actuation relies on the change in volume of a sealed liquid or solid under thermal loading. The principle also uses the phase change from liquid to gas or from solid to liquid to gain a larger volume expansion. The mechanical work generated in such a thermodynamic process exceeds the energy stored in an electrostatic or electromagnetic field. The actuation material of the thermopneumatic valve can be gas, liquid [77], or solid [78-82].

Solid Actuation Material: A photoresist-like thermally responsive hydrogel, for example, has been formulated, surface micromachined, and integrated into parylene microchannels to realize a valve [78-80]. It showed a 2.5-fold polymer volume increase by changing the water temperature from 25^{o}C to 10^{o}C. Hydrogels undergo reversible volume change (swelling) with pH [78], glucose concentration, and the temperature [79, 80] of the liquid in which they are immersed, thus plugging the microchannel when used as a valve.

A sealed patch of paraffin has been used as a thermopneumatic actuator [81, 82]. This actuator uses the high volumetric expansion of paraffin heated above its melting point, providing large displacements and forces while using low power. Both technologies, however, are very slow and require a low temperature fabrication process, which is not compatible with the standard probe process.

Liquid Actuation Material: The advantage of using liquid as an actuator material is the ability to generate large forces over a significant distance, since gaseous molecules

will freely flow within a closed cavity to reach equilibrium pressure throughout. Fabrication of thermopneumatic valves can be straightforward [77]. No exotic materials are required, other than possibly the working fluid, and batch processing is feasible for most of the fabrication steps.

1.5.2.6 Electrochemical Valves

Electrochemical valves are actuated using gas microbubbles generated by the electrolysis of water:

$$2H_2O \rightarrow 2H_2\uparrow + O_2\uparrow$$

The generated gases have a volume that is about 600 times that of the water volume needed for it. This ratio exceeds that of thermopneumatic actuators. The pressure inside the bubble is proportional to the surface tension σ and the radius of curvature R of the meniscus. The reverse reaction converts the two gases back to water. The reaction needs a catalyst such as platinum. Platinum is able to absorb hydrogen. The hydrogen-platinum bond is weaker than the hydrogen-hydrogen bond. Therefore, the energy barrier required for freeing hydrogen atoms from H_2 and bonding with oxygen is lower than in the gas phase. The benefit of this method is that, once formed, only a minimal holding current is required to compensate for parasitic losses from leakage and any back-reactions, depending on the half-cell voltage created between the electrode and the gas. The valve shown in (Figure 1.12) [83, 84], for example, is bistable and consumes only 4.3μW. The low operating voltage of 2.5V is a further advantage. One operational cycle (fully closed to fully open and back) requires approximately 120 seconds, which is very slow compared to electrostatic and piezoelectric valves. Though electrochemical actuators are suitable for low power applications, they are not suitable for this research due to their

very slow response times.

1.5.3 A Comparison of Actuation Schemes by Valve Metric

Actuator Type	Robustness	Actuation Voltage	Response Time	Leak Rate	Compatibility
Bimetallic	—	↓	—	↑	↓
Shape Memory Alloy	↓	—	↑	↑	↓
Electromagnetic	—	—	↑	—	↓↓
Electrostatic	↓↓	↓↓	↑↑	—	↓
Piezoelectric	—	—	↑	—	↓↓
Thermopneumatic	↑	↑↓	↑	↑	↑
Electrochemical	↑	↑↓	↓	↑	↑
Capillary-Force	—	↓	↑↓	—	↓

Table 1.1: A summary of the various actuation schemes and their relative merits by microvalve metrics. Key: ↑= better, —= neutral, ↓= worse, ↑↓= design dependent.

1.6 Conclusion

After examining the different schemes, thermopneumatic and electrochemical actuation were initially chosen for this research. But considering the speed of actuation, thermopneumatic actuation exhibits better compatibility with the needs of chronic drug-delivery systems. The results of this research are described in the following chapters. In chapter 2, two different designs for pneumatic microvalves are described. Chapter 3 describes the fabrication of pneumatic microvalves and their testing. Chapter 4 presents a feasibility study of process compatible thermopneumatic microvalves. Finally, chapter 5 introduces the future work needed for the realization of thermopneumatic microvalves and full drug-delivery microsystems.

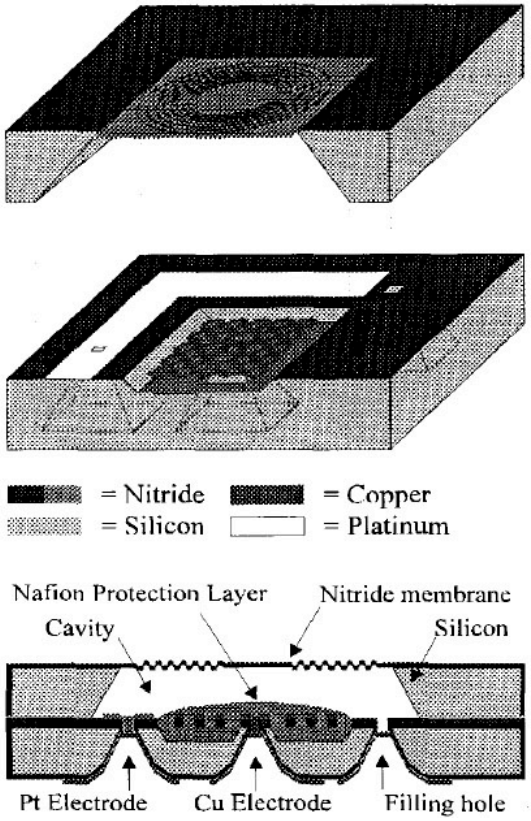

Figure 1.12: Schematic design of a micromachined electrochemical actuator [84].

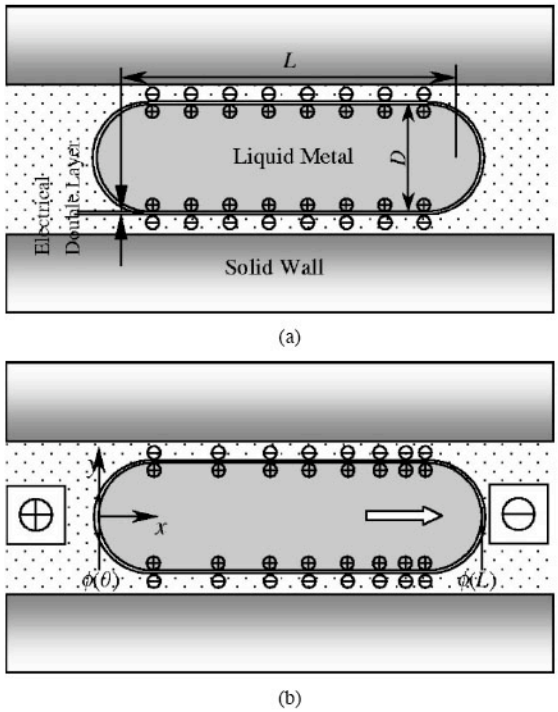

Figure 1.13: Electrocapillary effect (a) initial state (b) electrowetting state [85].

CHAPTER 2

Design, Simulation of a Drug-Delivery Probe with Pneumatically-Actuated Corrugated Microvalves

After examining the different approaches to microvalves presented in chapter 1, thermopneumatic actuation was chosen for this research. One of the fundamental challenges to any microvalve is the need to develop both a valve structure and its actuation mechanism. In order to explore the valve structure independent of the actuation mechanism, a pneumatically-actuated microvalve was initially designed, fabricated, and tested. It uses a separate external pressure source for actuation. This configuration has the advantage of fully isolating the valve from its actuator. With an external pressure source, the drive force may be arbitrarily chosen, allowing the flow and sealing characteristics of the valve to be explored without any actuator force limitations.

Section 2.1 describes the modeling of the microchannels and pneumatically-actuated microvalve. Sections 2.2 and 2.3 then present two designs for the microvalve to improve sealing capabilities in blocking mode. Section 2.4 discusses the conclusion of this chapter.

2.1 Modeling of the Microchannels and Microvalve

The basic concept of this microvalve is a normally-open dual-channel structure as shown in (Figure 2.1), with the one channel passing the fluid and the other channel acting as an actuator. Actuation from an external pressure source is applied through an actuation

channel attached to the bottom cavity. The actuation channel provides a large pressure on the cavity walls below the circular diaphragm. Since the cavity walls, except for the flexible diaphragm, are thick, the actuation pressure drives the flexible diaphragm up to block drug flow in the top channel as shown in Figure 2.1.

To design the feature sizes of the microvalve structure, simulations were performed using FLUENT and FEMLAB to determine the sizes of the drug-delivery and actuation channels and the gap spacing above the diaphragm (Figure 2.1(a)). The mechanical strength of the diaphragm was simulated to determine the appropriate radius, the number of corrugations, and the thickness of the diaphragm.

2.1.1 Microfluidic Simulations

One crucial part of any microfluidic system is the network of microchannels. A micr ochannel is a passive component connecting various parts of the fluidic system together. The widths of microchannels vary from hundreds of microns to hundreds of nanometers, depending on the application [32]. Flow can be considered as laminar, transitional, or turbulent, and is dependent on the fluid density and viscosity, characteristic velocity, and geometry of the channel.

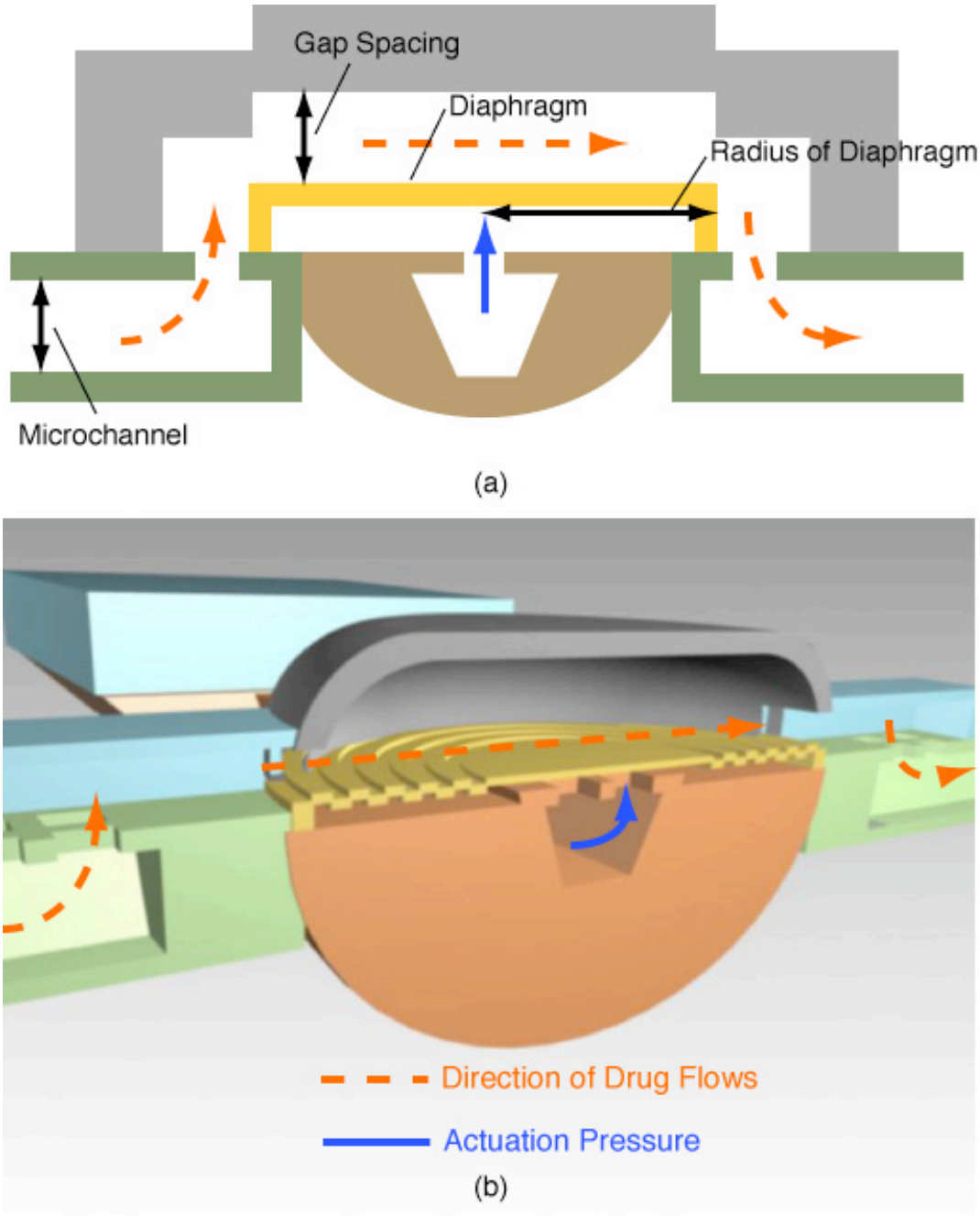

Figure 2.1:The basic concept of the microvalve; (a) 2D cross section view (b) 3D cross-section view with an indication of drug flows and the actuation pressure path.

For most simple microfluidic channels in which the width and height are less than 1mm and velocities are less than a centimeter per second, the flow will be laminar [86]. Flow patterns will typically be functions of Reynolds number, a measure of the ratio

between inertial forces and viscous forces in a particular flow. This dimensionless number is defined as

$$\mathrm{Re} = \frac{\rho V D}{\mu}, \tag{2.1}$$

where ρ is the fluid density (kg/m^3), V is the mean fluid velocity (m/s), D is the pipe diameter, and μ is the fluid dynamic viscosity (Pa·s or N·s/m^2). In circular tube flows, Reynolds numbers smaller than about 2,100 typically indicate laminar flow, while values greater than 4,000 are turbulent. Between these numbers, the flow may switch between laminar and turbulent conditions and is considered *transitional*. The dimensions of the microchannels in this research produce Reynolds numbers much less than 1, resulting in laminar flow behavior.

Based on laminar flow, the pressure difference across a tube of known dimensions can be calculated using the *Navier-Stokes equations* (nonlinear, second order, partial differential equations), which are the governing differential equations of motion for incompressible Newtonian fluids. For a horizontal tube, the pressure drop across the tube, ΔP [Pa], is directly proportional to the volume flow, Φ [m^3/s], for fully developed laminar flow

$$\Delta P = R \cdot \Phi \tag{2.2},$$

with R [Pa•s•m^{-3}] as the channel resistance, a constant that depends on the tube geometry. The pressure drop across a valve can be estimated using the channel geometry as schematically shown in Figure 2.2. The channel has a square cross-section of side b [m], while the step-like valve area has a length l [m] and a gap spacing y_i [m]. Considering this geometry for the channel, the pressure drop may be calculated [87] by using (2.2):

$$\Delta P = \frac{2 \cdot k_{shape} \cdot l \cdot \mu}{D_h^2 \cdot A} \cdot \Phi \tag{2.3}$$

where A[m] is the flow area, D_h[m] is the hydraulic diameter (defined as $D_h = 4 \cdot A/P$) the wetted perimeter of the flow cross-section area is P[m], k_{shape} is a constant that depends on the shape of the flow cross section area, μ is the viscosity of the fluid (10^{-3} Pa·s for water) , and l is length. Some resistance formulas for circular, rectangular, square and triangular cross-sections are presented in Table 2.1. Chen et al. [32] performed careful experiments with multiple microfabricated fluid delivery devices and found a k_{shape} of 27.5.

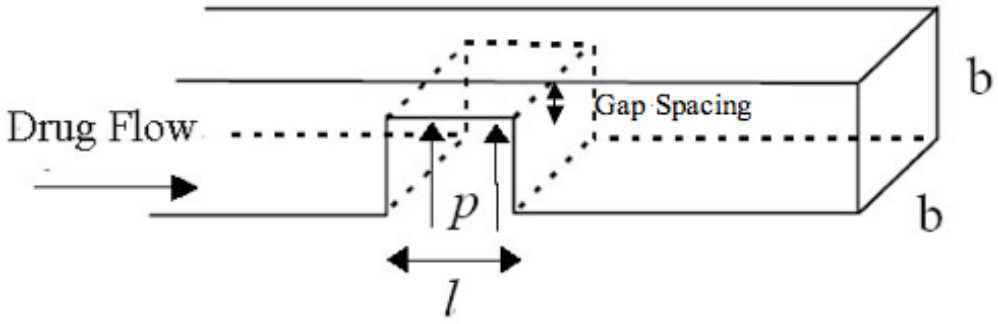

Figure 2.2: Schematic of a microvalve segment showing the cross-sectional area of the fluid path across the valve.

Channel Shape	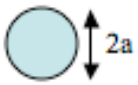	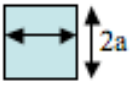	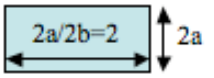	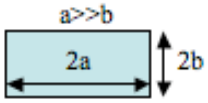	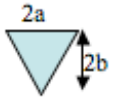
Shape Constant k_{shape}	16	14.2	15.5	24	13.3
Hydraulic Diameter, D_h[m]	2·a	2·a	$\frac{4a \cdot b}{a+b}$	4·b	1.04·a
Area, A[m^2]	$\pi \cdot a^2$	$4 \cdot a^2$	4·a·b	4·a·b	$1.41 \cdot a^2$
Resistance, R[Ns/m^5]	$\frac{8 \cdot l}{\pi \cdot a^4}\mu$	$\frac{1.78 \cdot l}{a^4}\mu$	$\frac{31(a+b)^2 \cdot l}{64a^3 \cdot b^3}\mu$	$\frac{3 \cdot l}{4a \cdot b^3}\mu$	$\frac{17.4 \cdot l}{a^4}\mu$

Table 2.1: Shape constant, hydraulic diameter, area and flow resistance for different types of channel cross section, with channel length, l [m], and fluid viscosity μ [Ns/m^2][88].

To find the appropriate gap spacing for the microvalve (Figure 2.1 and Figure 2.2), the pressure drop across the valve was simulated using MATLAB. A flow channel having a cross-sectional area of 338μm^2 with a 4mm-long shank and a microvalve having a circular diaphragm of 200μm-radius were used for this analysis (Figure 2.3). We assumed that the highest viscosity chemical that needs to be delivered through a chronic drug-delivery system is bee venom, the viscosity of which is three times higher than water. If the limit of viscosity is chosen as 0.005 Pa·s and we assume a drive pressure of 9000Pa, the required gap spacing above the microvalve having a 200μm-radius circular diaphragm for an open flow of 500pL/sec should be at least 3~4μm (Figure 2.4).

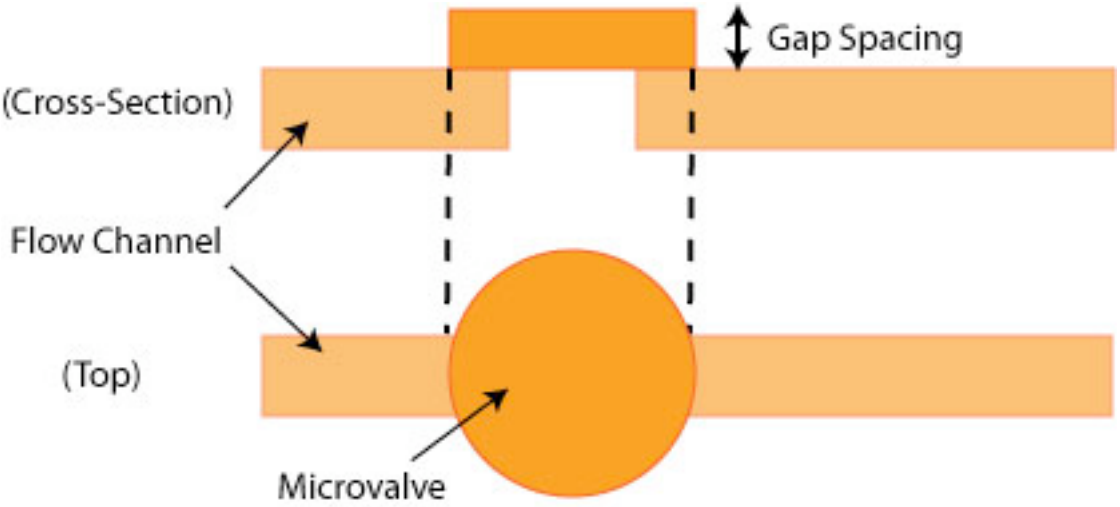

Figure 2.3: The cross-section and top views of the simulated model. A flow channel has a cross-sectional area of 338μm^{2}with a 4mm-long shank and a microvalve has a circular diaphragm of 200μm-radius.

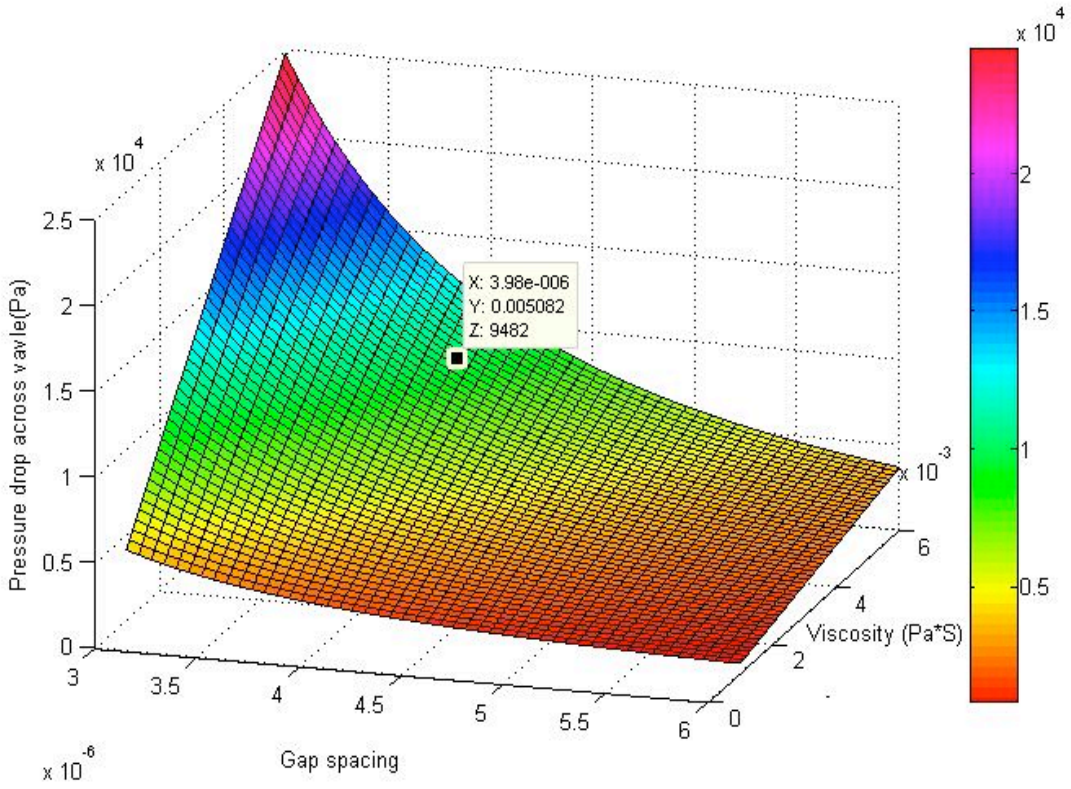

Figure 2.4: The simulated pressure drop across a microvalve under different viscosities and gap spacings with a flow channel having a cross-sectional area of 338μm^{2}at flow rate of 500pL/sec.No actuation pressure applied.

For an open flow rate of 500pL/sec and a 3μm-gap spacing (Figure 2.2), the total pressure drop across the entire drug-delivery system was simulated by FLUENT (Figure 2.5). Figure 2.6 and Figure 2.7 show that the pressure drop for water through a 50μm length of microchannel having a cross-sectional area of 338μm^2 at flow rate of 500pL/sec is 90Pa. Therefore, a 4mm-long drug-delivery probe with flow channels, excluding a microvalve, has a pressure drop of 7200Pa (49.9 Torr). The bottom picture of Figure 2.6 is for methanol at an open flow rate of 500pL/sec. The pressure drop through 50μm for methanol is 49Pa and for a 4mm length probe is 3920Pa (27.1 Torr).

The pressure drop across the microvalve without a flow channel for water at a flow rate of 500pL/sec is 1210Pa as shown in Figure 2.7(a). Figure 2.7(b) shows 0.0285 m/s

for the velocity of water at the outlet. Based on two simulations (Figure 2.6, Figure 2.7), the expected total pressure drop across the entire system for water is 8410Pa (7200Pa (from flow channels) + 1210Pa (from the microvalve)). Pressure ejection is the method used on the Michigan drug delivery probe. In operation, nitrogen pressure is applied to the fluidic drug reservoir, and the fluid in the channel moves along the direction of the pressure gradient. Drugs were previously delivered by 1-2 psi (6~12kPa) pressure pulses having duration of 100msec [65]. Therefore the expected total pressure drop across the entire system of 8410Pa is acceptable for this project.

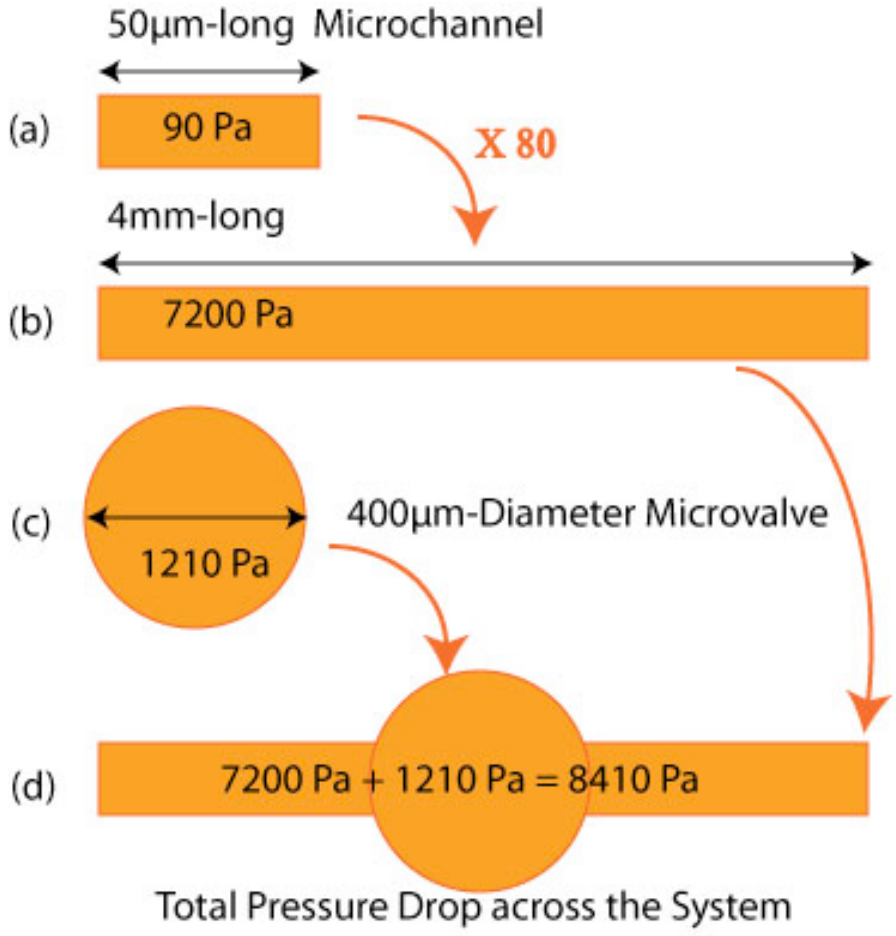

Figure 2.5: The pressure drop simulated using Fluent. (a) 50µm-long microchannel with a cross sectional area of 338µm^2 (Figure 2.6), (b) 4mm-long microchannel with a cross sectional area of 338µm^2, (c) a microvalve of 400µm diaphragm diameter (Figure 2.7), (d) Total system.

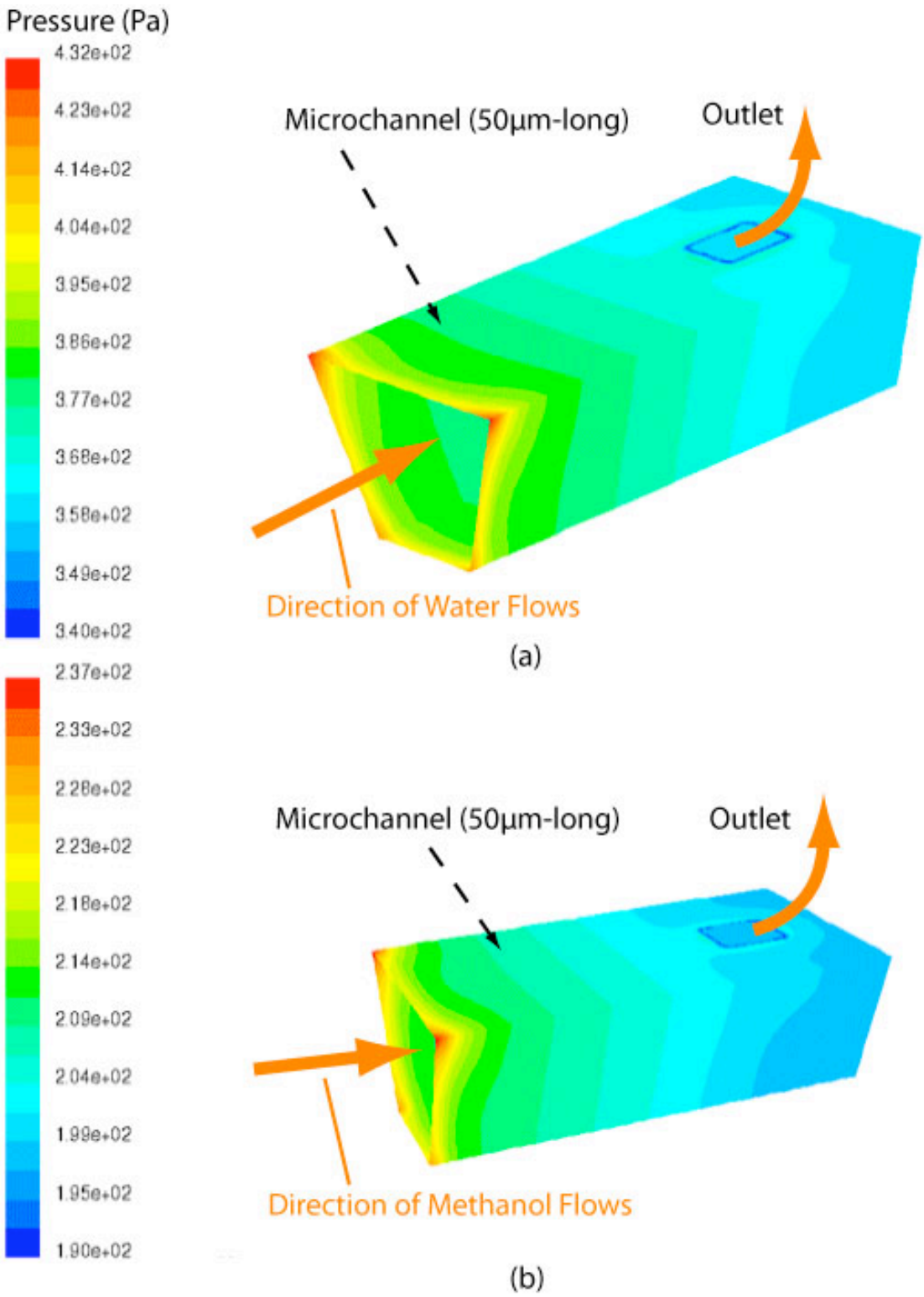

Figure 2.6: Microfluidic 3D Simulations for finding the pressure drop across a microchannel having a cross-sectional area of 338µm^2 at flow rate of 500pL/sec (a) for water, (b) for methanol.

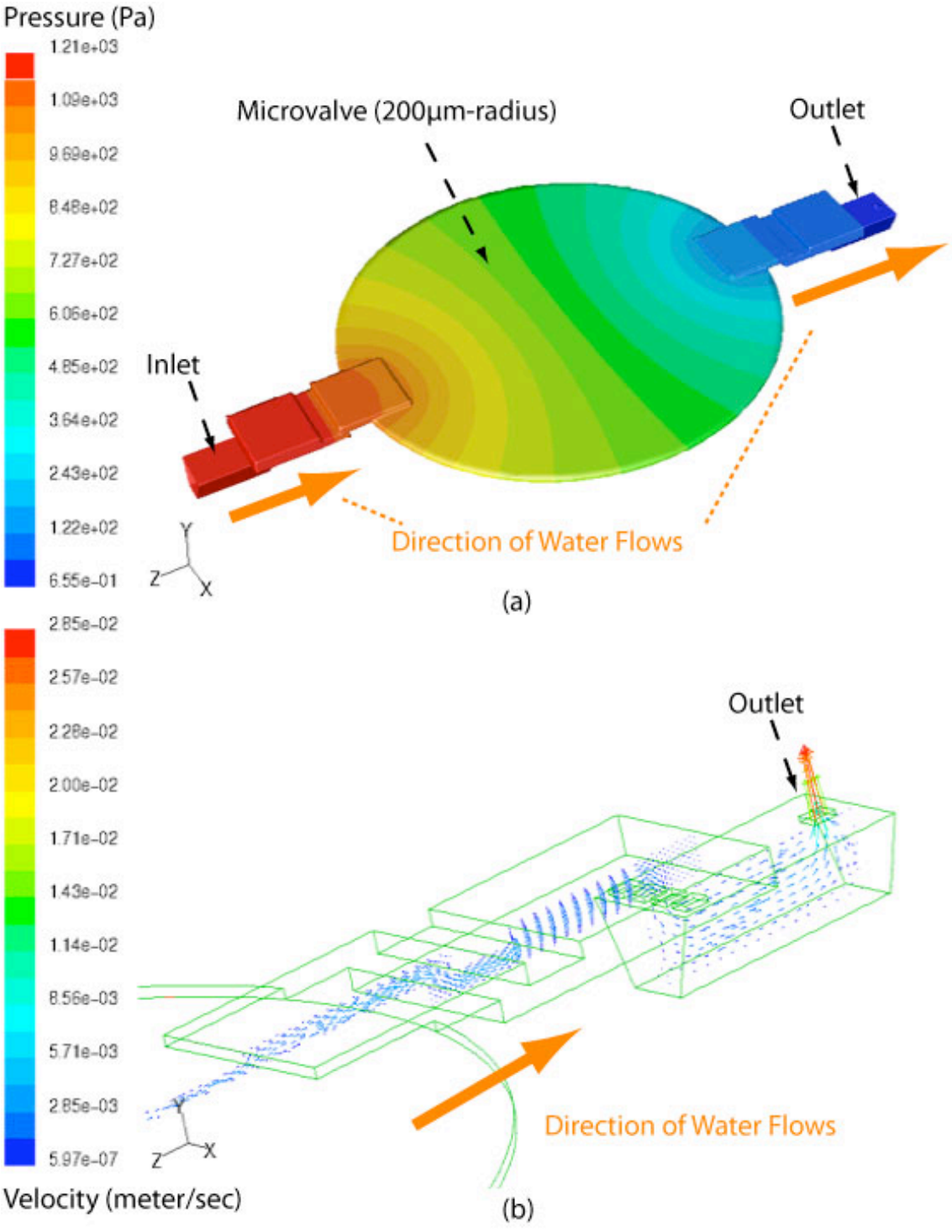

Figure 2.7: (a) Pressure drop (1210Pa) for water across the microvalve having a diaphragm of 200µm-radius with a gap spacing (Figure 2.2) of 5µm at the open flow rate of 500pL/sec, (b) Drug velocity at the same flow rate of 500pL/sec.

2.1.2 Simulation of Corrugated Diaphragm Deflection

The performance of membranes is important for the success of the valve-actuator. In active valves, for example, membranes capable of large deflection can be used to transform pressure into displacement. In classical mechanics, the linear theory for membranes made of isotropic, homogeneous, linear elastic materials can be derived based on the following simplified assumptions: The thickness, h, of the membrane is small compared with the other dimensions of the membrane. The nonlinearity which occurs for deflections more than 25% of the membrane thickness, regardless of its radius, is the result of tensile stress caused by the stretching of the membrane [89].

-Flat membranes

Due to the fabrication process, some internal stress may be present in the membrane. When a high internal stress, σ [Pa], is present, the relationship between the pressure difference P [Pa] over the membrane and the corresponding center deflection y[m] for a flat, square membrane of thickness, h[m], side length, 2a [m], Young's modulus, E [Pa], and Poisson's ration v is described by [90]:

$$\frac{Pa^4}{Eh^4} = \frac{3.41a^2}{Eh^2}\sigma \cdot \left(\frac{y}{h}\right) + \frac{1.98 \cdot (1 - 0.295v)}{1 - v} \cdot \left(\frac{y}{h}\right)^3 \tag{2.4}$$

The first term on the right side represents the resistance to bending introduced by the internal stress. The second term shows the geometrical non-linear effect for larger pressures as a result of stretching of the membrane. For example, silicon has a Young's modulus of about 170 GPa; silicon nitride, depending on the deposition process, varies as E= [200-300] GPa, σ= [-50-170] MPa, and polyimide E= [3-10] GPa, σ= [20-80] MPa.

-Corrugated membranes

A way to increase the deflection, for the same size of the membrane, is to use corrugations instead of a more flexible material. The corrugation profile influences the performance of the membrane: sharp corners will lead to stress concentration, so a desirable shape would be a groove with a rounded bottom point and rounded edges [3]. Experimentally it has been shown that a corrugated membrane has a larger linear range than a flat one because of the reduction of the radial stress in the membrane. For shallow, sinusoidally corrugated membranes the deflection is given by [90]:

$$\frac{Pa^4}{Eh^4} = \frac{2(3+q)(1+q)}{3\left(1-\frac{v^2}{q^2}\right)} \cdot \left(\frac{y}{h}\right) + \frac{32}{q^2-9}\left[\frac{1}{6} - \frac{3-v}{(q-v)(q+3)}\right] \cdot \left(\frac{y}{h}\right)^3 \qquad (2.5)$$

where the corrugation quality factor, q, for sinusoidal profiles is [90]:

$$q^2 = \frac{s}{l}\left[1+1.5\frac{H^2}{h^2}\right]$$

where s is the corrugation profile, *l* is the corrugation frequency, and H is the corrugation depth (Figure 2.8). Thus, q varies from 1 (flat membrane: H=0 and s=1) to $q = \left[1+1.5\frac{H^2}{h^2}\right]$. The corrugation profile can be calculated by:

$$s = \pi R \cdot \frac{2 \cdot \arcsin\left(\frac{l}{4R}\right)}{\pi/2} \qquad \text{Sinusoidal profile}$$

$$\frac{s}{l} = \frac{a+2NH}{a} \qquad \text{Rectangular profile}$$

where N is the number of corrugations, and R= $(4H^2+l^2)$ / (16H). As the number and

frequency of the corrugations increase, the deflection increases, indicating an increase in mechanical sensitivity of the membrane [91].

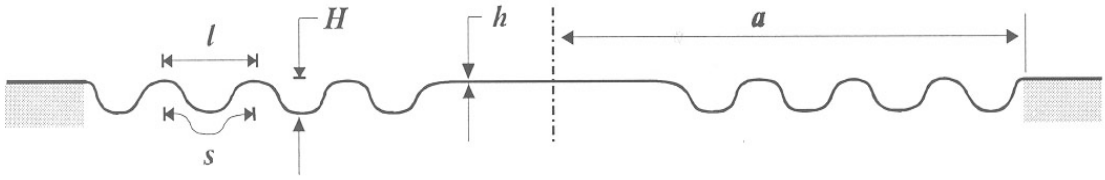

Figure 2.8: Schematic cross-sectional view of a circular corrugated membrane and its characteristic parameters: radius, a; thickness, h; corrugation depth, H, profile, s, and frequency, l, respectively.

-Corrugated Diaphragm of $SiO_2/Si_3N_4/SiO_2$

Based on equations (2.4) and (2.5), the deflection of a diaphragm of $SiO_2/Si_3N_4/SiO_2$ is shown in Figure 2.9 with 5 corrugations. Under the same pressure the corrugated diaphragm shows 1.4 times the deflection that the planar (flat) diaphragm does. The presence of corrugations reduces internal stress [92], and for large corrugation depths the mechanical sensitivity of the membrane only weakly depends on internal stress. The effects of internal stress cannot be treated as easily as for planar membranes, where a simple term is added to the pressure-deflection equation (2.4). Therefore, the finite element method (FEM)[92] becomes necessary in modeling the effects of different corrugation profiles and membrane thicknesses on the pressure-deflection characteristics.

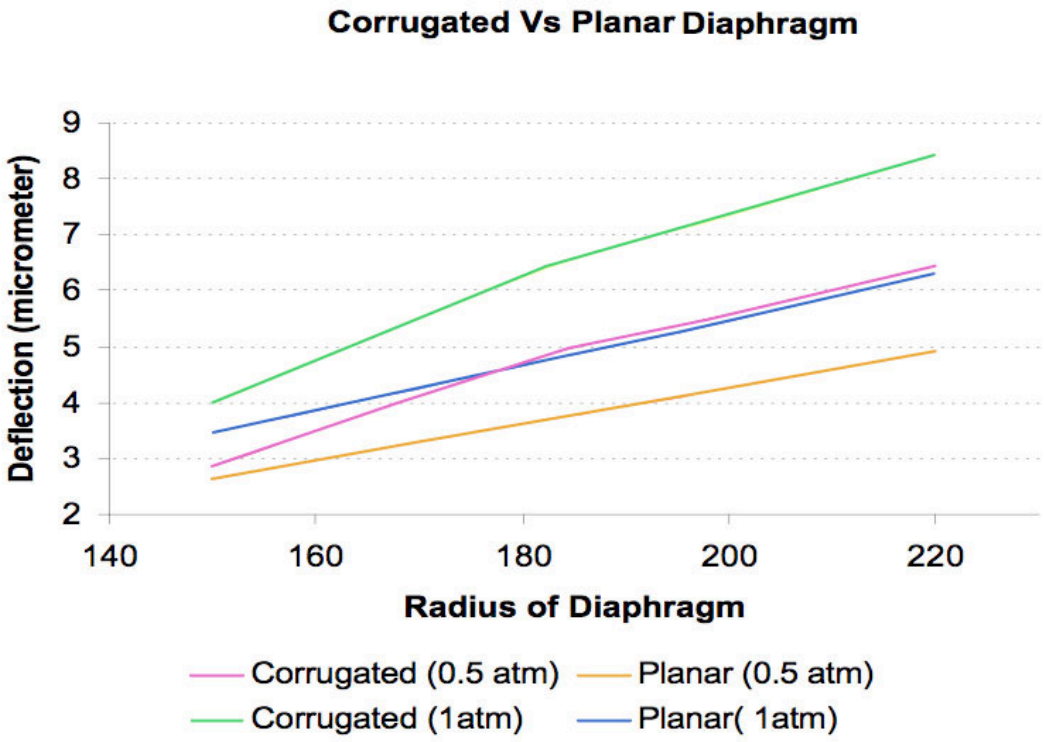

Figure 2.9: Calculated deflection of corrugated and planar diaphragms of $SiO_2/Si_3N_4/SiO_2$ having a thickness of 4000/2000/4000Å as a function of diaphragm size for 0.5atm and 1atm drive pressures.

ANSYS software was chosen to perform the FEM simulation of corrugated diaphragm deflection. To model the diaphragm material properties, the material is assumed to behave as linear elastic. For the finite element model, a coarse mesh was used since the geometry is not complex. Due to the symmetrical shape of the diaphragm, a two-dimensional PLANE82 is used as the element type. ANSYS software includes a parametric solver that was used to find the optimum diameter and thickness of the diaphragm for various drive pressures. Figure 2.10 shows the required actuation pressures to get a 7μm deflection of a corrugated diaphragm made of $SiO_2/Si_3N_4/SiO_2$ as a function of diaphragm radii (150μm~250μm) and thickness as (0.5μm~1.5μm). Based on these simulation results, diaphragm radii of 180, 200 and 220 μm with diaphragm thickness of 1~1.5 μm were fabricated to characterize the deflection of corrugated diaphragm in

chapter 3.

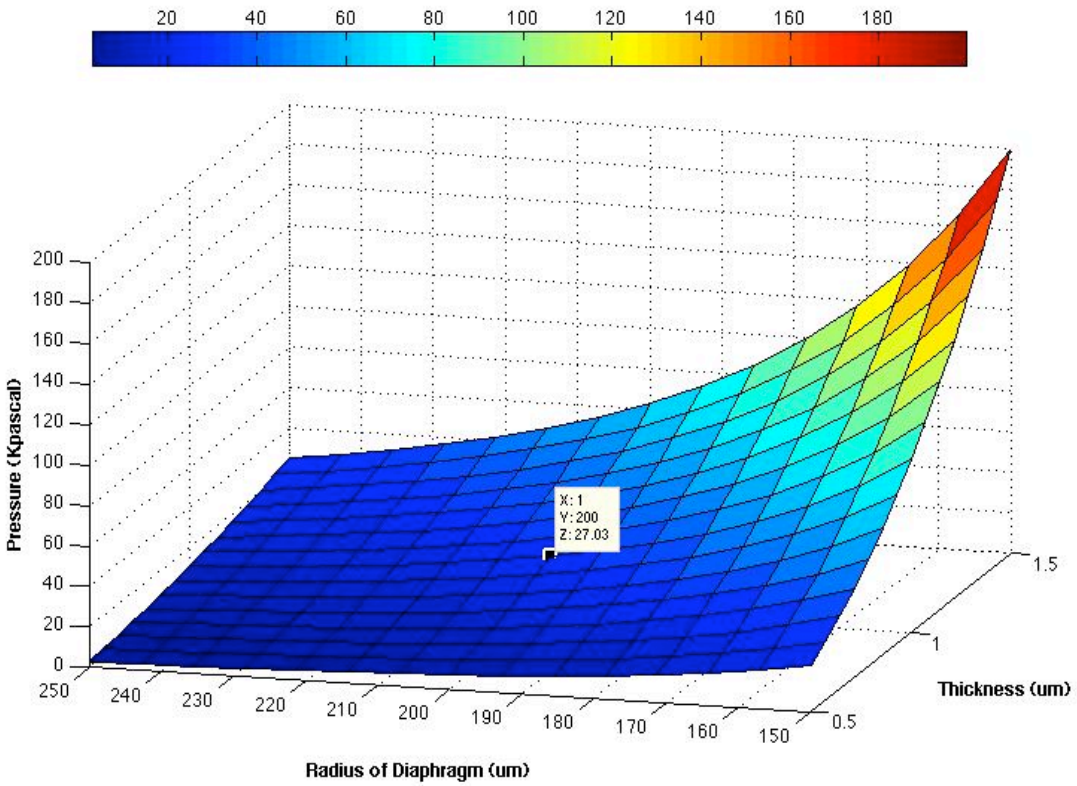

Figure 2.10 The required actuation pressure for the 7μm -deflection of diaphragm of $SiO_2/Si_3N_4/SiO_2$ as a function of the radius and thickness of the diaphragm. Through the simulation, the diaphragm radii of 180~200μm with the diaphragm thickness of 1~1.5μm was chosen for the testing. .

-Flat / Corrugated Membrane of Parylene

To reduce the actuation pressure and therefore the overall power required for the application of a thermopneumatic microvalve, a flexible and biocompatible material such as parylene was also investigated for the diaphragm of the microvalve. Based on equations (2.4) and (2.5), the deflection of a diaphragm of parylene, which has a much smaller Young's modulus than $SiO_2/Si_3N_4/SiO_2$ is substantially larger than that of a diaphragm of $SiO_2/Si_3N_4/SiO_2$ under the same applied actuation pressure. Figure 2.11

shows the required actuation pressures to get a 7μm deflection of a corrugated diaphragm made of Parylene as a function of diaphragm radii (150μm~250μm) and thickness (0.5μm~1.5μm). The simulations performed using 5 corrugations of the diaphragm show that the required actuation pressure of 0.7kPa to get a 7μm deflection of a parylene diaphragm is about 30 times lower than the 27 kPa required for a $SiO_2/Si_3N_4/SiO_2$ diaphragm. Figure 2.12 and Figure 2.13 show the required actuation pressures for a 7μm-deflection of $SiO_2/Si_3N_4/SiO_2$ and parylene diaphragms.

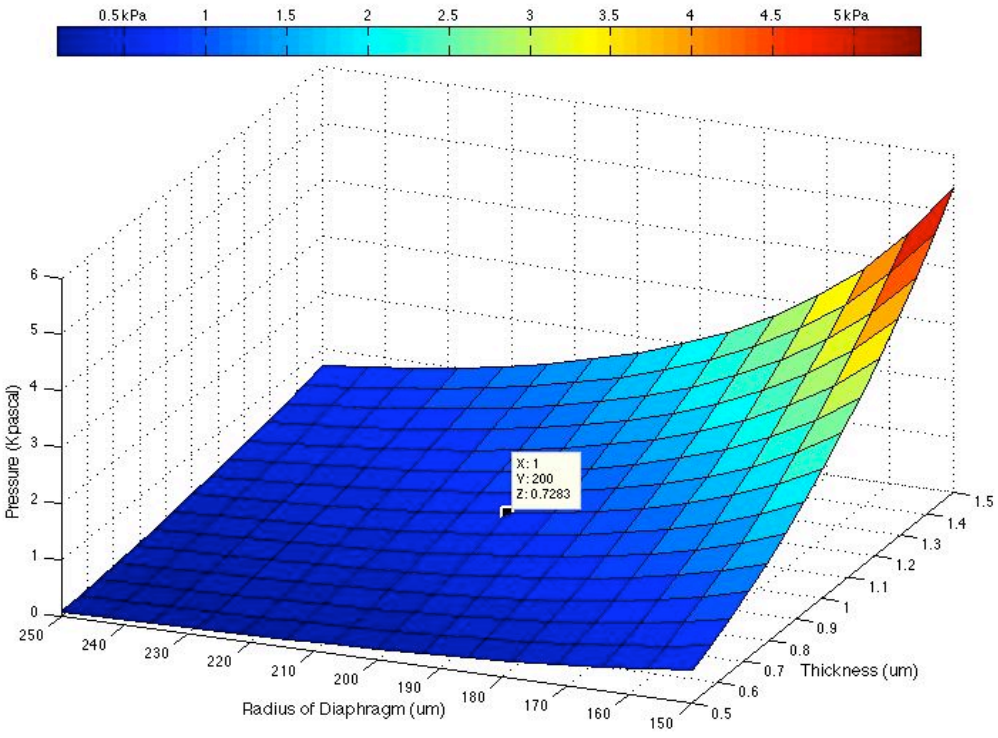

Figure 2.11: The required actuation pressure for the 7μm-deflection of diaphragm of parylene as a function of the radius and thickness of the diaphragm. Through the simulation, the diaphragm radii of 180~200μm with the diaphragm thickness of 1~2μm was chosen for the testing.

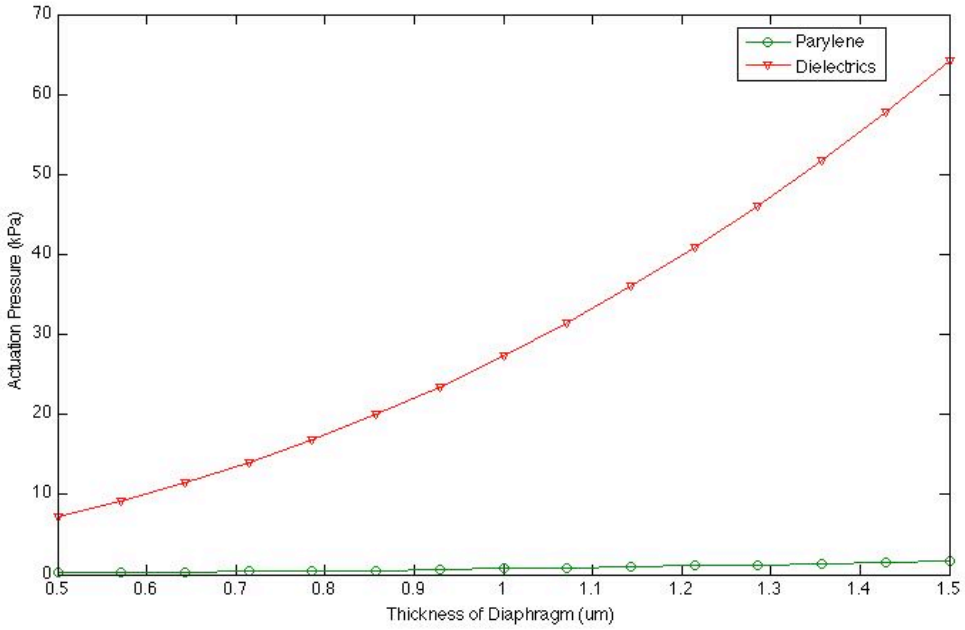

Figure 2.12: The required actuation pressures for a 7μm-deflection of $SiO_2/Si_3N_4/SiO_2$ and parylene diaphragms as a function of the thickness of the diaphragm with 200μm-radius of diaphragm.

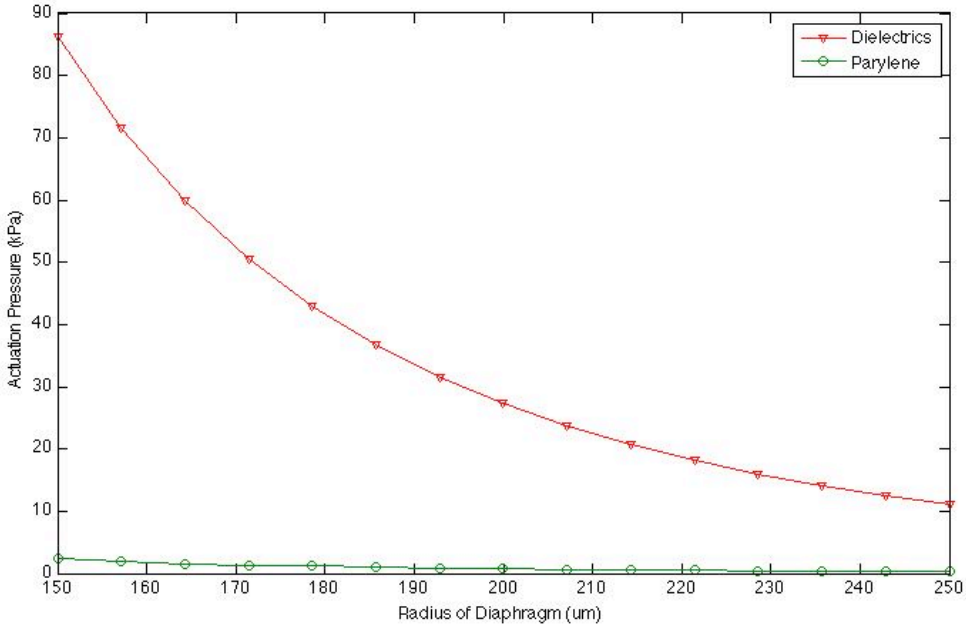

Figure 2.13: The required actuation pressure for a 7μm-deflection of $SiO_2/Si_3N_4/SiO_2$ and parylene diaphragms as a function of the radius of diaphragm with 1μm-thick diaphragm.

2.2 Designing a Pneumatically Actuated Microvalve (Version I)

Figure 2.14 shows the basic concept of a dual-channel structure with the top channel passing the fluid and the bottom channel acting as an actuator. Actuation from the external pressure source is applied through an actuation channel attached to the bottom cavity. The basic mechanism of the microvalve is that of a pneumatic actuator that has a membrane structure as the valve seat. The actuation channel provides a large pressure on the cavity walls below the corrugated circular diaphragm. Since the entire cavity wall, except for the 1μm-thick diaphragm, is surrounded by thick boron-doped silicon, the large actuation pressure drives the flexible diaphragm up to block the drug flow as shown in Figure 2.15. The valve is normally open with a gap of 5μm between the membrane and the valve cap. Using 2D axis symmetry, the 5.6μm-deflection of the corrugated diaphragm of $SiO_2/Si_3N_4/SiO_2$ required to block the drug flow was simulated at an actuation pressure of 35kPa as shown in Figure 2.16. The same thickness of deflection of Parylene diaphragm required to block the drug flow was simulated at an actuation pressure of 1.5kPa. One interesting observation for both simulations in Figure 2.15 and Figure 2.16 is that the 8μm-thick microvalve cap deflects around 0.6μm after the membrane contacts the bottom of the cap and then keeps pushing it out further with the actuation pressure.

Due to the process complexity of fabricating the rounded shape of the cap, a slight opening occurs between the cap and the deflected diaphragm along the outer edge of diaphragm during blocking mode, which results in leakage flow. Because of this problem, Figure 2.16 shows the flow path through the valve is beveled along 20μm of its outer edge to improve the ability of the diaphragm to seal to the valve cap. But possible

leakage still exists along the outer edge of diaphragm (Figure 2.17) due to the small gap shown in Figure 2.18. Inserting the dimensions of the gap into the equation (2.3), the hydraulic resistance of the microvalve calculated at 35kPa in blocking mode is $256x10^{15}$ Pa•s•m^{-3} (k=16, l=2πr=400πμm (200μm radius of diaphragm), μ=10^{-3} Pa•s). The calculated leak rate due to the small gap at an input pressure of 10kPa is 29 pL/sec. As mentioned in chapter 1, a typical cortical neuron can be recorded electrically over a distance of roughly 100μm. The negligible amount of injected chemical can arbitrarily be taken at about 0.5% of this 100μm-diameter sphere, which is equivalent to about 2.5pL. For example, for a 100mSec delivery pulse duration, the leak rate should be less than 25pL/Sec. Therefore the calculated leak rate for the version I valve is slightly above the required one.

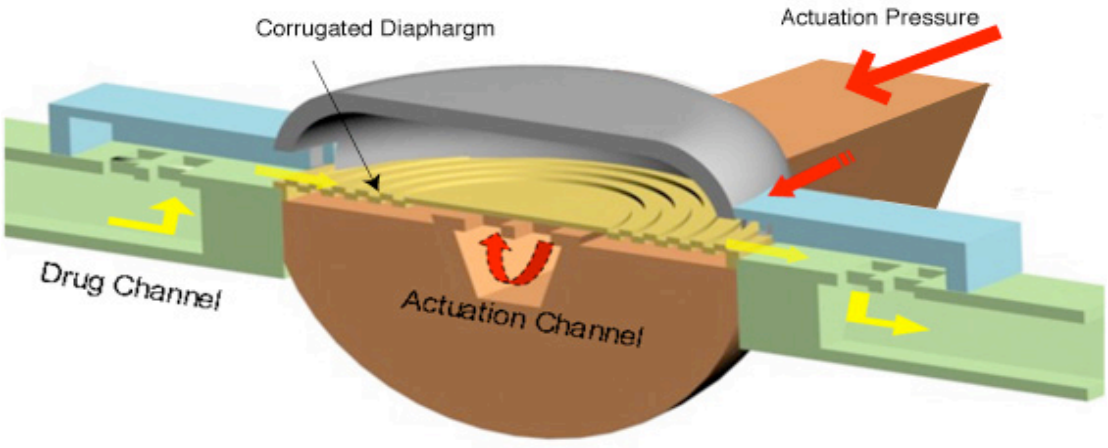

Figure 2.14: A cross-sectional view of a Version-I pneumatic microvalve with corrugated diaphragm.

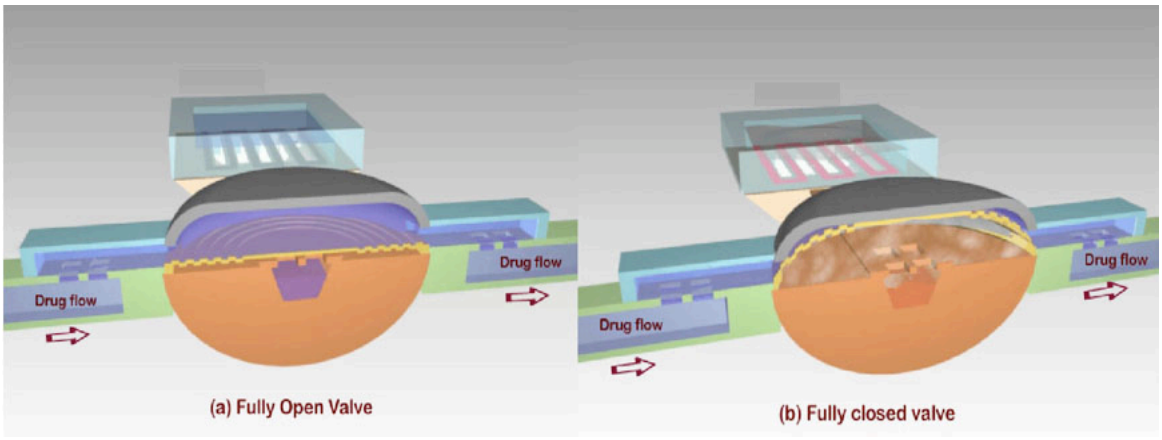

Figure 2.15: The actuation of a Version-I pneumatic microvalve.

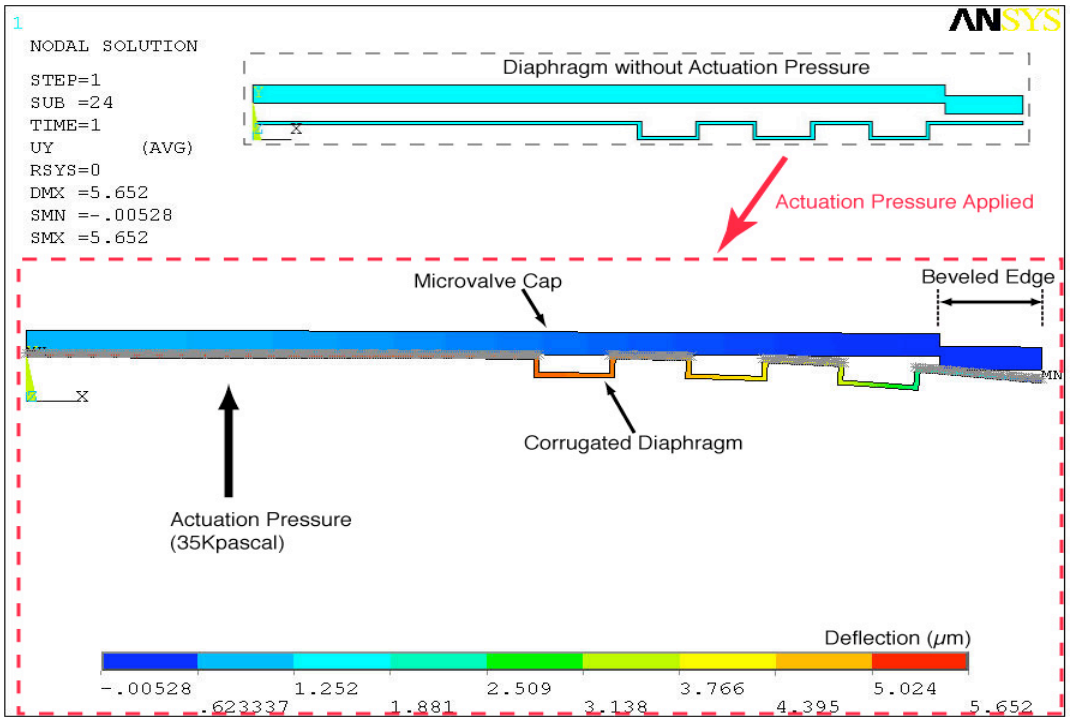

Figure 2.16: Under an actuation pressure of 35kPa, a diaphragm of $SiO_2/Si_3N_4/SiO_2$ deflects 5.6μm to close the drug flow area of the cavity.

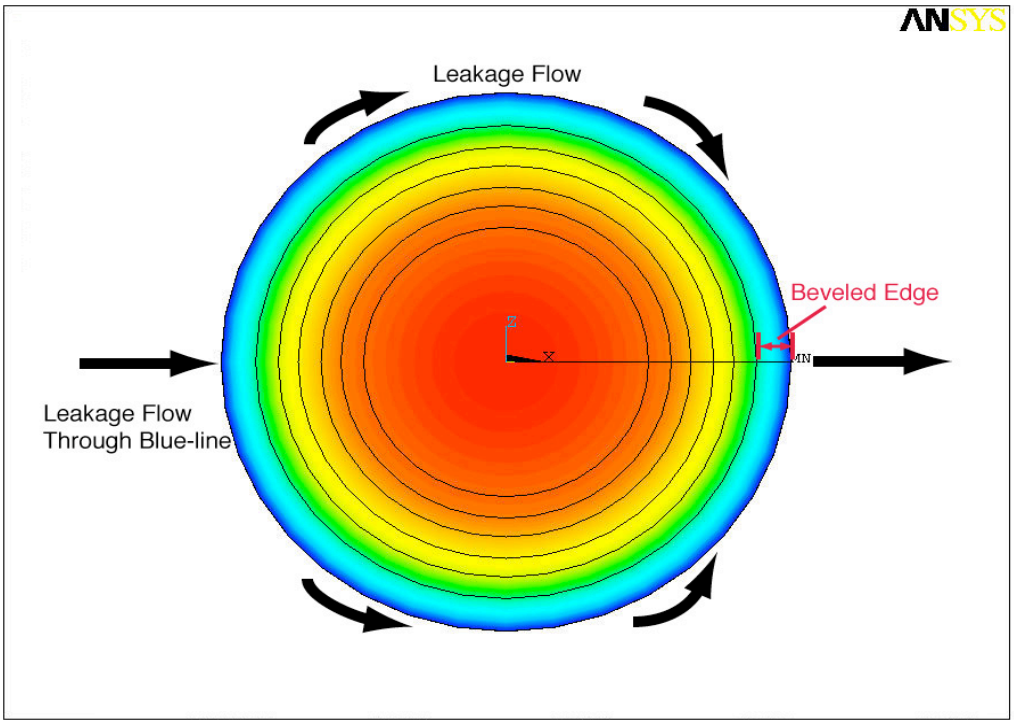

Figure 2.17: A top-view of a deflected circular diaphragm in blocking mode. The leakage flows along the outer edge of the membrane (blue colored line). The arrow indicates the direction of the leakage flow.

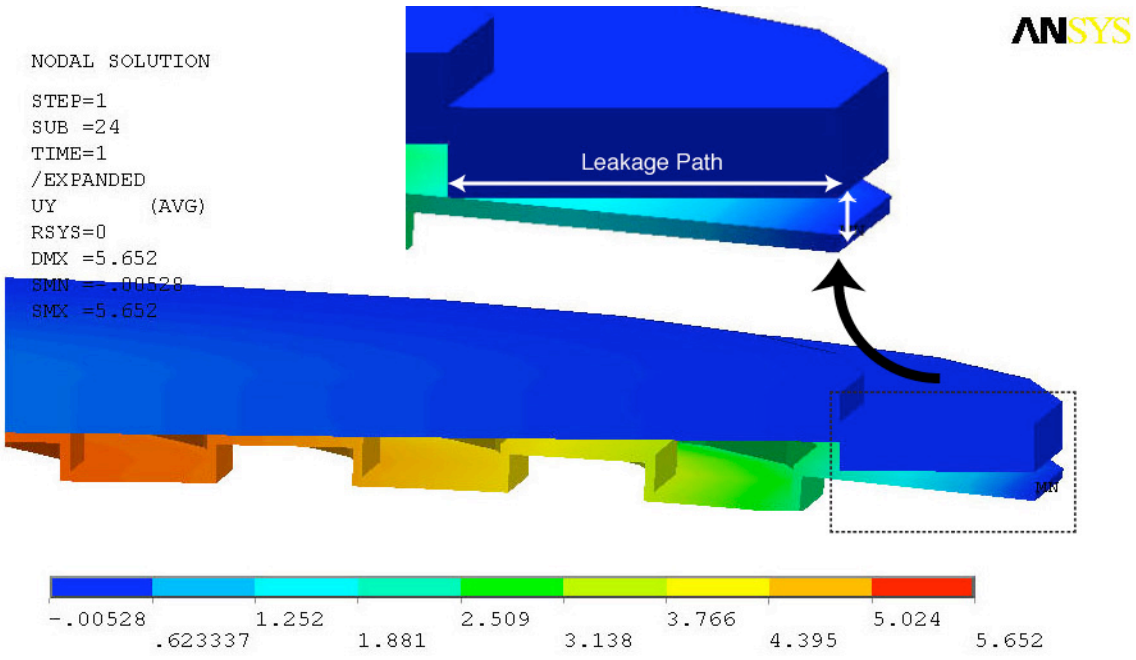

Figure 2.18: A cross-sectional view of a leakage flow path along the outer edge of a deflected diaphragm in blocking mode.

2.3 Designing a Pneumatically Actuated Microvalve (Version II)

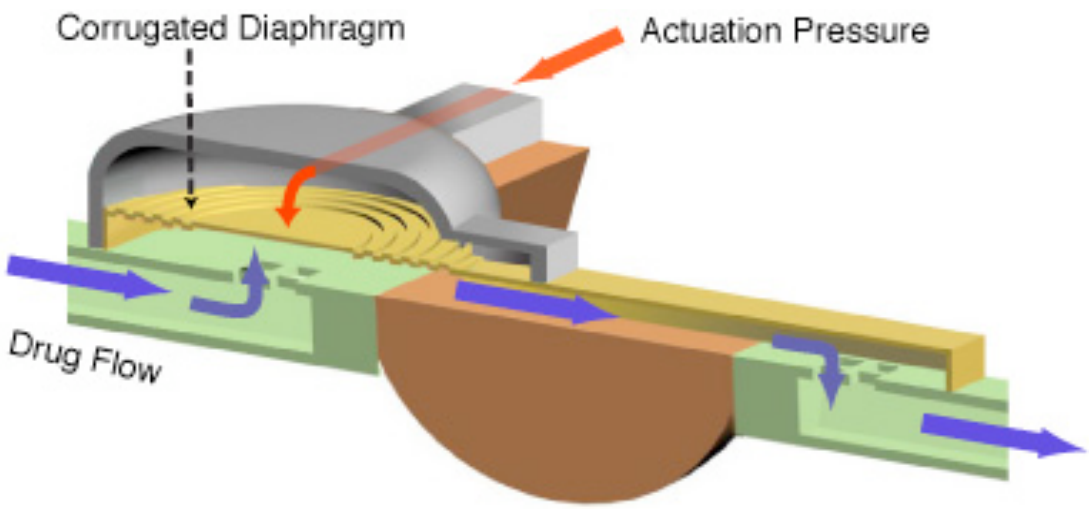

Figure 2.19: A cross-sectional view of a Version-II pneumatic microvalve with corrugated diaphragm.

An alternative configuration adjusting the geometries of microvalve was designed to improve the valve sealing. The basic idea of the Version II structure is the same as that of the Version I in that it has a dual-channel. The bottom channel here passes the fluid, and the top channel acts as the actuation channel. The basic mechanism of the microvalve is the same as that of the Version I. The actuation channel applies a large pressure to the cavity walls above the corrugated circular diaphragm. Since the cavity walls, except for the 1μm-thick diaphragm, are surrounded by 7μm-thick dielectrics, the actuation pressure drives the flexible diaphragm down to seal the inlet port of the bottom channel as shown in Figure 2.19. The opening diameter of the inlet port is 20μm. The valve is normally open with a gap of 5μm between the membrane and the flow channel. Using a three-dimensional SOLID92 element in ANSYS, the deflection of a corrugated diaphragm of $SiO_2/Si_3N_4/SiO_2$ with a radius of 200μm is simulated to close at an actuation pressure of 35kPa as shown in Figure 2.20. The simulation result shows that the center of the

diaphragm deflects about 0.77μm (Figure 2.20) into the inlet port. Therefore, Version II can be expected to give better sealing than Version I after the membrane contacts the top of the flow channel orifice (Figure 2.21).

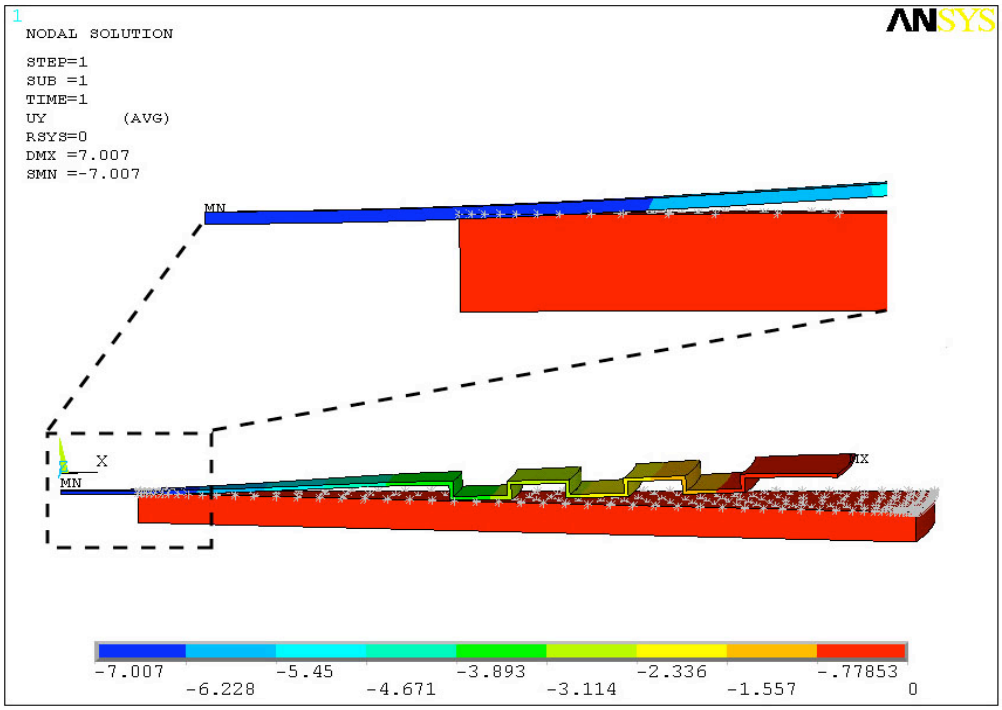

Figure 2.20: Under an actuation pressure of 35kPa for version II, a diaphragm of $SiO_2/Si_3N_4/SiO_2$ deflects 7μm to close the drug flow area.

One interesting observation is that the first corrugation from the center of diaphragm contacts the top of the flow channel and it would result in further improvement of valve sealing ability as a beneficial ring seal. Based on these simulations, the Version II is expected to have lower leakage than Version I in blocking mode without changing the open flow rate.

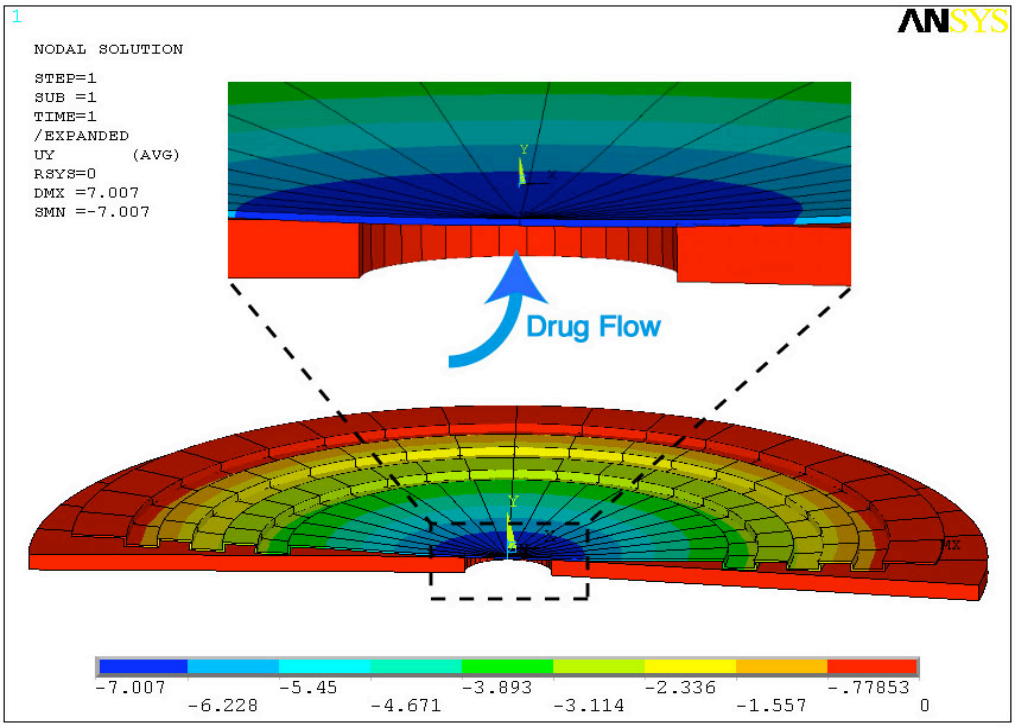

Figure 2.21: A cross-sectional view of a fully- deflected $SiO_2/Si_3N_4/SiO_2$ diaphragm of version II at 35kPa actuation pressure.

2.4 Conclusions

The feasibility of the basic designs developed for the prototype pneumatically actuated normally-open valve structure was verified, as demonstrated by the simulations of diaphragm deflections as a function of an actuation pressure and pressure drops at open flow and in blocking mode. Two different configurations, Version I and Version II, of microvalve structure were designed. Both structures were capable of having an open flow rate of 500pL/sec at an applied input pressure of 8.5kPa, which meets the design target of 500pL/sec at an applied input pressure of 10kPa as discussed in chapter 1. Version II was designed to increase the valve sealing ability in blocking mode.

CHAPTER 3

Fabrication and Testing of a Pneumatically-Actuated Corrugated Microvalve

This chapter describes the development of a pneumatically-actuated process compatible microvalve with a drug-delivery probe which is able to selectively deliver chemicals at the cellular level as well as electrically record from and stimulate neurons in vivo. The drug-delivery probe is bulk-micromachined and directly process compatible with formation of thin-film electrode arrays [13] for electrical recording and stimulation on the same substrate.

Section 3.1 describes in detail the formation of a surface-micromachined parylene microvalve structure. Section 3.2 describes in detail the formation of a bulk-micromachined microchannel, the Version I and Version II microvalve made of $SiO_2/Si_3N_4/SiO_2$. Section 3.3 shows the open flow rate and leak rate testing of a drug-delivery system with the Version I and II microvalve.

3.1 Fabrication of a Parylene Microvalve

To reduce the actuation pressure and therefore the overall power required for the application of a thermopneumatic microvalve, a flexible and biocompatible material such as parylene was first investigated for the diaphragm of the microvalve. Parylene is the generic name for members of a unique polymer series. The basic member of the series, called Parylene N, is poly-para-xylylene, a completely linear, highly crystalline material. Parylene C, the second commercially available member of the series, is produced from the same monomer modified only by the substitution of a chlorine atom for one of the aromatic hydrogens. Due to the uniqueness of the vapor phase deposition, the parylene polymers can be formed as structurally continuous films from as thin as a fraction of a micrometer to as thick as several mils. Because the thermal process has great influence on the composite layer of parylene, a photoresist layer was used as a sacrificial layer and Al/Cr was used as a feedthrough for etching the sacrificial layer (Figure 3.1a). The photoresist remained completely covered by parylene to form a diaphragm. Another sacrificial photoresist was deposited on top of the parylene to define the valve (Figure 3.1b). Then the metal was electroplated over the photoresist as a ceiling for the valve to maximize the deflection of diaphragm (Figure 3.1e and f). The sacrificial photoresist is etched out via the etch-through (Figure 3.2b). A free-standing diaphragm made of parylene 2μm-thick was successfully fabricated (Figure 3.3). To measure the deflection of this diaphragm, a pressure housing which has a transparent cover was used. The pressure generator was attached to the pressure housing to provide the static actuation pressure for the deflection. Figure 3.4d shows a 5μm deflection of this diaphragm for 20kPa actuation pressure, which is lower than the simulated result for a diaphragm made

of $SiO_2/Si_3N_4/SiO_2$ for the same deflection.

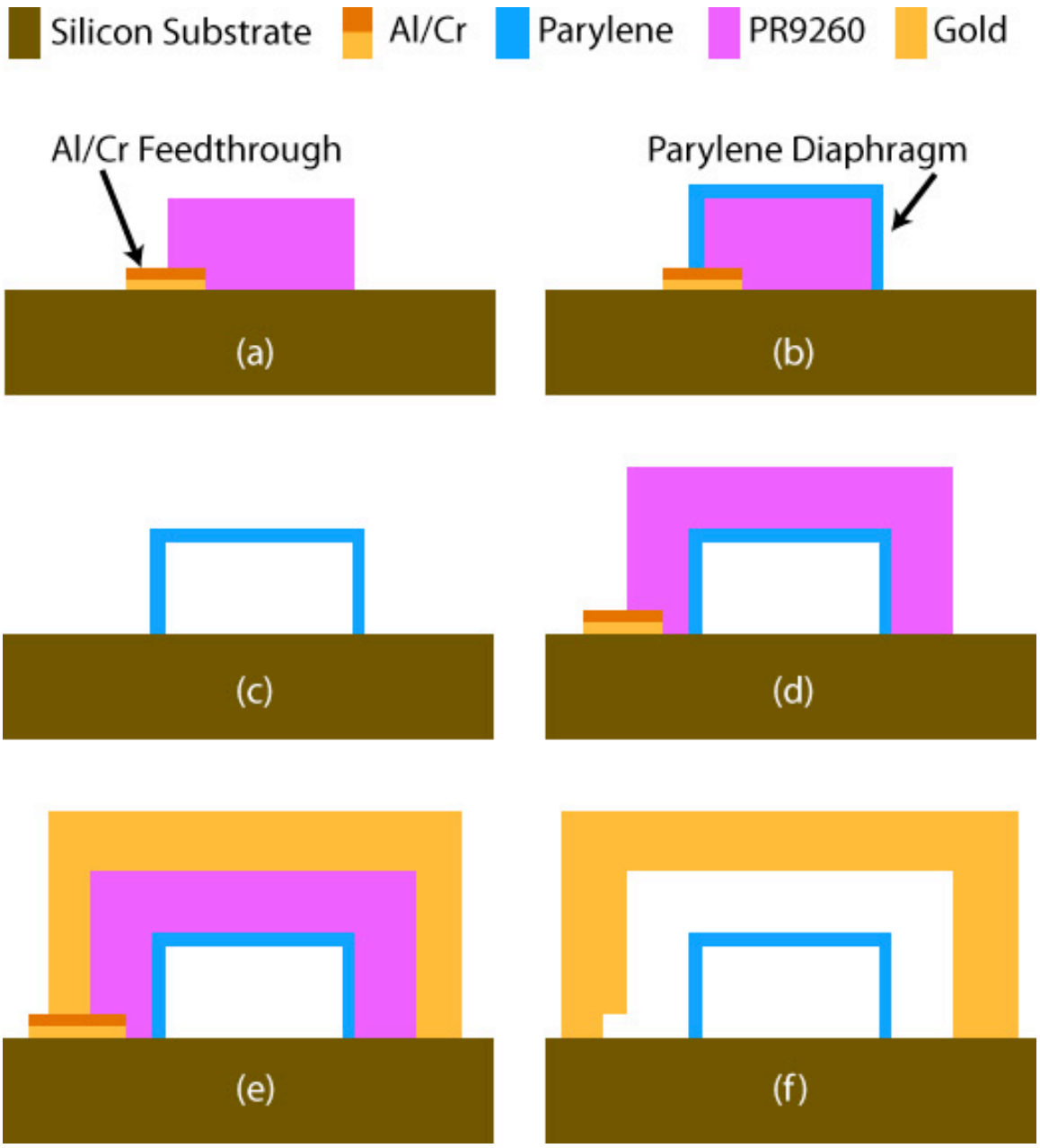

Figure 3.1:Top view of chamber formation (a) Sputter Al/Cr feedthrough and deposit photoresist (PR9260); (b) Deposit parylene on top of the photoresist; (c) Remove the first sacrificial layer (PR9260) and deposit parylene; (d) Deposit the second sacrificial layer (PR9260) and pattern; (e) Gold was electroplated; (f) After the removal of the sacrificial layer through the etch-through, then sputter gold.

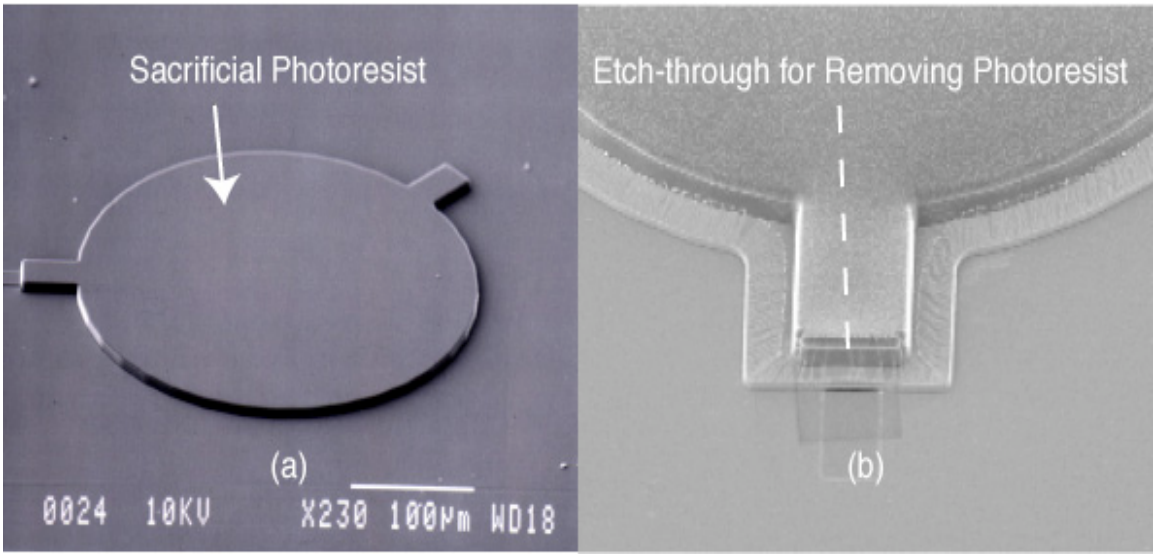

Figure 3.2: Fabrication of a Parylene Microvalve (a) deposit sacrificial photoresist, (b) etch sacrificial photoresist via etch-through. Parylene diaphragm remains after the etching.

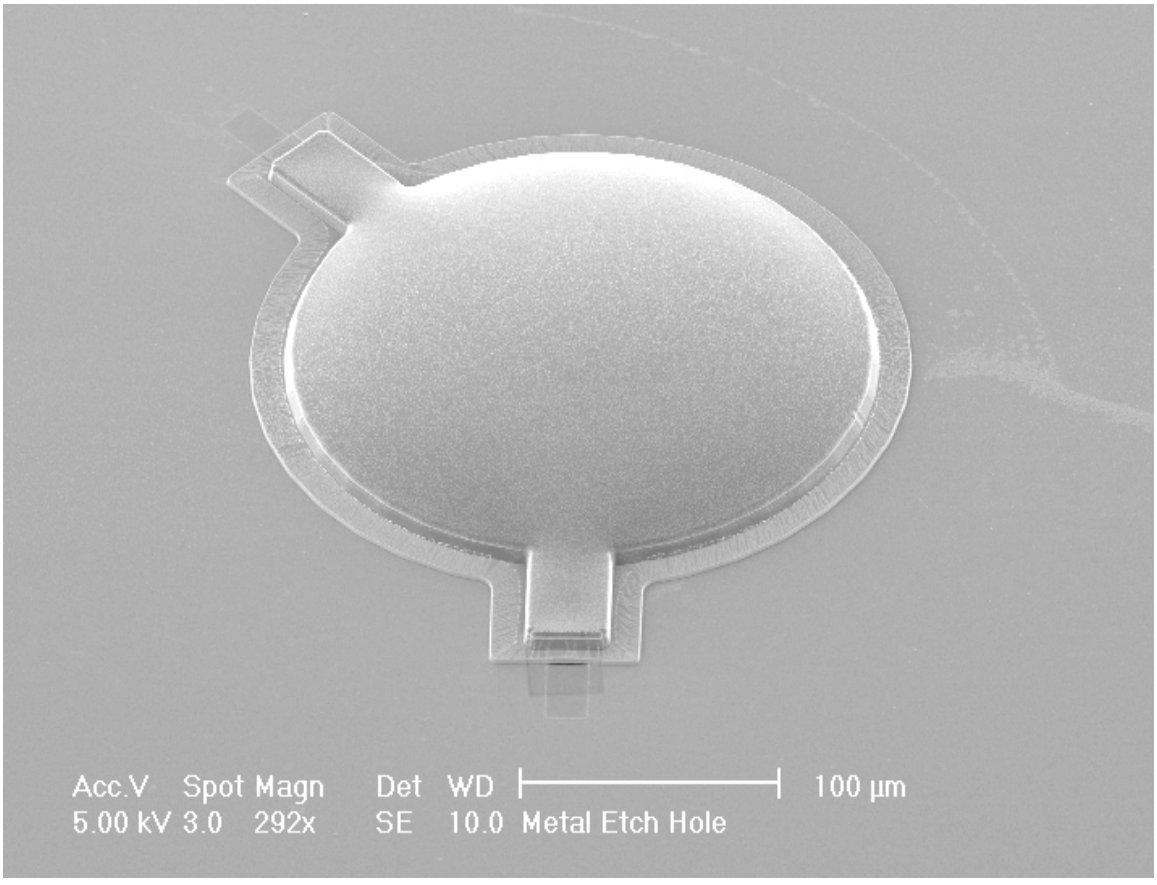

Figure 3.3: Free standing diaphragm made of 2µm-thick Parylene.

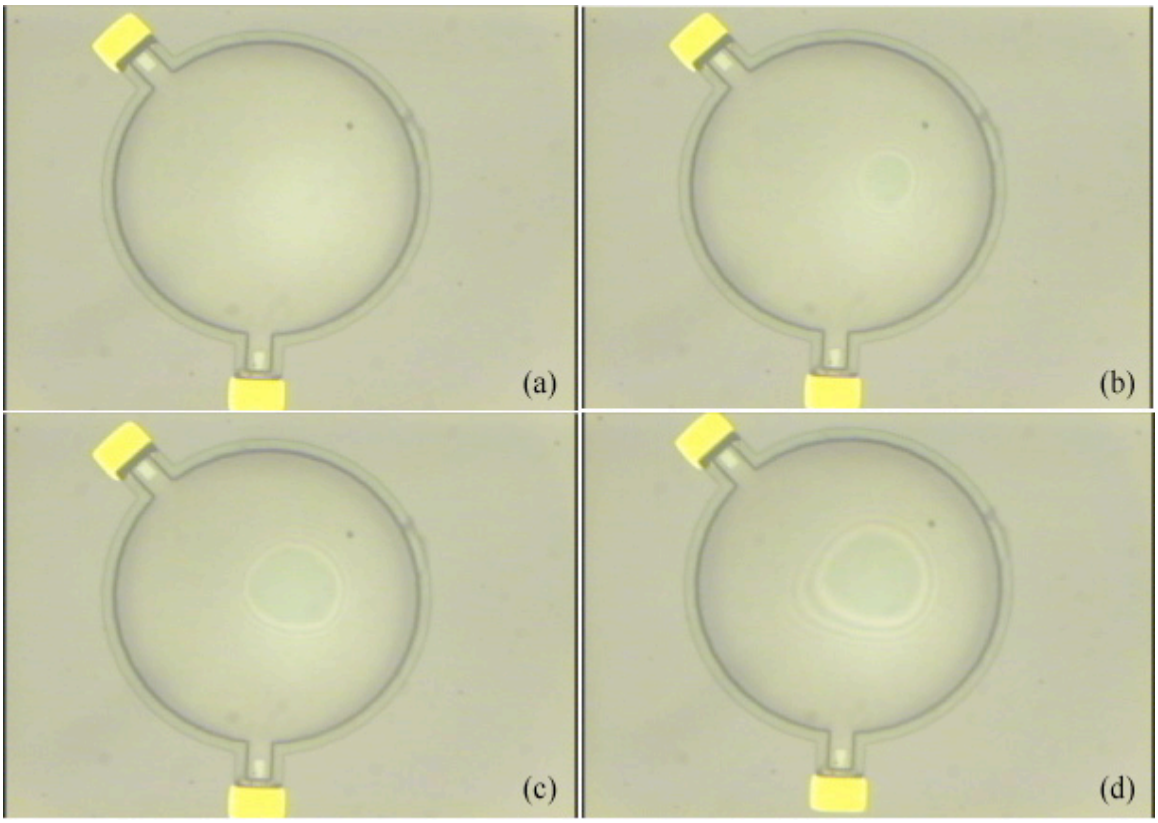

Figure 3.4: The deflection of parylene diaphragm at (a) no actuation pressure (b) 7.5kPa (c) 15kPa (d) 20kPa.

Though microvalves made of parylene were previously reported [93-95], it is hard to claim that the parylene can be compatible with this research, because the reported valves were not bulk-micromachined and EDP or similar wet-etching processes, such as TMAH, were not used. For a microvalve in an implantable chronic drug-delivery device, the reliability of the microvalve under many number of valve cycles is a key requirement of selecting the material of the valve diaphragm. In the past, unfortunately, this technology could not be used further because the parylene layer exposed to EDP (>110^{o}C) for 100 minutes was too brittle to be reliable as the valve diaphragm (Figure 3.5), though new process now enables to use parylene with wet-etching process.

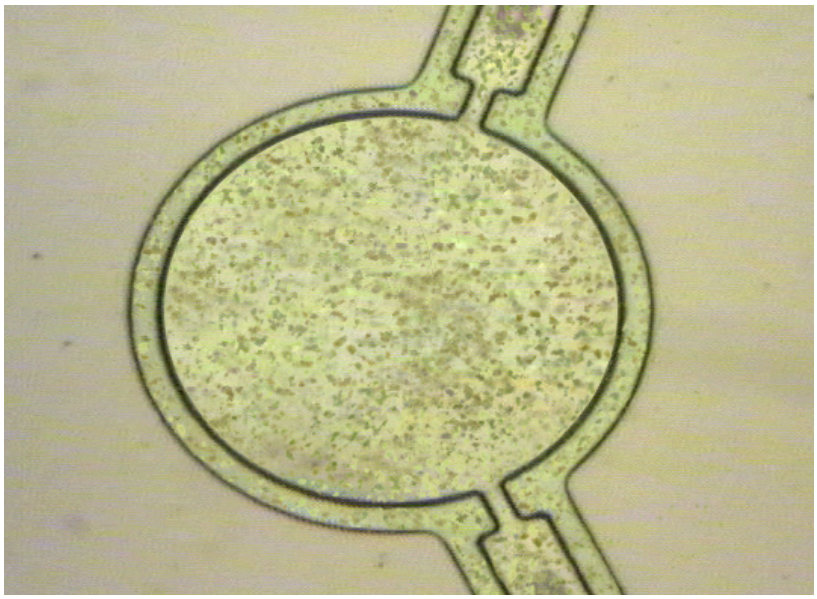

Figure 3.5: Top view of the parylene diaphragm after100-minute etching in EDP at 110^{o}C.

3.2 Pneumatic $SiO_2/Si_3N_4/ SiO_2$ Microvalve Fabrication

3.2.1 Version I Pneumatic Microvalve

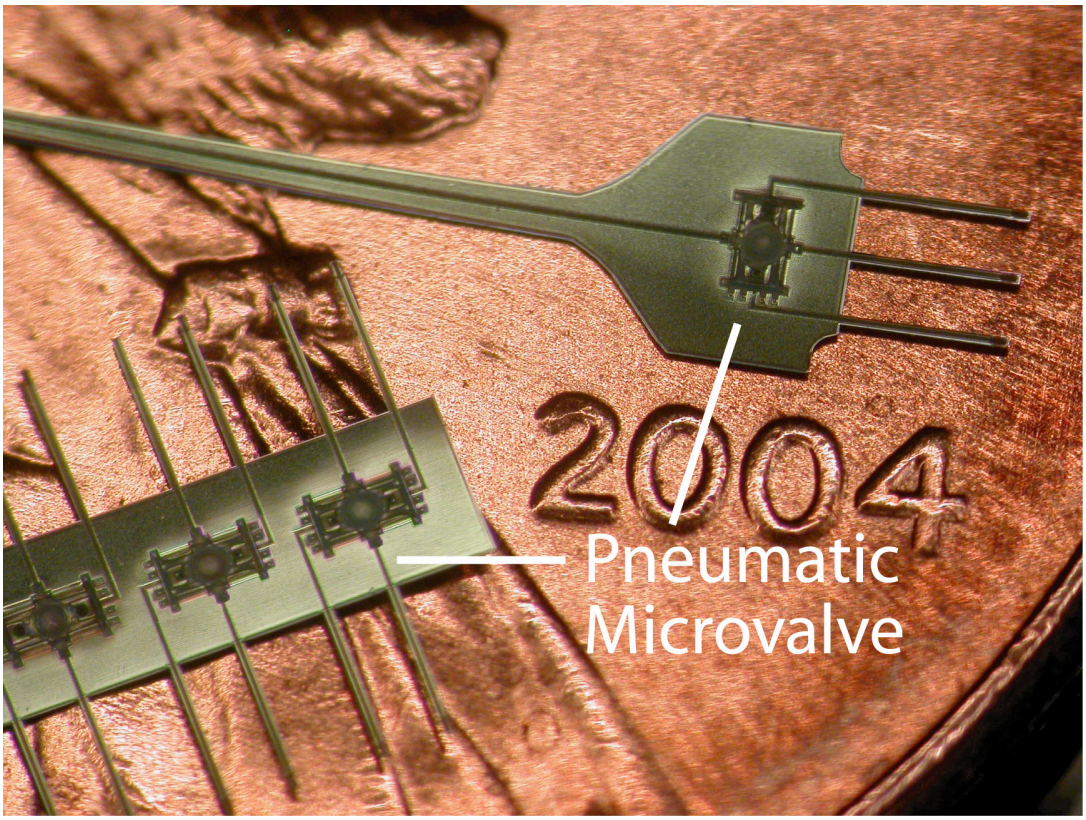

Figure 3.6: A drug-delivery probe with version-I integrated pneumatic microvalve.

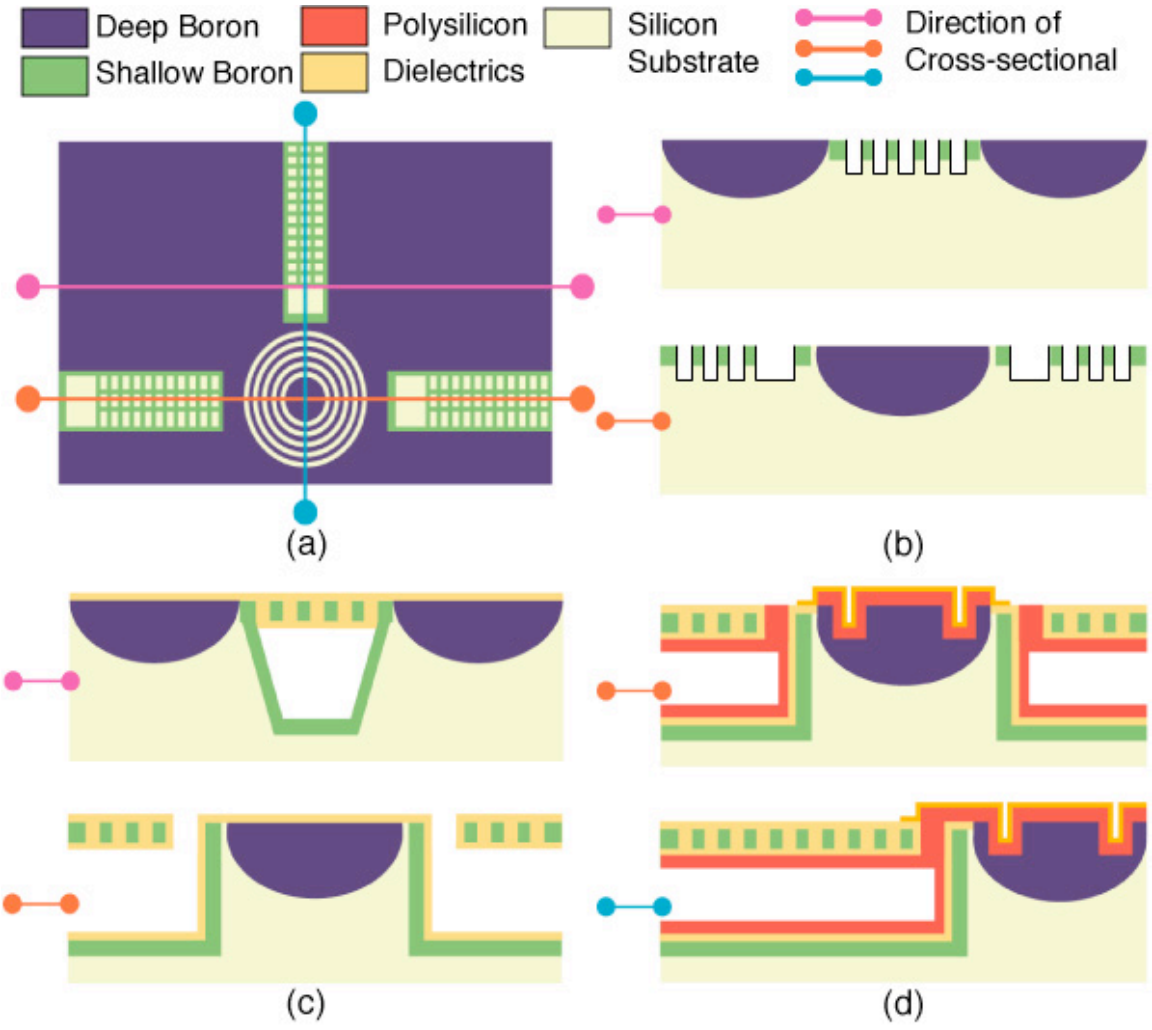

Figure 3.7: (a) Top view of microvalve and channel formation; each color line stands for the direction of cross-sectional view for the following fabrication steps; (b) Deep boron diffusion; Shallow boron diffusion; DRIE for etching trenches; (c) EDP etching; Shallow boron diffusion; LPCVD silicon dioxide/silicon nitride/silicon dioxide to fill trench gap; (d) CVD polysilicon for a first sacrificial layer and pattern; LPCVD silicon dioxide/silicon nitride/silicon dioxide and pattern.

The Version I microvalve is shown in Figure 3.6 and is realized using a 13-mask process (Figure 3.7). Fabrication of the microvalve takes only two masks in addition to the normal probe with microchannels. The process begins with blank (100) silicon wafers. The first step is a boron diffusion to define the probe shape using patterned a 1.2µm-thick silicon dioxide layer which is grown over the entire wafer in 3 hours at a temperature of 1100^{o}C. The second step forms the buried channels. Screen masking structures with 2µm

openings are patterned along the <110> direction in the silicon [81]. 4μm-openings are used for the output port of the actuation channel, which delivers the drive pressure to the corrugated diaphragm. 4μm-deep trenches for the channels and corrugations of the valve diaphragm are etched with a deep reactive ion etcher (DRIE), which selectively etches silicon anisotropically by creating a chemically-reactive RF plasma and a DC bias. This etching process needs to penetrate through the shallow boron layer and into the lightly-doped silicon beneath. Once formed, the trenches are connected by undercutting the undoped silicon between the trenches to form the drug-delivery channels (Figure 3.8) and actuation channels (Figure 3.9) using 50 minutes in ethylenediamene pyrocatechol (EDP) at 110^{o}C. An unsealed 20~25μm-deep channel is formed with shallow boron ribs on the ceiling spaced by the trench areas. Then, the low-pressure chemical vapor deposited (LPCVD) 1.2μm thick $SiO_2/Si_3N_4/SiO_2$, which normally isolates the electrodes from the substrate, also seals the channel by filling in the trench gaps (Figure 3.10). Wider openings not fully sealed by dielectrics (Figure 3.11) still have enough space to deliver actuation pressure (Figure 3.12). Following the formation of the microchannels in the probe substrate, the space between the substrate and the valve diaphragm is formed using a 3μm-thick CVD sacrificial polysilicon layer.

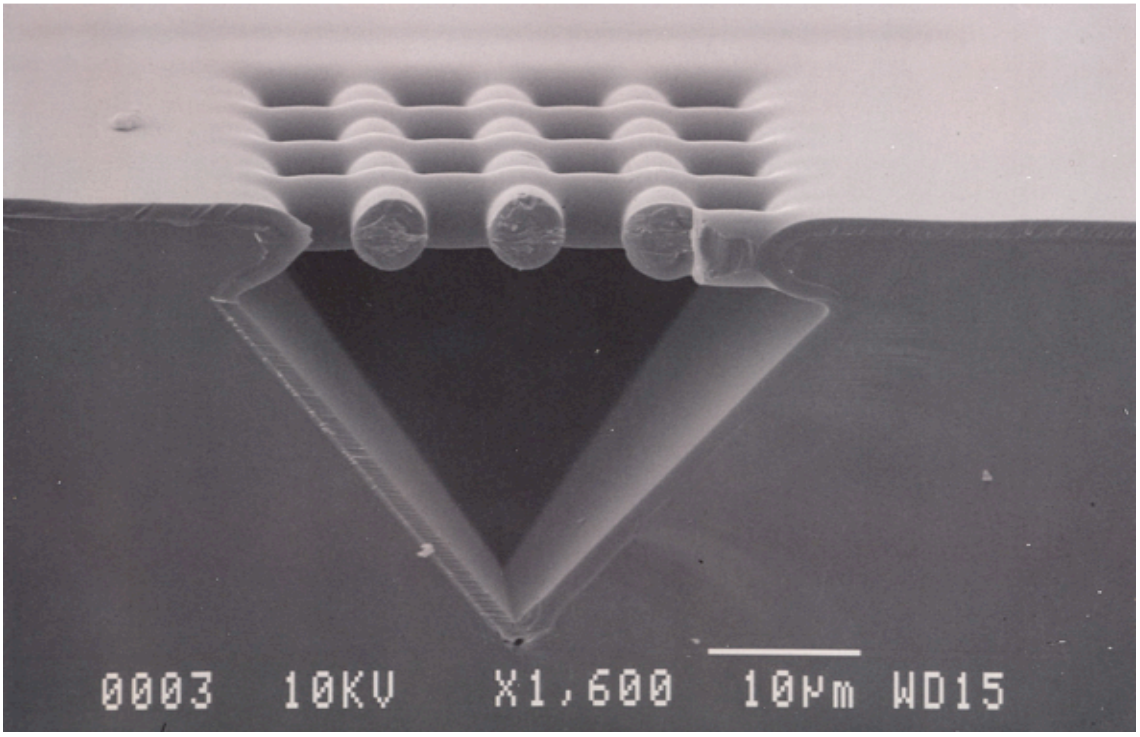

Figure 3.8: Cross-section of a drug-delivery microchannel after 50-minutes of EDP etching.

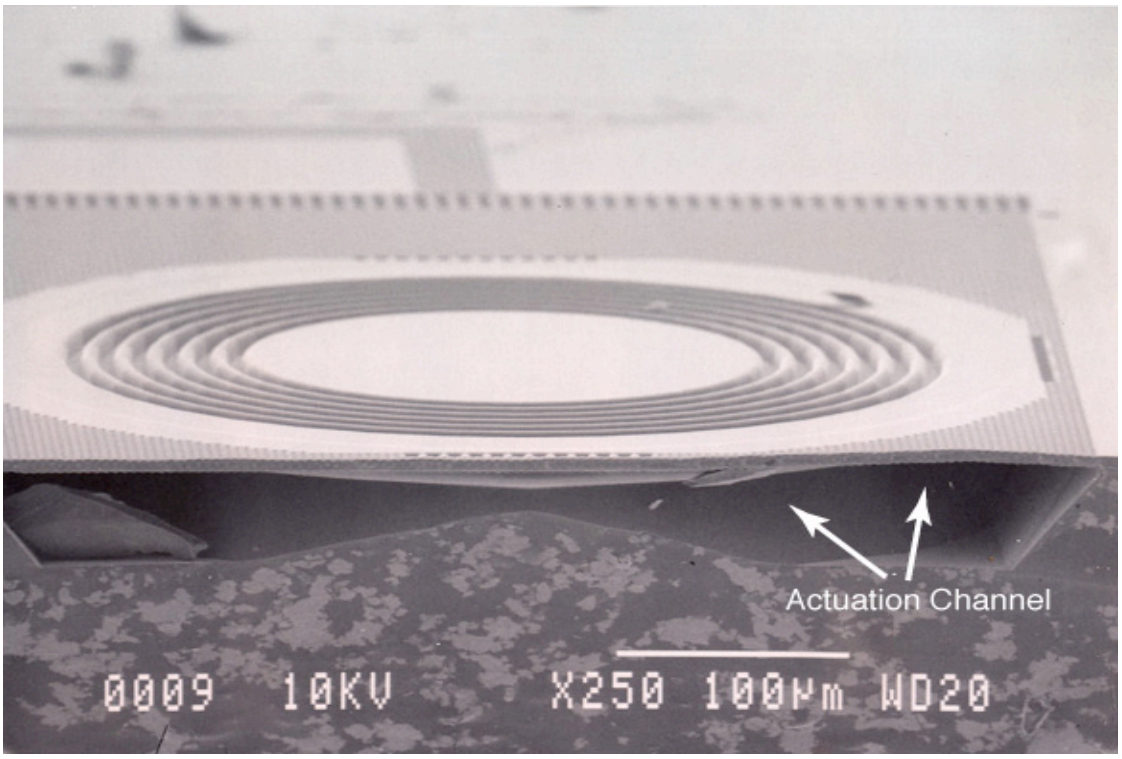

Figure 3.9: Actuation channels after EDP etching. To reveal the cross-section of actuation cavity the silicon wafer was cleaved.

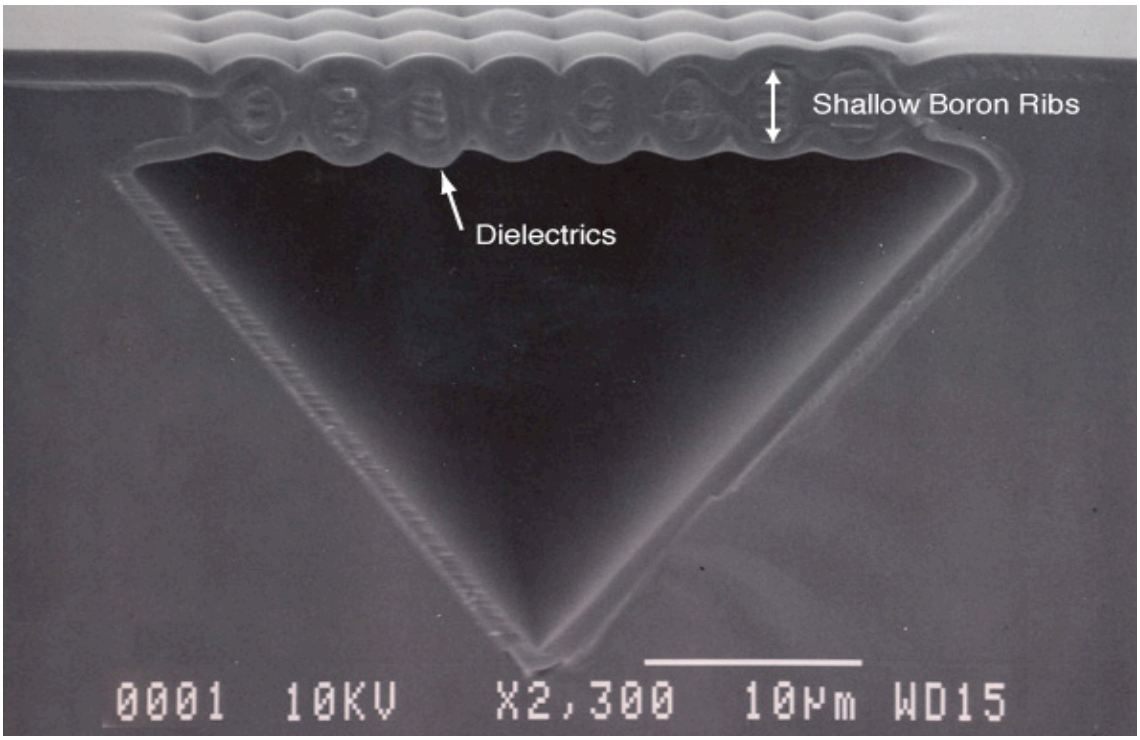

Figure 3.10: Cross-section view of microchannels covering by LPCVD stacked dielectrics.

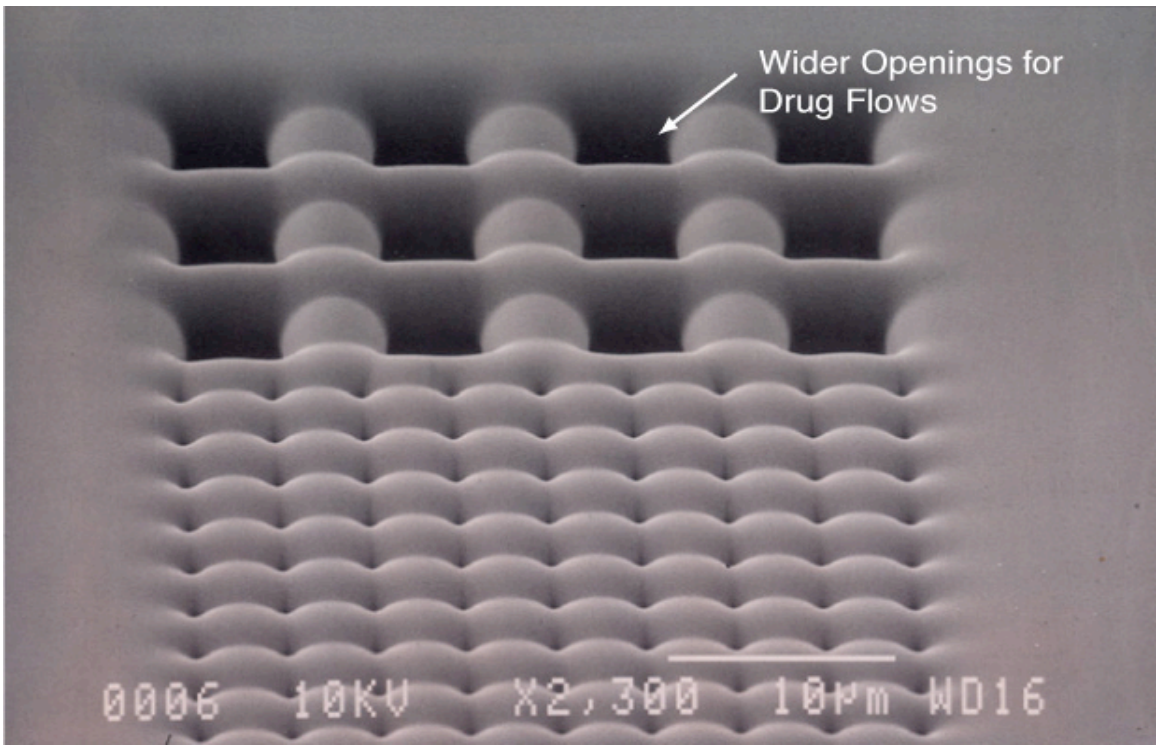

Figure 3.11: Top view of microchannels after filling in trench gaps through stacked dielectrics. The wider trench gaps are open for drug flows. The diagram of the wider openings is shown in Figure 3.12.

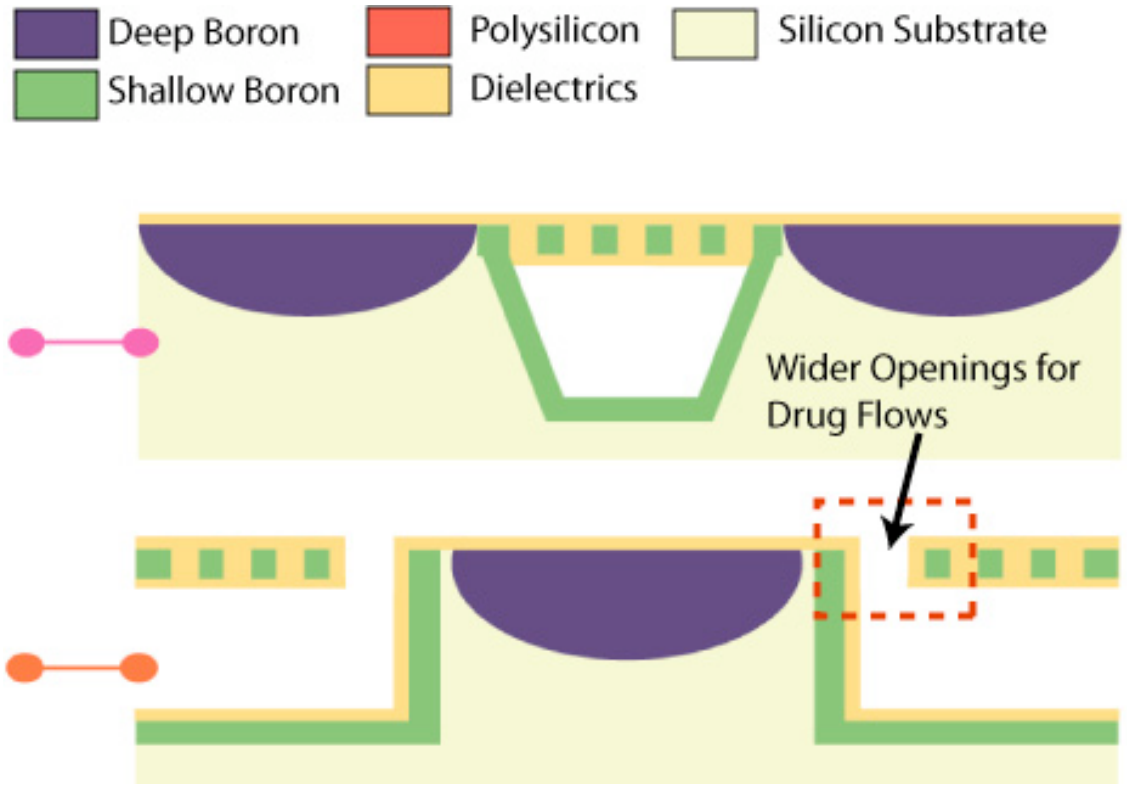

Figure 3.12: Cross-section view of the wider openings for drug-flows. Except wider trenches,

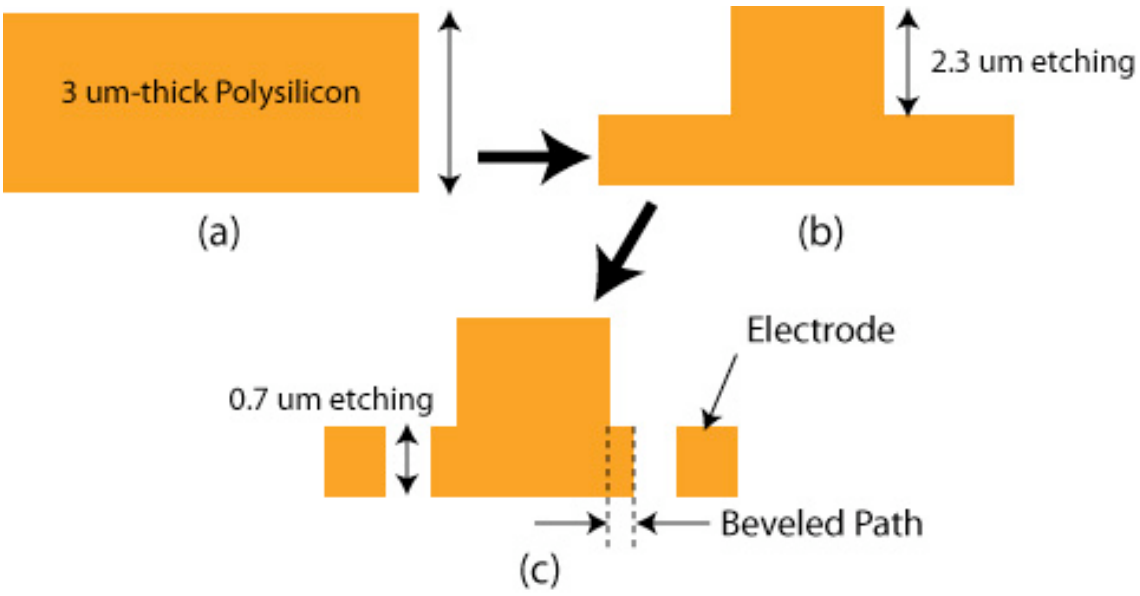

Figure 3.13: (a) Cross-section view of the 3µm-thick polysilicon; (b) Using DRIE, the 2.3 µm-thick polysilicon is etched out; (c) Using DRIE, the electrodes and the beveled path are patterned.

The polysilicon is then patterned to form the probe electrodes and is beveled along 20μm of its outer edge to improve the ability of the diaphragm to seal to the valve cap as simulated in chapter 2. To fabricate the beveled path and the electrode, the deposited polysilicon was patterned with two masks (Figure 3.13). Because the target thickness of the electrode should be 0.7 μm thick, 2.3 μm-thick polysilicon is etched using DRIE. Then using DRIE the electrodes and the beveled path are patterned. Stress-compensated 1μm-thick silicon dioxide/silicon nitride/silicon dioxide dielectrics are then deposited to form the corrugated diaphragm itself and to passivate the electrodes. Etch access holes are formed around the perimeter of the diaphragm (Figure 3.14) to allow removal of this first sacrificial polysilicon layer. The sacrificial layer is removed using a 3 hour tetramethyl ammonium hydroxide (TMAH) etch. The locations of the etch access holes (Figure 3.14) are very critical to shorten the etching time (Figure 3.15) and therefore maintain the target thickness of the diaphragm, which could be thinned during TMAH etching. When the etch access holes were not located in the center of diaphragm and the, the polysilicon layer still remained after the 3hrs TMAH etching (Figure 3.16). By testing 7 wafers for various etching times, 13 locations of the set for etch access holes were chosen (Figure 3.14). Test structures were fabricated and tested to find the proper locations of the holes and the required etching time. After diaphragm release, the etch holes are filled by depositing additional 2 μm-thick silicon nitride/silicon dioxide dielectric (Figure 3.17).

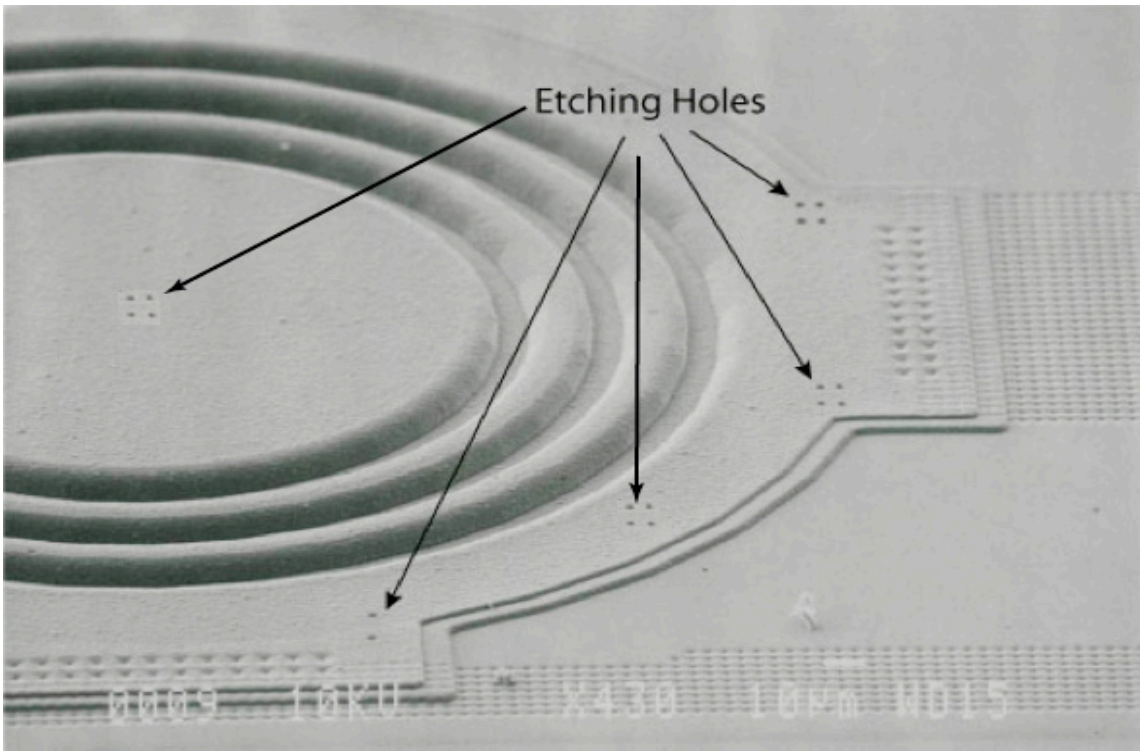

Figure 3.14: Etch access holes of 1.5µm diameter are formed using a Plasmatherm RIE.

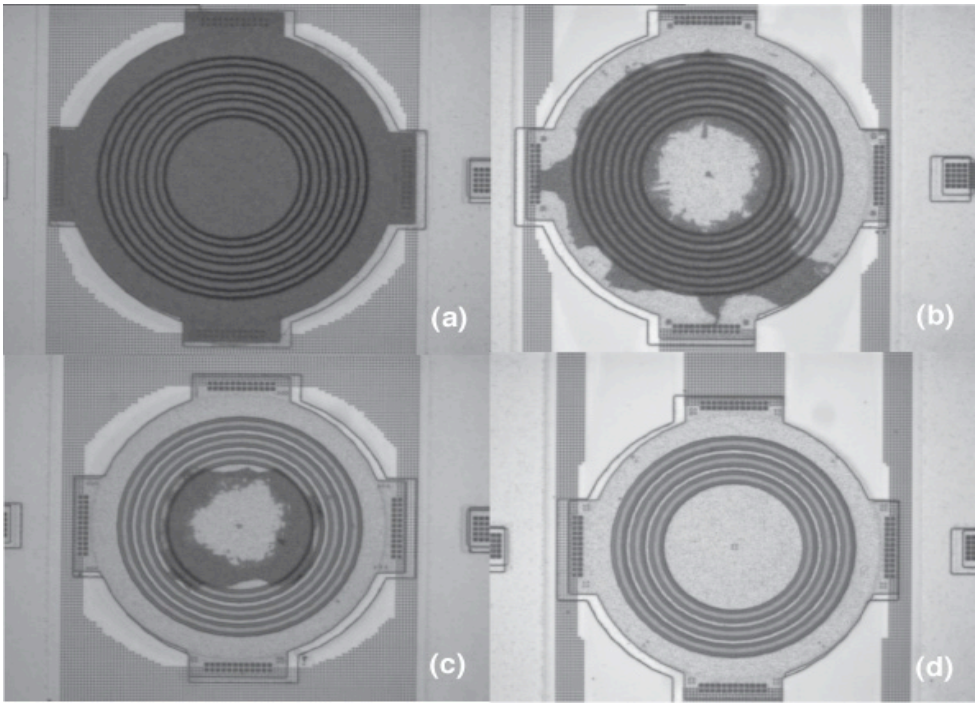

Figure 3.15: (a) The dark circular shape in diaphragm area is the CVD sacrificial polysilicon; (b) After 1 hr TMAH etch; (c) After 2hrs TMAH etch; and (d) After 3hrs TMAH etch the diaphragm is fully released and a fully etched out cavity is shown through the transparent diaphragm. The cavity is connected to actuation channel through wider openings.

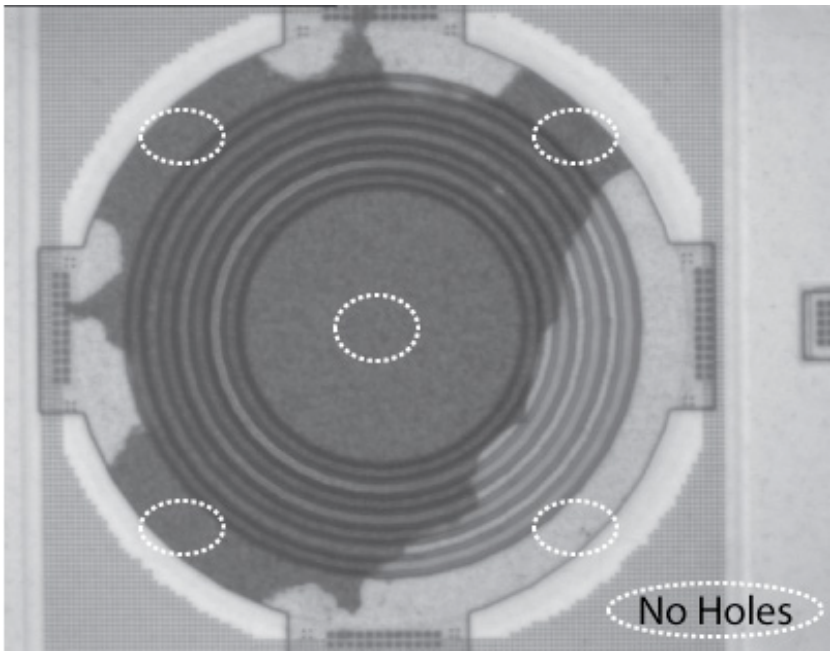

Figure 3.16: Various locations of the etch access holes were evaluated. The sacrificial layer made of polysilicon were partially removed after 3 hrs TMAH etching without having the etch access holes in the white circles.

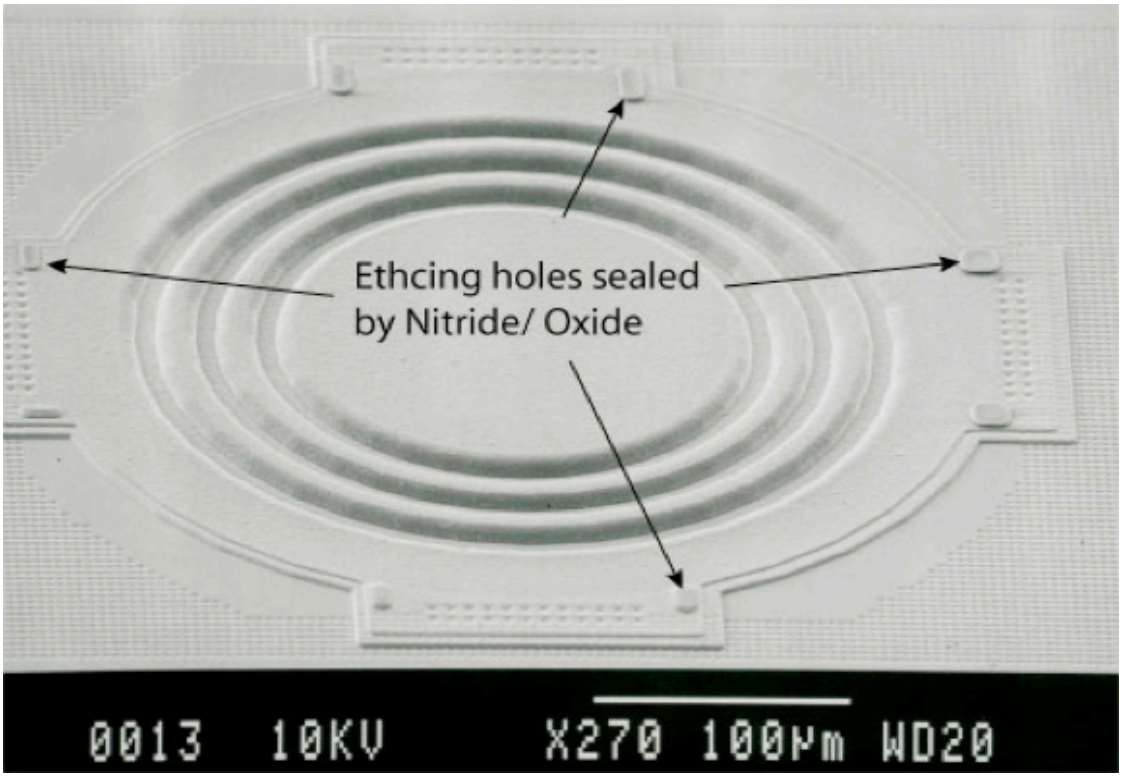

Figure 3.17: The etch holes are filled by depositing additional dielectrics.

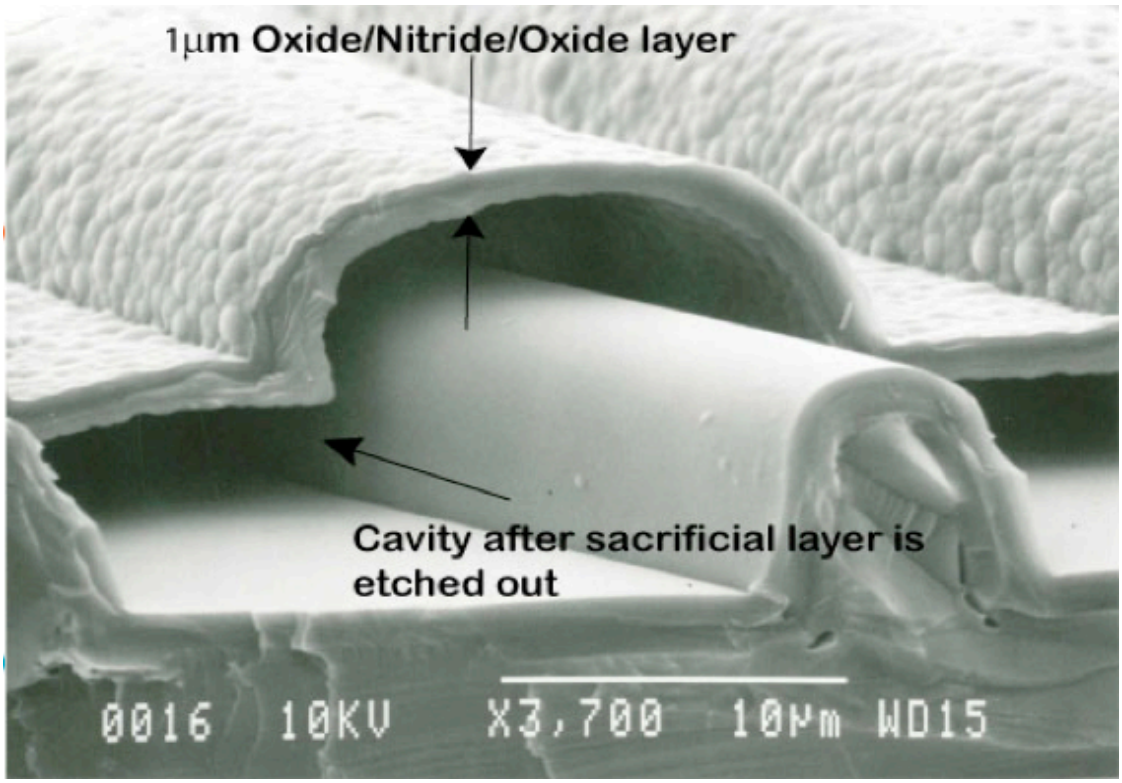

Figure 3.18: Corrugated diaphragm made of 1μm-thick $SiO_2/Si_3N_4/SiO_2$.It shows the clean cavity without having any polysilicon residue.

A 3μm-thick sacrificial polysilicon layer is now deposited to form the flow path through the valve. A second set of etch access holes are patterned to allow removal of this second sacrificial polysilicon layer. After the second sacrificial layer is removed by a 4 hour TMAH etch (Figure 3.19), a 7μm-thick stress-balanced silicon dioxide/ silicon nitride/ silicon dioxide stack is deposited and patterned to form the cap. (Figure 3.20) The thick cap limits the deflection of diaphragm (Figure 3.21). Contacts are then etched to the sites and bonding pads followed by sputtering iridium on the sites and gold on the bonding pads. The probe is then released using EDP.

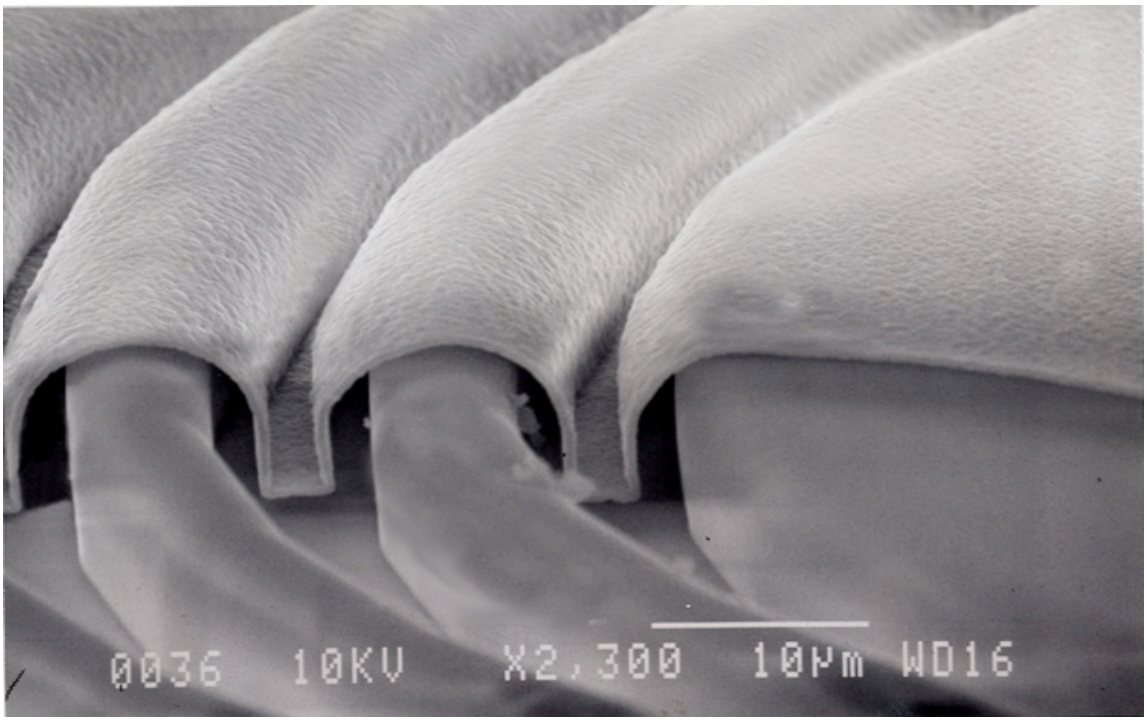

Figure 3.19: Corrugated diaphragm after the second polysilicon sacrificial layer is removed. To confirm that the corrugated diaphragm remains properly after 4hrs TMAH etching, the top ceiling was removed.

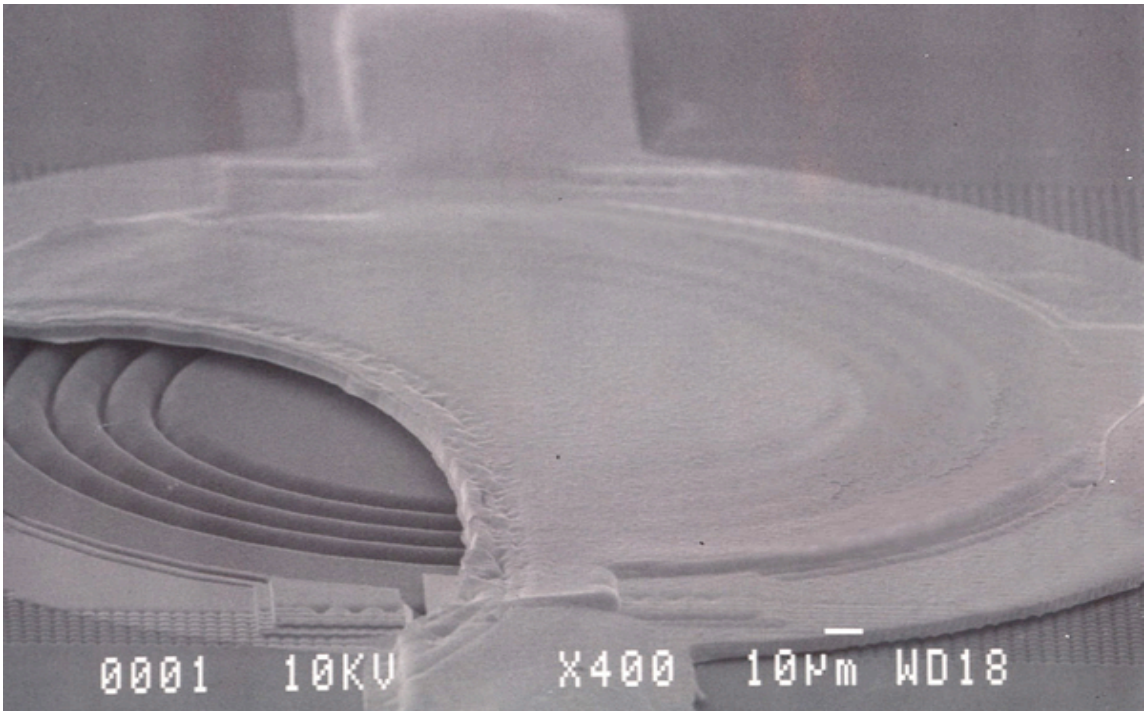

Figure 3.20: The pneumatic microvalve with a corrugated diaphragm after probe is released by EDP. To show the corrugation of the valve diaphragm below the ceiling, a partially opened structure was chosen as a sample.

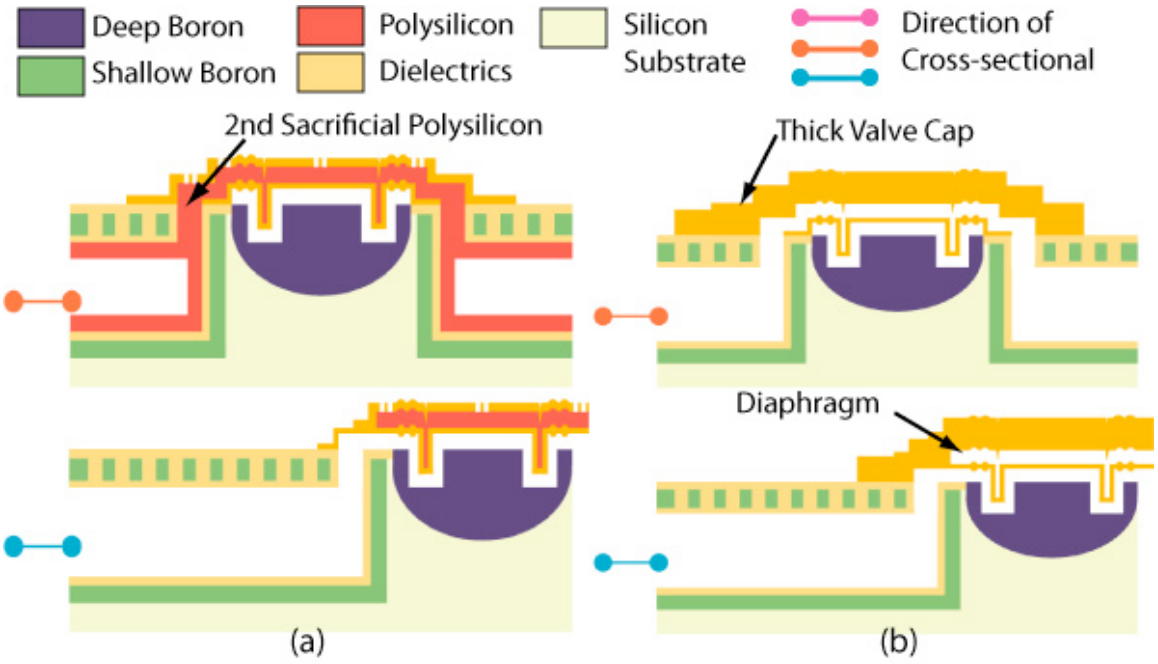

Figure 3.21: (a) TMAH etching to remove the second sacrificial polysilicon (b) LPCVD silicon dioxide/silicon nitride/silicon dioxide to fill trench gap, then PEDVD dielectrics to form the cap

3.2.2 Version II Pneumatic Microvalve

As mentioned in chapter 2.2, the Version II pneumatic microvalve (Figure 3.22) was designed to implement better valve sealing than the Version I. The fabrication was performed using the same 13-mask process as required for Version I. The major difference is that the bottom channel passing the fluid is defined using the first sacrificial polysilicon layer (Figure 3.23), and the top channel acting as an actuation channel is fabricated using the second sacrificial polysilicon layer (Figure 3.24). The rest of the fabrication process is the same as the Version I.

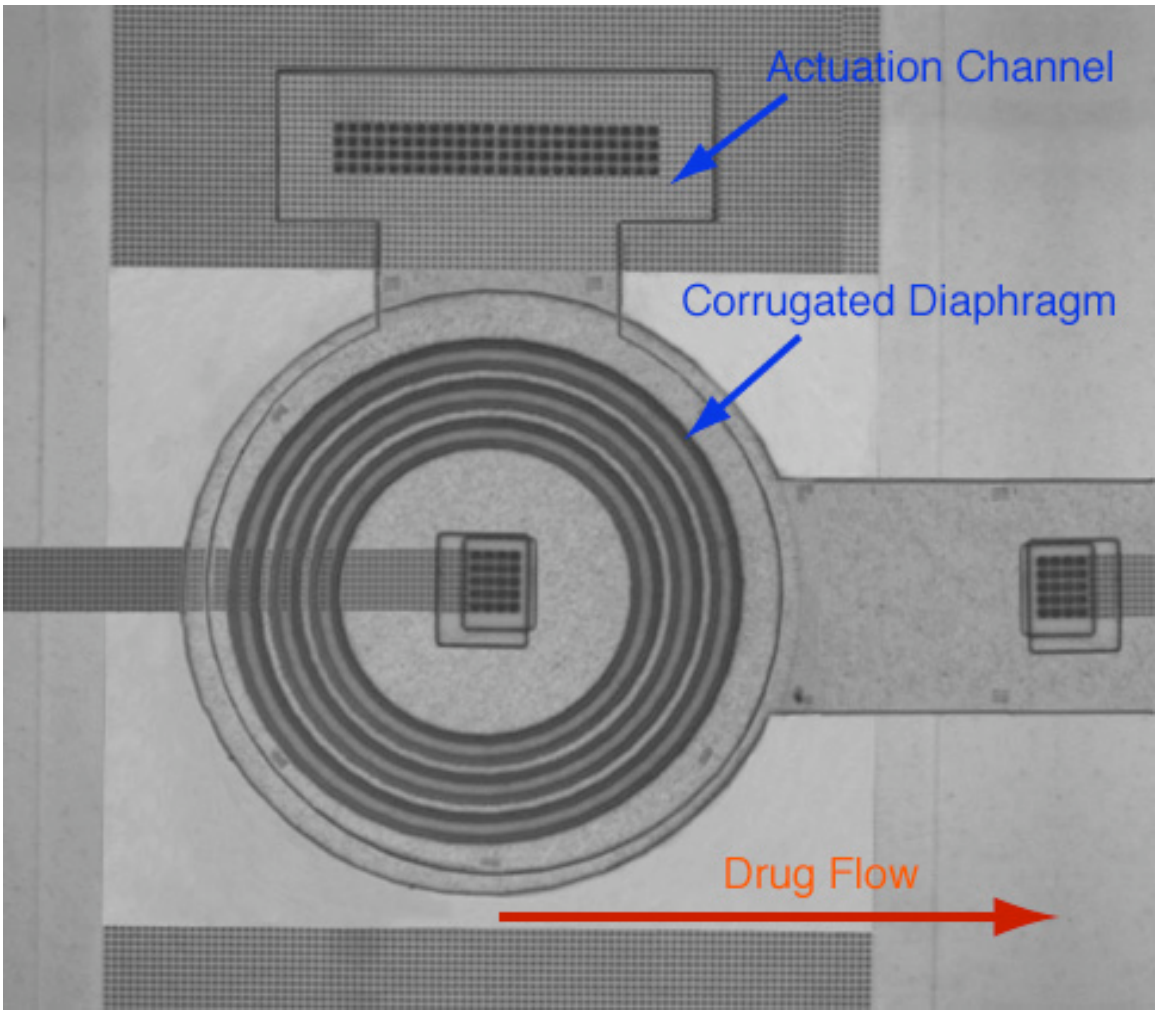

Figure 3.22: Top view of the Version II pneumatic microvalve

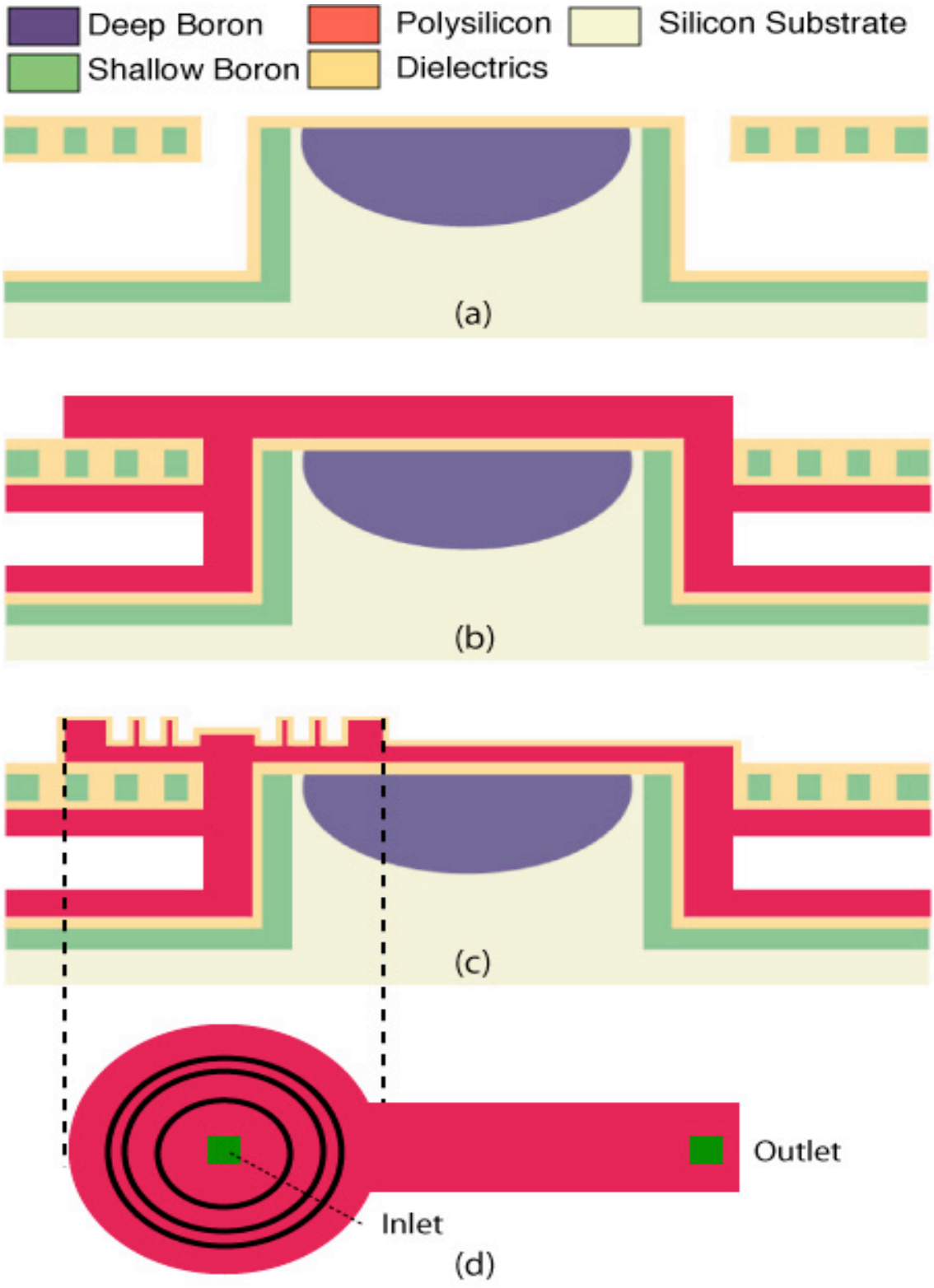

Figure 3.23:The cross-sectional view of fabrication process for the Version II microvalve, (a) Define microchannels; (b) CVD polysilicon for a first sacrificial layer; (c) Pattern and deposit the dielectrics for a valve diaphragm; (d) The top-view of the patterned polysilicon

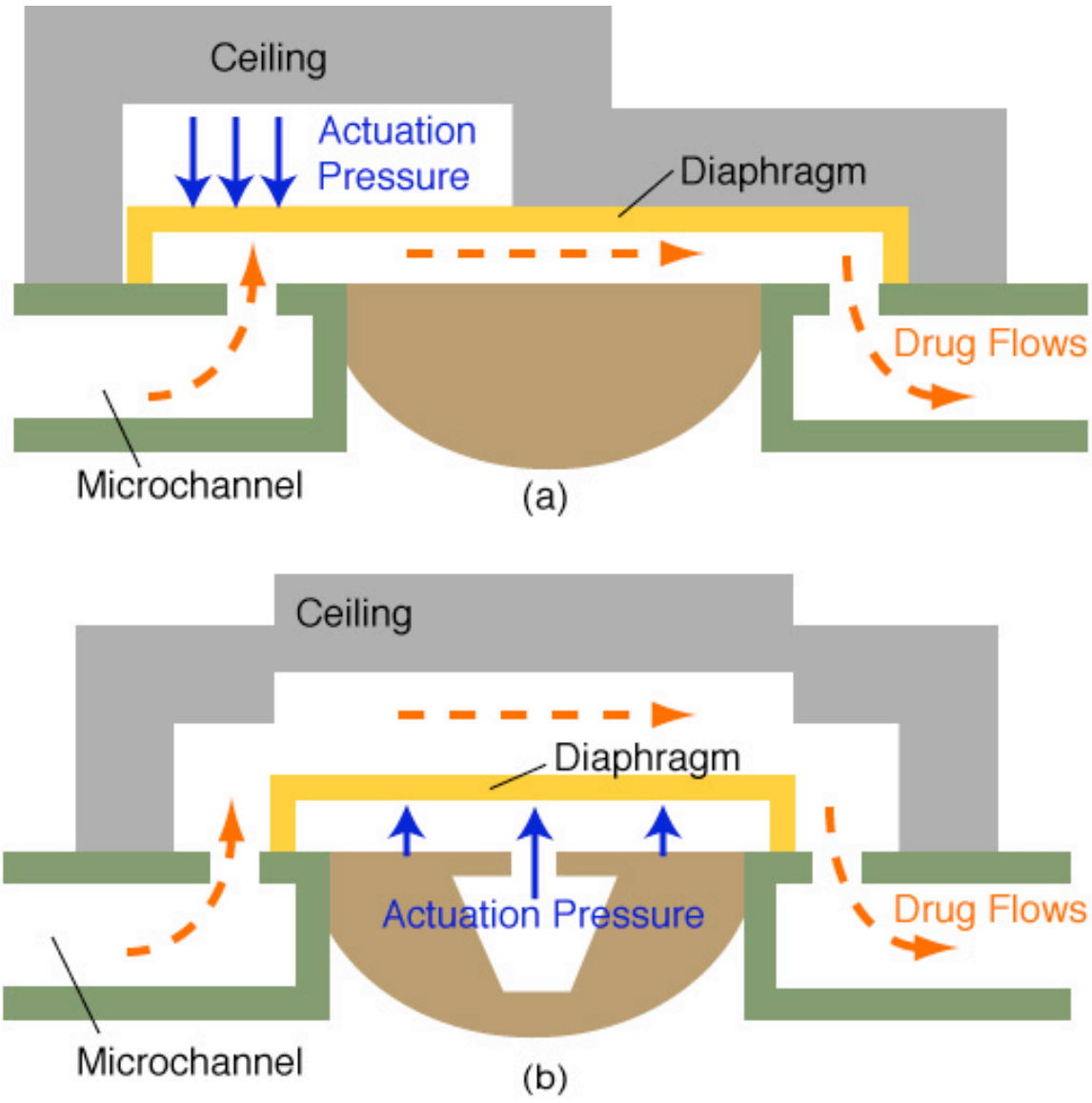

Figure 3.24: (a) Cross-sectional view of the Version II microvalve with the bottom channel passing fluid and the top actuating channel; (b) Cross-sectional view of the Version I microvalve with the bottom actuation channel and the top channel passing fluid.

3.3 Testing of a Drug-delivery System with a Pneumatic Microvalve

3.3.1 Test Configurations

To confirm that the fabricated microvalve is suitable for a chronic drug-delivery device, it is necessary to do a feasibility test that measures the flow hydraulic resistance across system and the leak rate over a certain pressure range. To measure the hydraulic flow resistance and leak rate across the drug-delivery system, the flow testing tools were set up as shown in Figure 3.25. The flow is driven using a volume flow controlled syringe pump (WPI UltraMicroPump) and a micro syringe (Hamilton 0.5µL). Pressure is measured with a differential pressure transducer (Omega P26). The fluid is filtered through a 0.2 µm in-line filter (Corning, Inc.) to remove trace particulates.

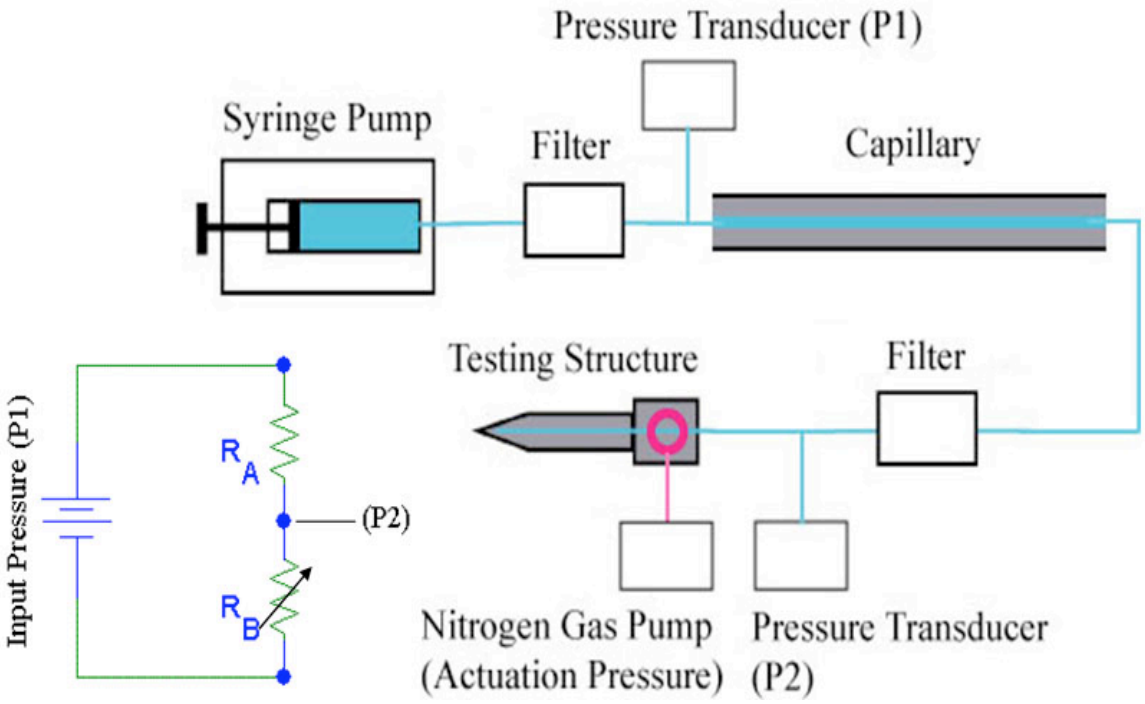

Figure 3.25: Schematic diagram of the flow testing tools illustrating pneumatic microvalve characterization. A small diagram shows a pressure-equivalent circuit. R_A is the hydraulic flow resistance of the capillary and filter, and R_B is the hydraulic flow resistance of the drug-delivery probe.

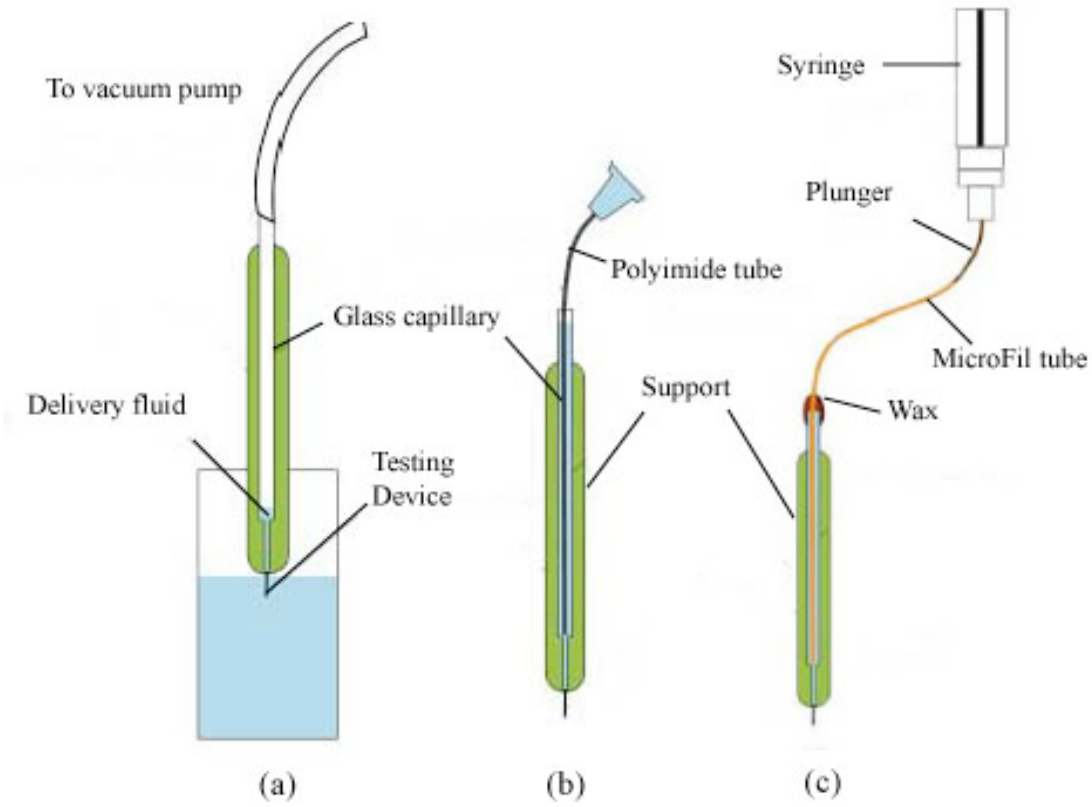

Figure 3.26: Preparation of the probe prior to fluid delivery. (a) back-fill, (b) using a MicroFil polyimide tube to fill the glass capillary, (c) syringe and testing device assembly.

The large surface-to-volume ratios of microfabricated fluid channels result in significant surface tension effects [39]. Consequently, it is important to ensure that there are no exposed surfaces in the flow system. This includes bubbles, leaks, foreign particulates, and stationary volumes of fluid. Complete saturation of the flow system was ensured by using the following procedure [39]: the testing device was first back-filled with fluid using a vacuum pump system (Figure 3.26a); then a flexible polyimide tube (WPI MicroFil) was inserted into the glass capillary until it made contact with the upstream tip of the device (Figure 3.26b); and finally a syringe assembly (Figure 3.26c) provided the required flow through the device. The seal between the syringe and the glass capillary of the device assembly was maintained with wax.

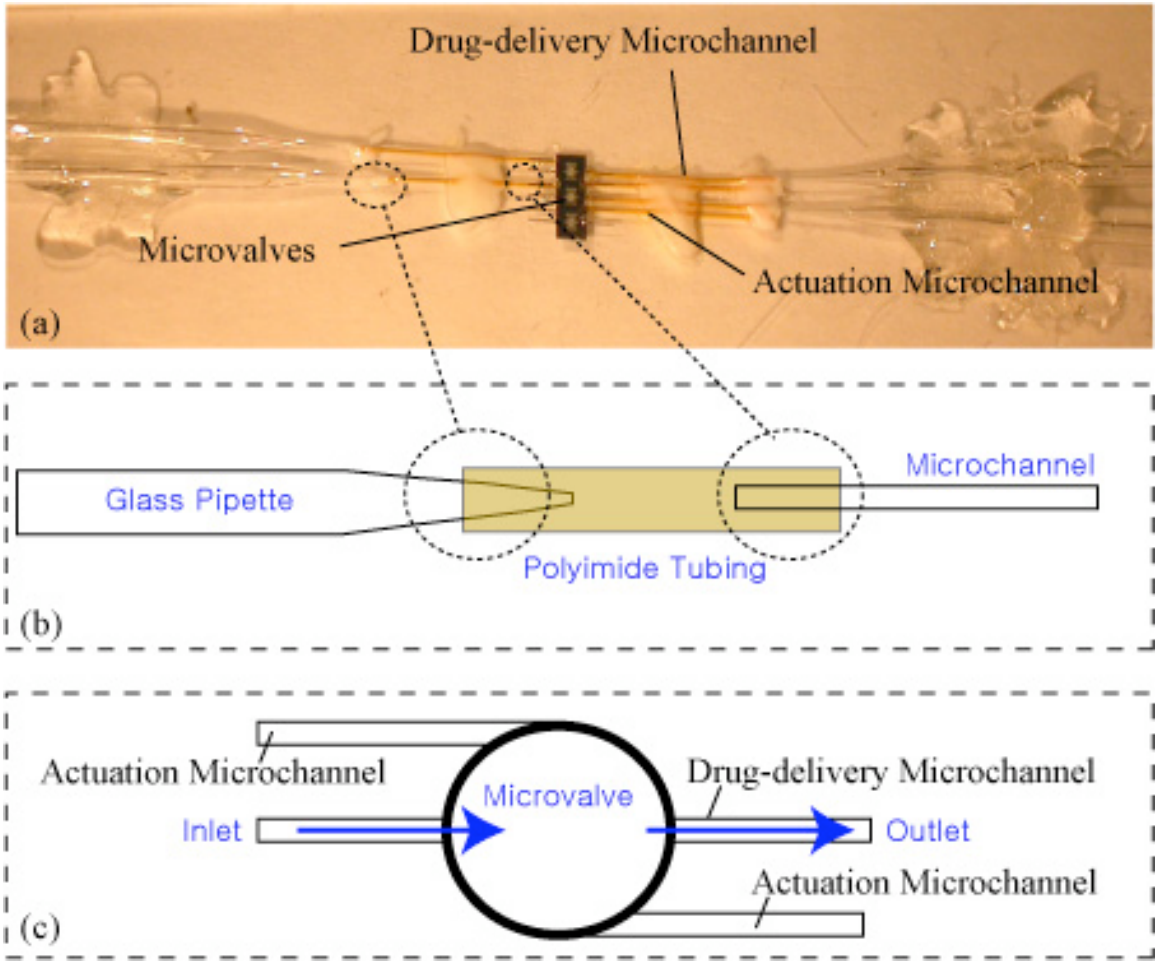

Figure 3.27: (a) A picture of the testing device. (b) The diagram of showing the connection between glass pipette and microchannel through the polyimide tubing; (c) Each device has three pneumatic microvalves. Each microvalve has two actuation channels and one drug-delivery channel

3.3.2 Pressure Drop Measurement for the Version I Microvalve

The pressure difference across the Version I microvalve and its series microchannel has been analyzed to understand the open drug delivery rate as a function of drive pressure. A pneumatic microvalve is composed of two channels. One is for drug-delivery and the other is for actuation (Figure 3.27). A first experiment was performed to measure the pressure variation (P2) across the system for water for different input pressures (P1)

as shown in Figure 3.28. No pressure is applied to the actuation channel so that the valve was open. A 30μm-ID, 10cm-long capillary (Polymicro Inc.) with a hydraulic resistance of $5x10^{15}$ Pa•s•m^{-3} was used as a reference, and a valve diaphragm radius of 200μm was used. As shown in Figure 3.28 and Figure 3.29, the total hydraulic resistance of the entire testing system was around $19.5x10^{15}$ Pa•s•m^{-3} at an input pressure of 10kPa, so that the hydraulic resistance of the open-microvalve was $14.5x10^{15}$ Pa•s•m^{-3}. At a flow rate of 513pL/sec (Figure 3.29), the pressure drop across the system was 7438Pa, which is slightly lower than the simulated result of 8410Pa by FLUENT and equation (2.2). The discrepancy probably results from the fact that the gap distance of the cavity over the diaphragm is larger than that of the simulated one.

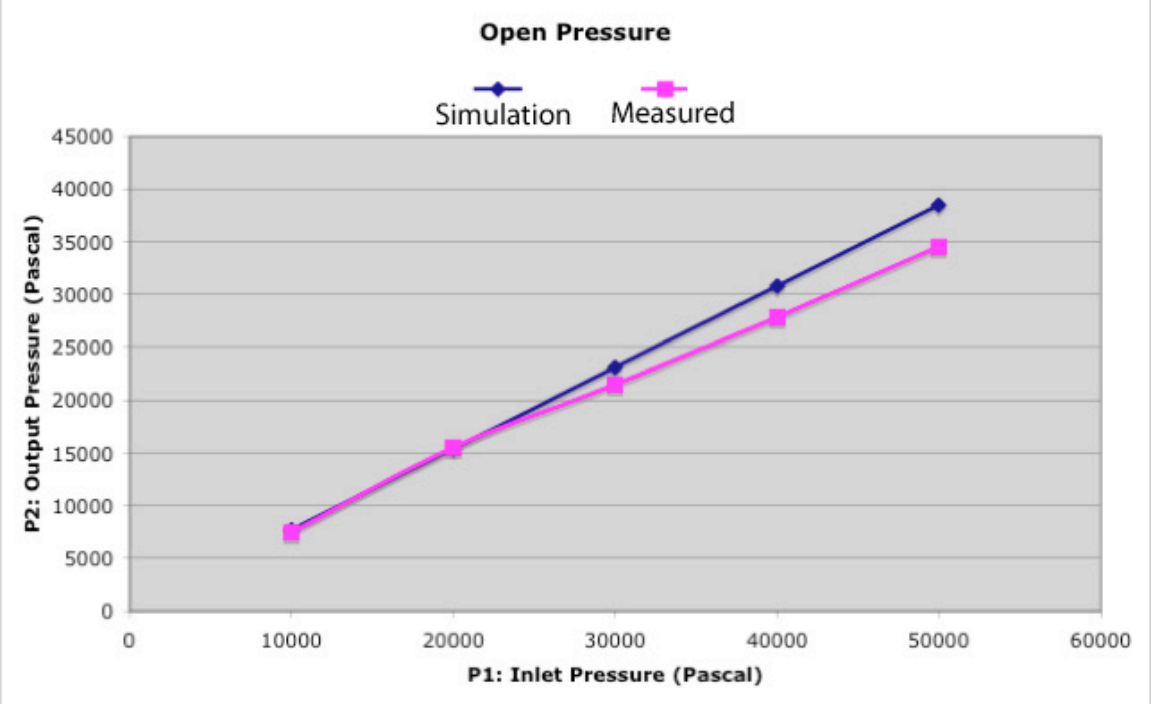

Figure 3.28: The pressure variation across the testing device as a function of inlet pressure

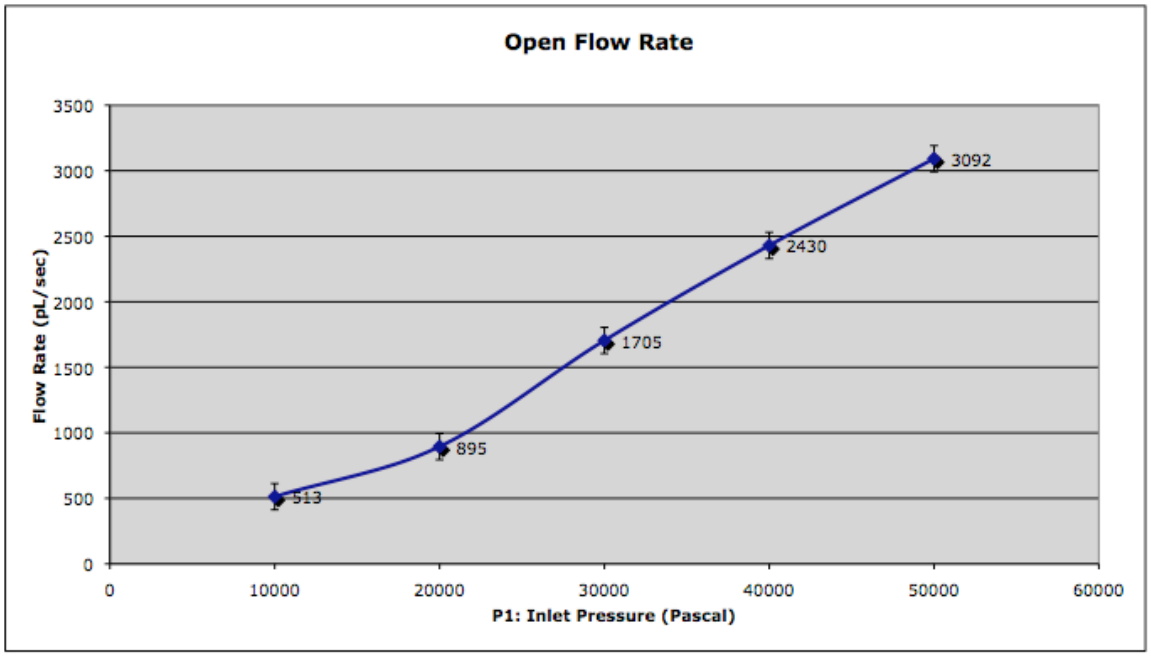

Figure 3.29: An open-flow rate variation as a function of inlet pressure (P1)

As the input pressure (P1) increases, the cross-sectional area of the liquid-path in the microvalve increases due to the liquid pressure on the flexible microvalve diaphragm, driving it to increase the channel depth. Consequently, the hydraulic flow resistance decreases. This results in the nonlinearity in the flow rate (Figure 3.29) as the input pressure (P1) increases. Except for this nonlinearity, the predicted and measured data values match to within a few percent on average, confirming to the usefulness of the model developed in chapter 2.

3.3.3 Leak Rate Measurement for the Version I Microvalve

The pressure difference across the microvalve has been measured (Figure 3.30) to understand the leak rate (Figure 3.31) as a function of actuation drive pressure at a fixed input pressure of 10kPa. A 10cm-long reference capillary was used with an inner diameter of 15μm (Polymicro Inc.) and a hydraulic resistance of 80×10^{15} Pa•s•m^{-3}. Valve

diaphragm radii of 180, 200, and 220μm were used. For diaphragm radii of 180, 200, and 220μm, the measured leak rates are 32, 21, and 15pL/sec, respectively, at the actuation pressure of 35kPa. The hydraulic resistance of the microvalve (200μm diaphragm radius) was calculated at 35kPa in blocking mode in chapter 2 to be $256x10^{15}$ $Pa•s•m^{-3}$. The calculated leak rate at the actuation pressure of 35kPa was 29pL/sec, which is slightly higher than the measured one. This results from the fact that the cross-sectional area of the leak liquid-path in the microvalve in blocking mode decreases due to the surface roughness of polysilicon and dielectrics.

These experiments show that the closed leak rate for a diaphragm radius of 200μm at 10kPa input pressure (P1) is 21pL/Sec and the open flow rate is 513pL/Sec at the same pressure. As discussed in chapter 1, the minimum effective flow rate of an injected chemical can be arbitrarily taken as 500pL/Sec and a negligible amount of injected chemical can be arbitrarily taken at about 0.5% of a 100μm-diameter sphere, which is 25pL/Sec for 100mSec pulse-duration (5% of the minimum open flow rate). Therefore, the experiments showed that this valve structure fulfills the requirements of leak rate (<25pL/Sec) and the minimum open flow rate (>500pL/Sec) at 10kPa input pressure (P1).

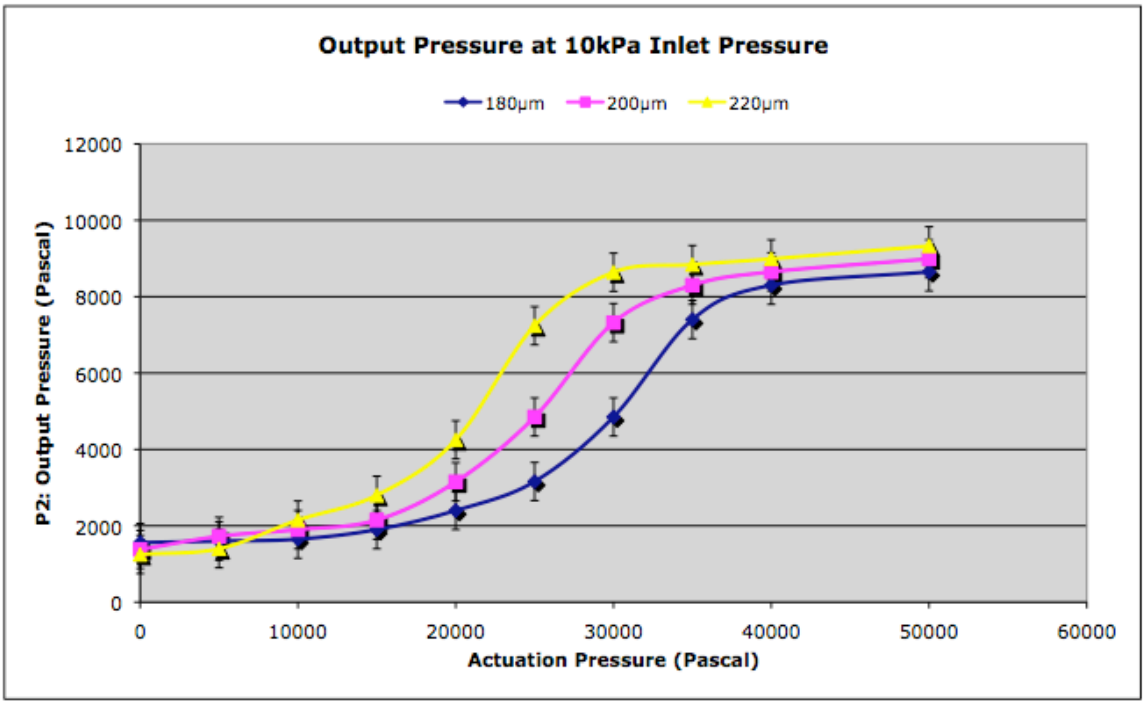

Figure 3.30: The pressure (P2) variation across the testing device as a function of actuation pressure at an input pressure (P1) of 10kPa

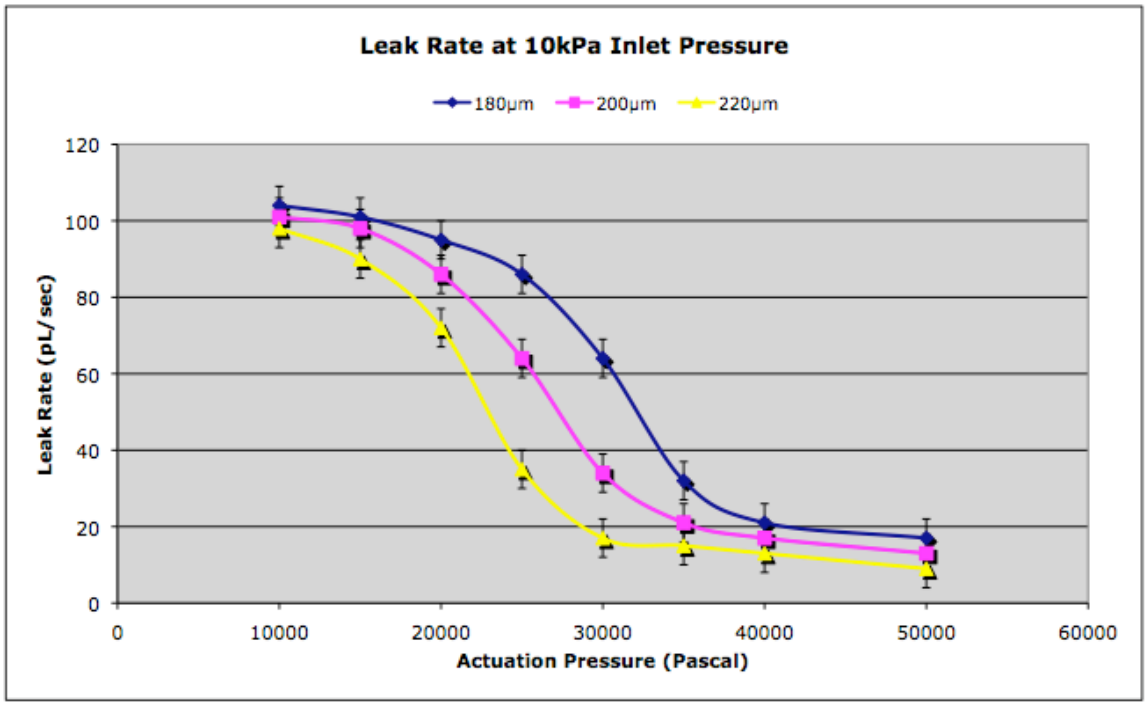

Figure 3.31: The leak rate measured as a function of actuation pressure at an input pressure (P1) of 10kPa

3.3.4 Pressure Drop Measurement for the Version II Microvalve

The pressure difference across the Version II valve and its series microchannel has also been analyzed to understand the drug delivery rate as a function of drive pressure. The experimental setup was the same as that of Version I (Figure 3.25). The pressure variation (P2) across the system for water was measured for different input pressures (P1) as shown in Figure 3.25. No pressure was applied to the actuation channel so that the valve was open. A 30μm-ID, 10cm-long reference capillary (Polymicro Inc.) with a hydraulic resistance of $5x10^{15}$ Pa•s•m^{-3} was used with a valve having a diaphragm radius of 200μm. As shown in Figure 3.32 and Figure 3.33, the total hydraulic resistance of the entire testing system was around $10.6x10^{15}$ Pa•s•m^{-3} at an input pressure of 10kPa, which indicates that the hydraulic resistance of the open-microvalve was $5.6x10^{15}$ Pa•s•m^{-3}, resulting in an open-flow rate of 943pL/sec (Figure 3.29). The pressure drop across the system was 5280Pa, which is lower than the pressure drop across Version I of 7438Pa. This results from the fact that the liquid-path in Version II is shorter than that in Version I. As the input pressure (P1) increases, the cross-sectional area of the liquid-path in Version II also increases due to the liquid pressure on the flexible valve diaphragm and consequently the hydraulic resistance decreases. Because the center of the Version II diaphragm is located above the inlet of the drug-flow channel, it results in the higher slope in the open-flow rate as a function of inlet pressure than Version I does at the input pressure of 50kPa (Figure 3.33).

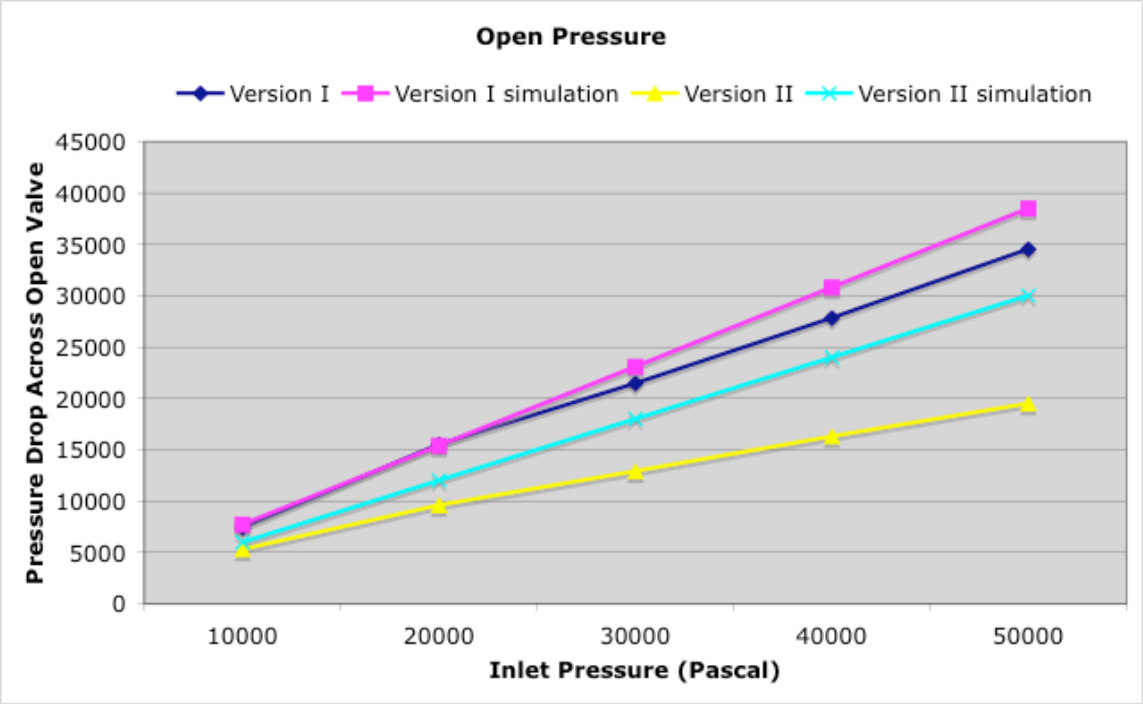

Figure 3.32: A pressure variation across the testing device having the version II microvalve as a function of inlet pressure (P1)

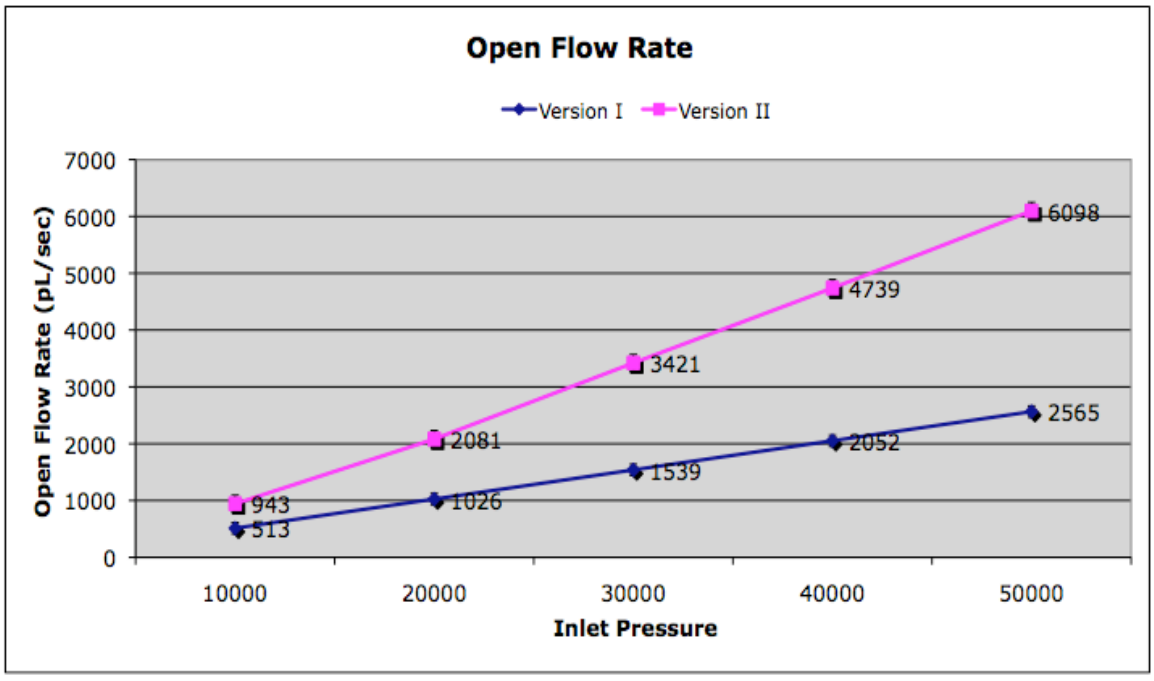

Figure 3.33: An open-flow rate variation as a function of inlet pressure (P1). The open flow rate of Version II has higher than that of Version I at the same inlet pressure

3.3.4 Leak Rate Measurement for Version II Microvalve

The pressure difference across Version II has been measured (Figure 3.34) to verify the improved sealing ability compared to Version I as a function of drive actuation pressure at the fixed input pressure of 10kPa. A 10cm-long reference capillary with an inner diameter of 15μm (Polymicro Inc.), and a hydraulic resistance of $80x10^{15}$ $Pa•s•m^{-3}$ was used with valve diaphragm radius of 200μm. Figure 3.34 shows that the output pressure for Version II starts to increase at a lower actuation pressure, which indicates that Version II requires less actuation pressure to work in blocking mode than Version I. The measured leak rate is 9pL/sec at an actuation pressure of 35kPa (Figure 3.35), which is three times lower than the Version I. This results from the fact that the gap spacing between the Version II diaphragm and the inlet of the drug-delivery channel is much smaller than the opening along 20μm of the outer edge of the Version I diaphragm at a differential actuation pressure of 35kPa above the inlet. The leak rate variation was also measured as a function of inlet pressure at the actuation pressure of 35kPa (Figure 3.36). The feasibility of Version II design was verified by not only fulfilling the minimum open flow rate (>500pL/Sec) at 10kPa input pressure (P1) but also meeting the design target of leak rate (<25pL/Sec).

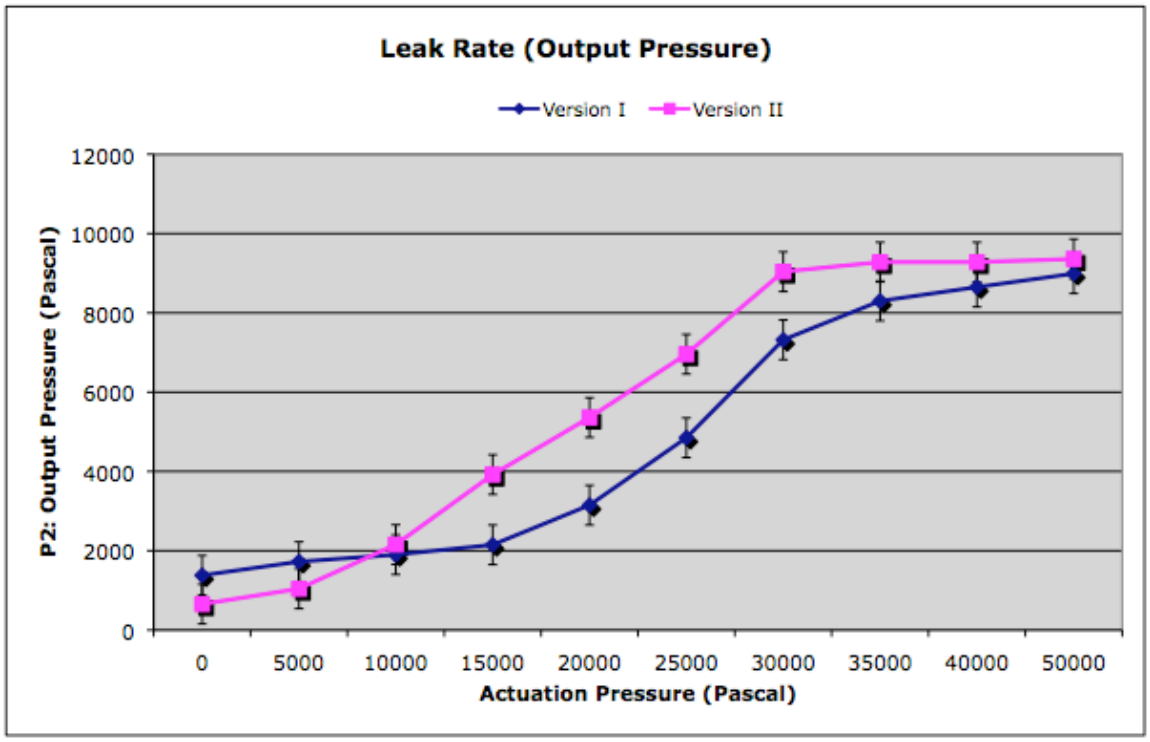

Figure 3.34: The pressure (P2) variation across Version II as a function of actuation pressure at an input pressure (P1) of 10k

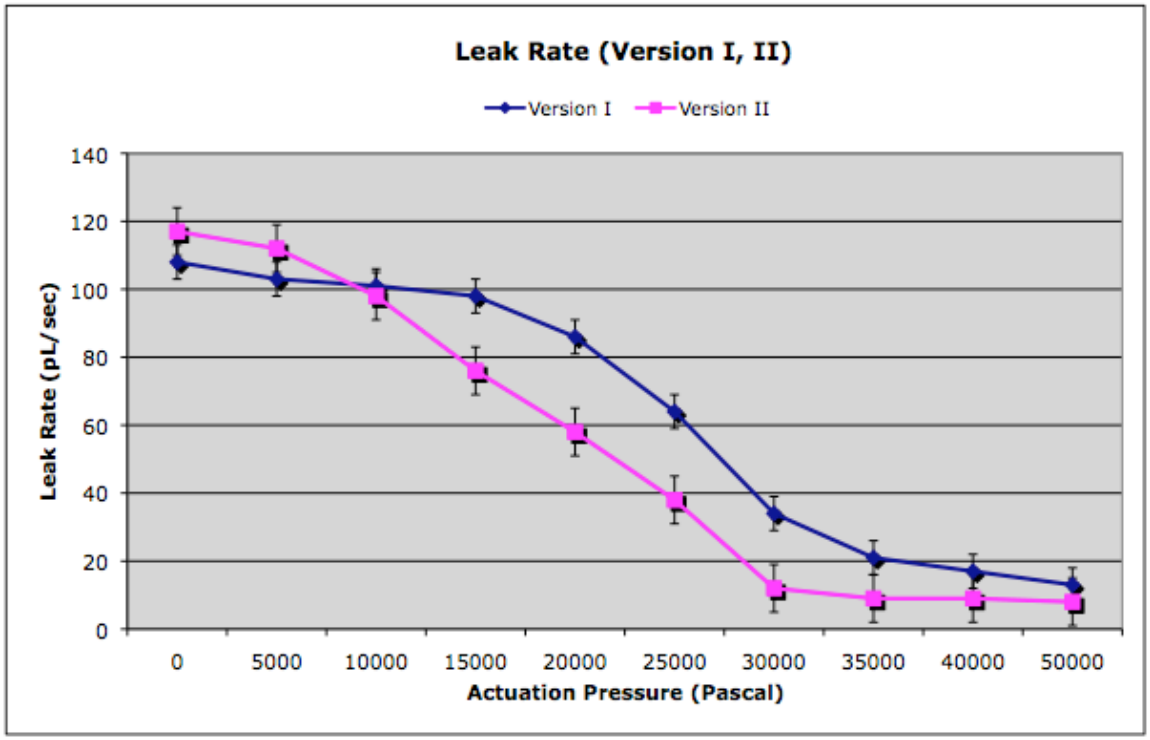

Figure 3.35: The leak rate of Version II measured as a function of actuation pressure at an input pressure (P1) of 10kPa

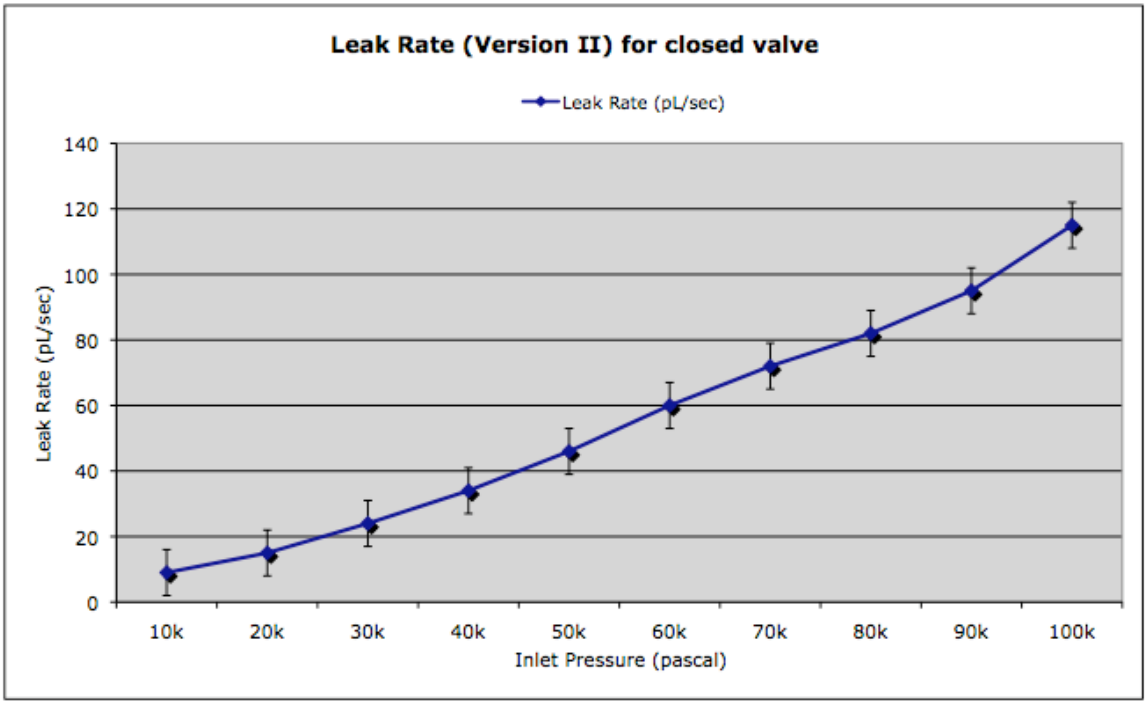

Figure 3.36: Leak rate vs. inlet pressure for the closed Version II valve, with 35kPa differential across diaphragms

CHAPTER 4

A Feasibility Study of Thermopneumatically-Actuated Corrugated Microvalves

The previous chapter dealt with the design, fabrication, and testing of devices with on-chip pneumatic actuation. Although such devices should be appropriate for some applications, it is ultimately desirable to study the feasibility of implementing a self-contained device that is controlled entirely by electrical signals. This chapter treats the conceptual development of a thermopneumatic actuator that can meet such a requirement.

Section 4.1 states the design considerations for a complete thermopneumatically-actuated microvalve. Section 4.2 then examines the simulation results.

4.1 Thermopneumatic Microvalve Design Considerations

As discussed in chapter 1, thermopneumatic actuation relies on the change in volume of a sealed liquid under thermal loading. The principle uses the phase change from liquid to gas to gain a larger volume expansion. The advantage of using liquid as an actuator material is the ability to generate large forces over a significant distance, since gaseous molecules will freely flow within a closed cavity to reach equilibrium pressure throughout.

The integrated microvalves on a neural probe must be compatible with current probe fabrication technology without adding too much process complexity (Figure 4.1). They

should also be compatible with chronic use in-vivo. In general, the requirements pertaining to flow rates may be met by a suitably dimensioned structure similar to the already-demonstrated, pneumatically-actuated flow element. Leak rate requirements may likewise be met if the drive pressure developed by the thermopneumatic actuator is capable of producing the 35kPa used to achieve the results of the pneumatic design (Chapter 2 and 3).

Pressure ejection has been used on the Michigan drug delivery probe. As discussed earlier, 50pL is the minimum amount of injected chemical to effectively change the neuronal environment. To achieve this amount, the chemical was delivered by 1-2 psi pressure pulses having durations of 100msec, which results in a flow rate of 500pL/Sec, the open flow rate of the drug-delivery probe with the on-chip pneumatic microvalve described in chapter 3.

Operating temperature: To find the energy required to create an actuation pressure of 35kPa, the thermal equivalent model must take into account the thermal sinking of the surrounding structure and the external fluid (Section 4.2). The microvalve on the microprobe should not produce a temperature rise of more than $2^{o}C$ in the surrounding tissue. The temperature rise of the surrounding tissue will also be analyzed when a microvalve is held closed for the pulse duration of 100msec.

Actuation-voltage: The use of high voltages within any organism is not attractive due to the risk of electrical leakage and shock. In order to avoid damaging the neural system, a low actuation voltage (< 10V) is required.

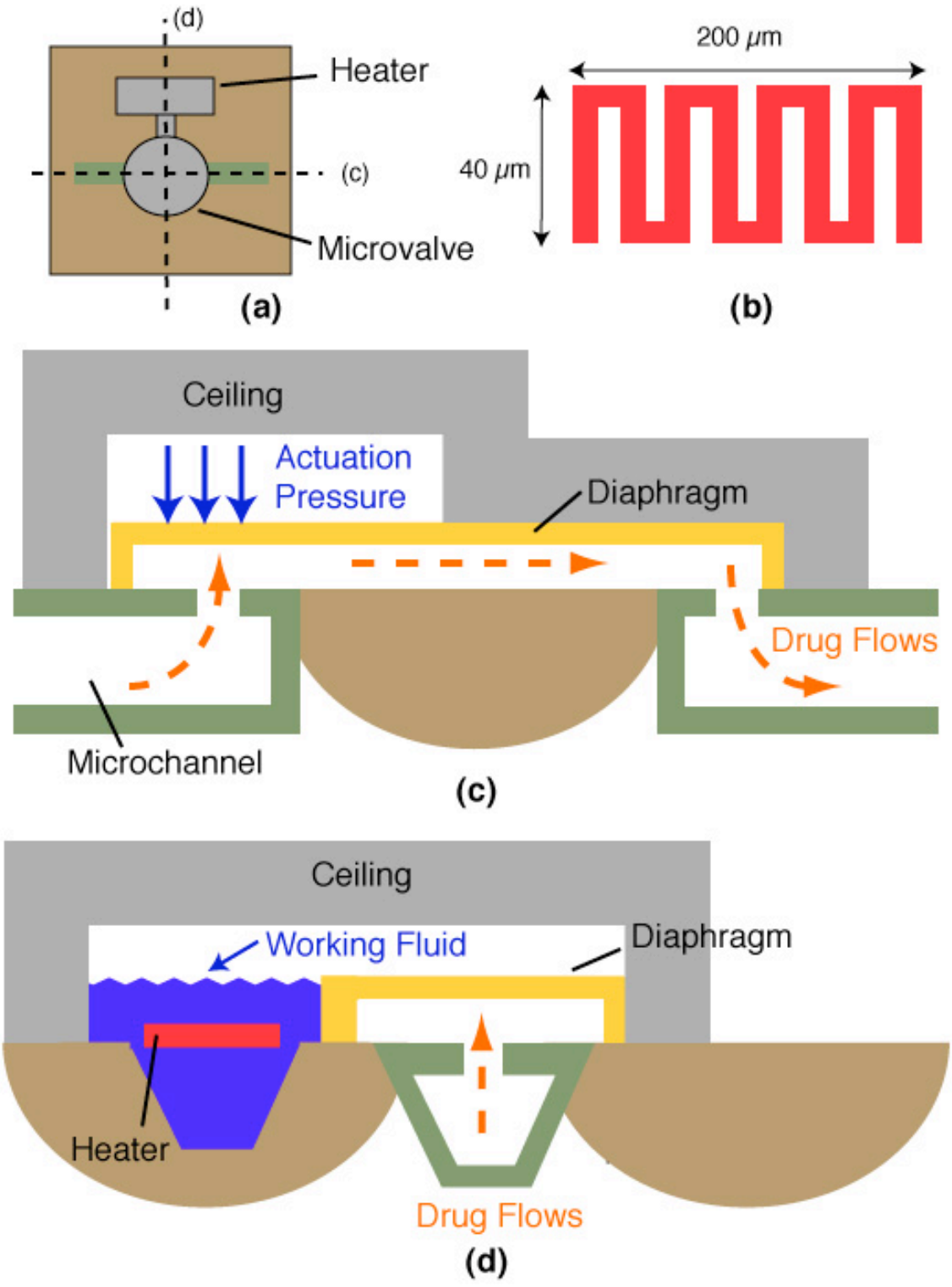

Figure 4.1: (a) Top view of the microvalve and heater; each line stands for the direction of cross-sectional view for the following diagrams; (b) Heater grid design (200μm × 40μm); (c) The cross-sectional view of microchannel and the valve diaphragm; (d) The cross-sectional view of the heater and the valve diaphragm. The working fluid is partially filled in the cavity.

Power consumption and Response time: The characteristics of power consumption, response time and operating temperature all interrelate for a thermally-actuated structure. Lower boiling point relative to ambient means less energy input is needed to reach the vaporization temperature of the operating fluid, or conversely, the same energy input yields a faster transient response.

Additionally, excess energy input beyond that required for actuation must be dissipated before the valve will open, prolonging the reset time for the device. Thus, an ideal system will input only enough power to achieve and maintain the required actuation pressure.

4.1.1 Heater Grid Design

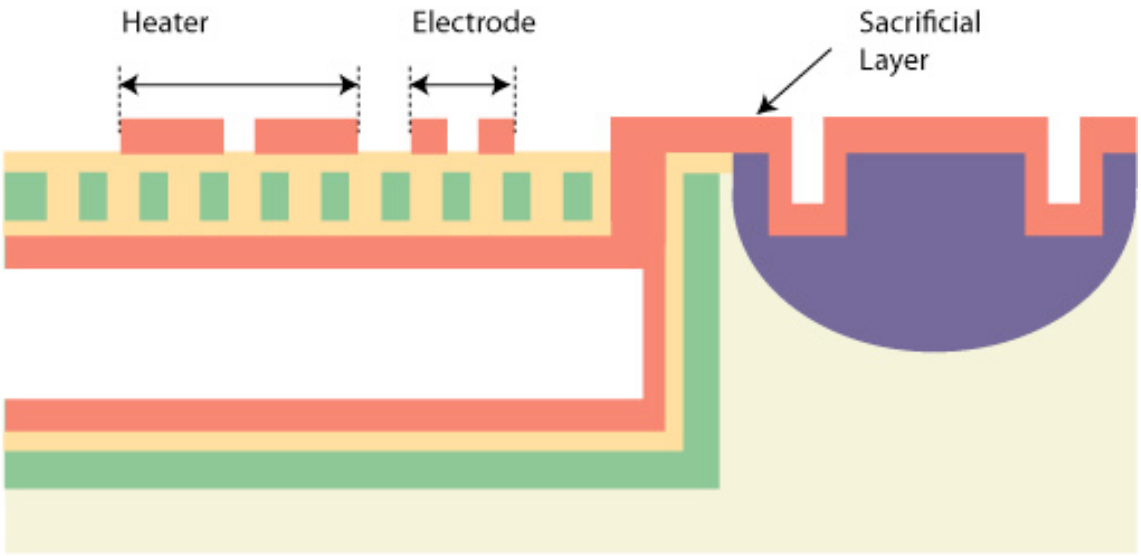

Figure 4.2: The cross-sectional view of heater, electrodes and the sacrificial layer formation. The polysilicon heater can be fabricated without adding any extra mask to the current pneumatic microvalve fabrication process.

Precise control of the grid resistance is necessary in order to construct a system that operates over a useful voltage range. For this device a nominal power output of 8mW at a heater resistance of 3.5kΩ was chosen. Thus the operating voltage was 5V. The heater is

defined with the same mask for patterning electrodes and the first sacrificial layer for the valve diaphragm (Figure 4.1, Figure 4.2). In the design of a driver to heat the working fluid, a 3µm minimum feature polysilicon heater is used with an assumed sheet resistance of 10 Ω/square. The serpentine driver overall length was chosen to be 200µm and the overall width was chosen to be 40µm (Figure 4.3). With these dimensions, the expected resistance contained within the driver is almost 3.5kΩ.

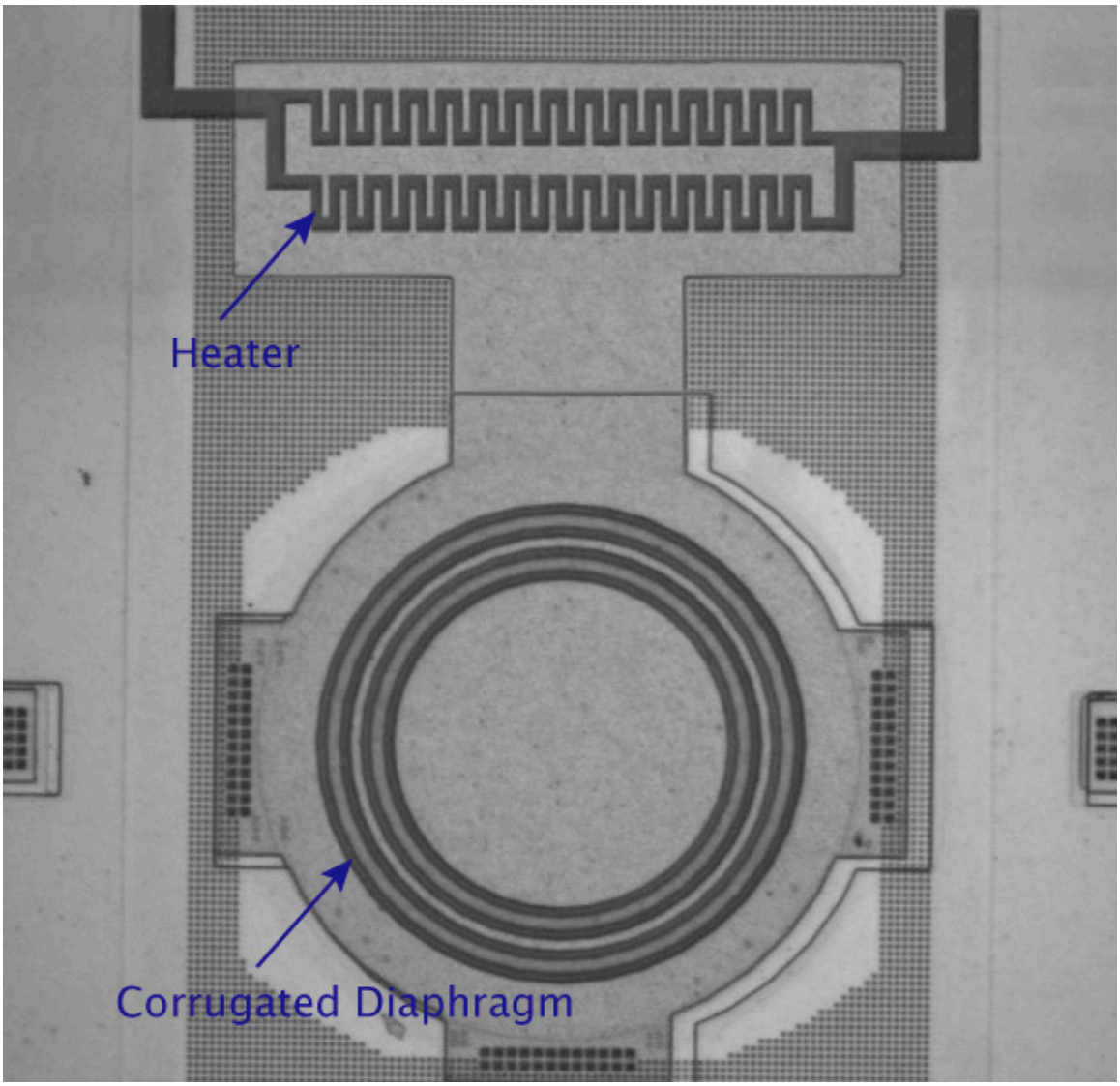

Figure 4.3: The serpentine heater was fabricated to confirm the process compatibility with the current fabrication process of the pneumatic microvalve.

4.1.2 Working Fluid

A number of different volatile liquids may serve as the working fluid. Table 4.1 enumerates several possibilities. Generally, a higher boiling point translates to a lower power requirement. Note that the boiling point of a working fluid is always specified at a specific pressure and will naturally rise with increasing pressure in the actuator cavity.

Name	Formula	Boiling Temperature at 760torr	Heat, $\Delta h_{t,g}$ [kJ/kg]	Molar mass, M [kg/kmole]
Trichlorofluoro-methane (Freon-11)	CCl_3F	24	180	137.4
Pentane	C_5H_{12}	36	357	72.2
Acetone	C_3H_6O	56	508	58.1
Methanol	CH_4O	65	1104	32.0
Hexane	C_6H_{14}	69	335	86.2
Benzene	C_6H_6	80	394	78.1
Trichloroethylene	C_2HCl_3	87	261	131.4
Propanol	C_3H_8O	97	696	60.1
Water	H_2O	100	2256	18.0
Tululene	C_7H_8	111	364	92.1
Chlorobenzene	C_6H_5Cl	132	N/A	112.6
Xylenes	C_8H_{10}	137	322	106.2

Table 4.1: Physical characteristics of some potential working fluids [96-98]

Since the working fluid should be stay in a liquid phase without any applied heat flows, the boiling temperature is the most important factor to be considered in choosing the material. The boiling temperature should be close to body temperature so that less hea ting of the device is required and consequently less power is lost to the ambient environm ent, but not close enough to result in phase-change when the body temperature accidentally goes up due to fever or excertion. The choice of a working fluid for this work was pentane, reflecting Rich and Bergstrom's earlier work. Pentane-filled devices

required actuation power in the tens to a few hundred milliwatts range [96, 97] in their structures.

Based on previous experiments [98], to achieve a pressure rise of 50 Torr, only 0.017pL of cyclopentane needs to be converted to a gas. To achieve 35kPa (250 Torr), 0.1pL of cyclopentane is required. Based on the size of the heater and the cavity of the working fluid in Figure 4.3; the designed volume has a capability of generating the actuation pressure of 35kPa.

Earlier work by Rich and Bergstrom determined that the most efficient thermopneumatic system contains just enough operating liquid to be completely vaporized upon actuation [98]. (Any additional liquid absorbs excess energy and increases the thermal time constant of the system.) Hence, the actuation cavity should be filled with vapor, having only a small fraction occupied by the working fluid (Figure 4.2b). For example, Rich's device required a 0.43% fill fraction to operate at maximum efficiency.

4.2 Thermal Analysis and Modeling

4.2.1 Two-Dimensional Thermal Circuit Modeling

A two-dimensional thermal analytical model of the thermopneumatic actuator may be constructed to obtain an approximate idea of the expected performance. Later the three-dimensional thermal FEM simulation results will be discussed. The first step in the two-dimensional modeling of this structure was to obtain an understanding of the heat flow around the surrounding structure and external fluid (Figure 4.4). To simplify modeling:

- A locally lumped model was used for one active valve in a microprobe.

- The electrical portion of the heater is assumed to be constant.
- Significant heat flow is assumed through the bulk Si surrounding the heater, not through the cavity of the heater.
- The forced convection through the drug flow is assumed to be negligible, since the flowrate is negligible when the valve is held closed.
- The vapor is assumed to be at uniform temperature within the heater cavity.

Within the device, conduction currents are assumed dominant. Resistance to thermal conduction, $R_{th,}$, through a volume of material may be expressed as:

$$R_{th} = \frac{L}{kA} \tag{4.1}$$

where L is the length of the volume parallel to heat flow, A is the cross-sectional area perpendicular to heat flow, and k is the thermal conductivity of the material. The thermal resistance has units of ^{o}C/W.

When time constants are involved, we must also calculate the thermal heat capacitance of the material. This is a measure of the energy required to heat the material by 1^{o}C; the thermal heat capacitance is given by

$$C_{th} = \delta \cdot LA \cdot \eta \tag{4.3}$$

where δ is the density of the material in gm/cm^3, LA is the volume (length times area) in cm^3 of the material considered at a particular node, and η is the specific heat of the material in J/gm-^{o}C. The thermal capacitance is important in determining thermal time constant, which determines the thermal response speed. The parameters of a few of the materials are given in the table 4.2.

	SiO_2	*Si_3N_4*	*Silicon*	*Polysilicon*	*Water*	*Pentane*
Density (gm/cm^3)	2.2	3.4	2.33	2.3	1	0.75
Specific Heat ($J/gm-^oC$)	0.745	0.691	0.68	0.68	4.18	1.783
Thermal Conductivity ($W/cm-^oC$)	0.014	0.16	1.45	0.2~0.25	0.0058	0.00136

Table 4.2: The density, specific heat and thermal conductivity of a few of the materials used in this device.

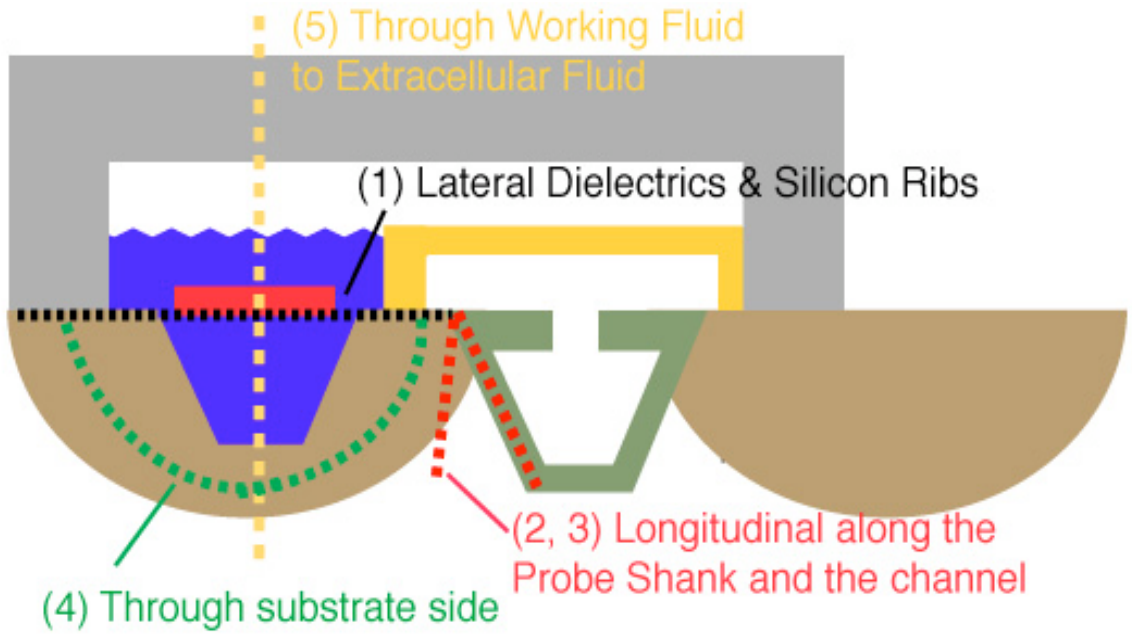

Figure 4.4: The conductive thermal flow paths with an integrated thermopneumatic valve

Figure 4.4 shows the cross-sectional view of a microvalve and heater. The triangular channel has a width of 30μm and a depth of 21.2μm, which results in a rather large cross-sectional area of $318\mu m^2$. The channel sidewalls and ribs are made of 4μm thick heavily boron-doped silicon. The channel is sealed by a 2μm-thick LPCVD oxide/nitride/oxide sandwich with an oxide to nitride thickness ratio of 4:1. The heater is formed by a 200μm-long, 40μm-wide, 1μm-thick polysilicon resistor.

Conductive thermal flow determines how well the heating is retained in the local area. Figure 4.4 shows the approximate heat dissipation mechanisms in the heater structure including the four conduction paths as follows:

1) Conduction through the lateral dielectrics and boron-doped silicon ribs to the edge of the dielectric ceiling (R_Lateral);

2) Conduction through the deep boron diffused silicon along the probe shank (R_Shank1);

3) Conduction through the dielectric and boron-doped silicon ribs along the longitudinal direction of the channel (R_Shank2)

4) Conduction from the actuator ceiling to the bottom of the channel through channel sidewalls (R_Bottom)

5) Conduction through the cyclopentane above the heater through the actuator ceiling and out to the extracellular fluid environment (R_Top, R_Ceiling, R_Water20, R_Water30, R_Water250).

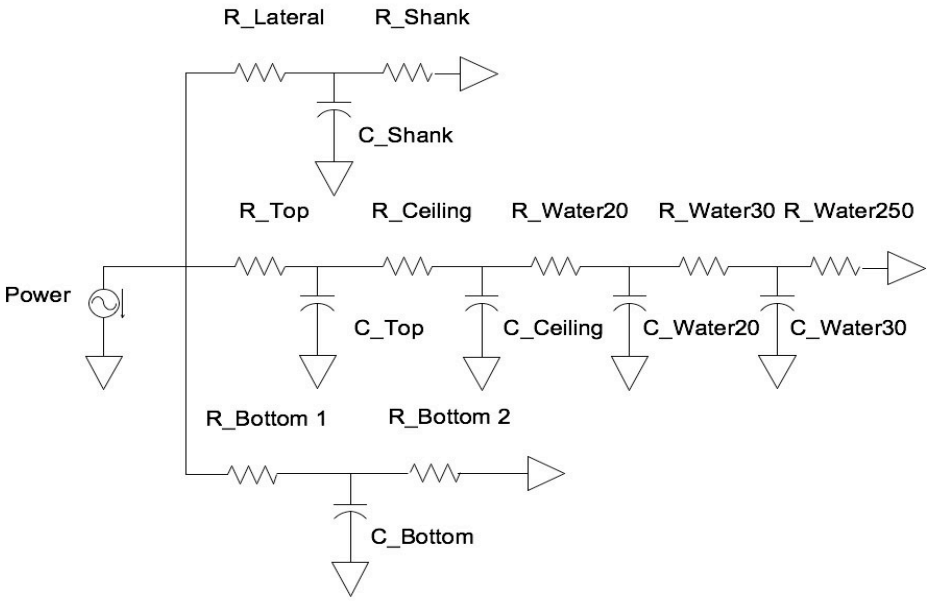

Figure 4.5: Two-dimensional thermal circuit used to model the drug-delivery probe

R_Top	R_Ceiling	R_Water20	R_Water30	R_Water250
10.6kΩ	42.3Ω	5kΩ	10kΩ	20kΩ
R_Bottom1	**R_Bottom2**	**R_Lateral**	**R_Shank**	**C_Top**
56kΩ	56kΩ	1kΩ	3kΩ	20nF
C_Ceiling	**C_Water20**	**C_Bottom**	**C_Lateral**	**C_Shank**
33.6nF	1.86uF	0.7uF	33nF	63nF

Table 4.3: Values for thermal equivalent resistances and capacitances of the thermal circuit (Figure 4.5)

All paths can be modeled based on the assumption that the heater area is considered as a lumped body at uniform temperature. Modeling in SPICE indicates (Figure 4.5) that a power of 8mW is needed to raise the heater temperature 7.5^{o}C. The power is held for 100msec. This gives an actuation delay of 6mSec for cyclopentane evaporation. The thermal relaxation time is 12mSec to bring the cyclopentane temperature back to within 1^{o}C of the starting temperature (Figure 4.6). While a microvalve is in blocking-mode for a short pulse-duration (100mSec), the temperature rise in the tissue environment adjacent to the microvalve should be less than 2^{o}C. If the valve is held closed for 100mSec, the heating of the surrounding extracellular environment 250μm away from the microvalve increases 2^{o}C (Figure 4.6). Using the parameters in table 4.3 and the two dimensional thermal modeling, the distribution of heat flow in the thermopneumatic microvalve was analyzed. As shown in Figure 4.7, the major distribution of heat flow is along the probe shank and above the heater cavity. Since the two-dimensional modeling did not fully consider the mass of entire probe shank and surrounding extracellular fluid, the three-dimensional modeling using FEM will be performed in the next section.

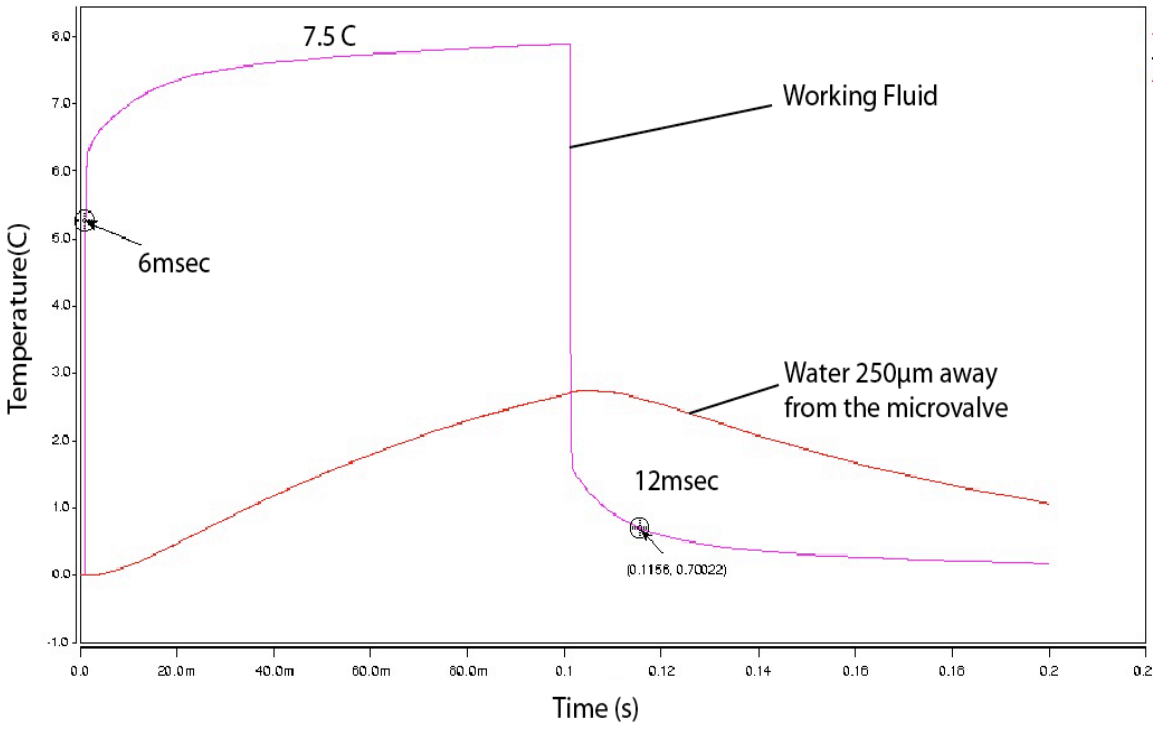

Figure 4.6: The two-dimensional probe thermal model with an integrated thermopneumatic microvalve using phase-change. Phase-change requires low power of 8mW for 100msec pulse-duration. As a result, the surrounding area is heated minimally.

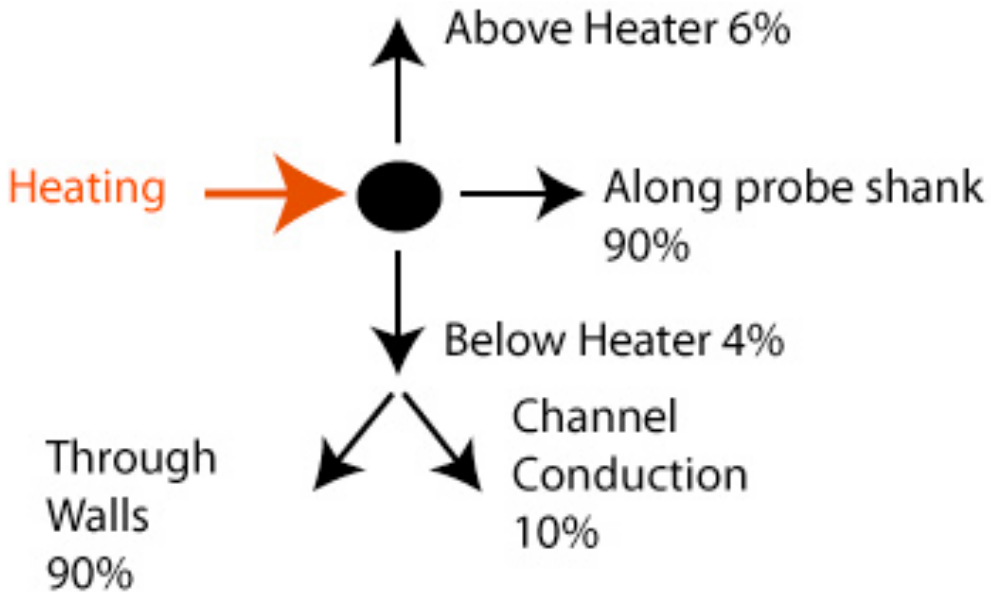

Figure 4.7: The distribution of heat flow in microprobe with an integrated thermopneumatic microvalve

4.2.2 Three-Dimensional Thermal Circuit Modeling

Since the 2-D thermal circuit was modeled to understand the distribution of heat flows in the thermopneumatic microvalve, the next step is to add the real mass of the microprobe and the extracellular fluid to the modeling. To do that, the three-dimensional modeling was performed using ANSYS. This finite-element modeling software would be the most accurate way to determine how the heater of the valve heats the surrounding structures. The structural model is shown in Figure 4.8. In the design, the assumption made is that the water as an extracellular fluid is maintained at an ambient temperature of 37^{o}C at a distance of 5mm away from the microvalve area.

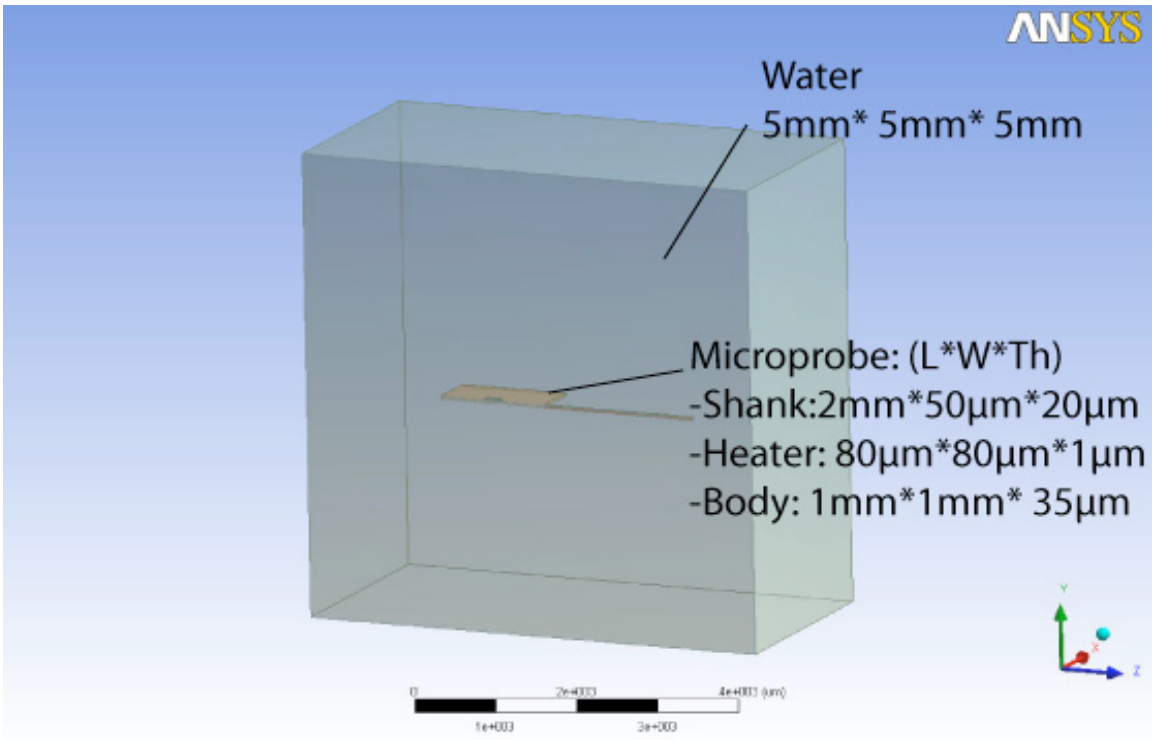

Figure 4.8: The three-dimensional ANSYS model of the microprobe with an integrated microvalve

The cavity of working fluid has a width of 90µm and a length of 90µm, which results in a cross-sectional area of 8100µm^2. The heater is formed by a 80µm-long, 80µm-wide, 1µm-thick resistor. The results of this simulation can be seen in Figure 4.9. The

temperature is indeed confined to the immediate area above and beneath the microvalve with minimal heating of the extracellular fluids. Figure 4.9 shows that the major distribution of heat flows is along the probe shank. To confirm this, the probe body was selected and the temperature of the probe body was separately evaluated in Figure 4.10. While the temperature of the working fluid is maintained at 42^{o}C, the temperatures at 500μm and 1.5mm down along the probe shank are 38.3^{o}C and 37.8^{o}C, respectively (Figure 4.10). Figure 4.11 shows the transient time analysis. While a microvalve is in blocking-mode for a short pulse-duration (100mSec), the temperature rise in the tissue environment adjacent to the microvalve was analyzed. The heater temperature is higher than the temperature of working fluid and will be capped at 42^{o}C to produce the phase change of the working fluid. Since the pressure cavity has a low internal thermal mass (consisting of the heater and liquid pentane), its temperature rises within a 10mSec after power application. After this initial transition a much slower increase takes place as the rest of the probe and the extracellular fluid, which has a comparatively large thermal mass, continues to heat. Similarly, upon termination of input power, the actuator cavity quickly drops to the temperature of the rest of the probe and then slowly decays back to ambient as the probe cools. The static thermal modeling was also simulated to evaluate the temperature rise of the surrounding structures for longer pulse-duration (>100mSec) and it confirmed no higher temperature rise of the probe than that generated by the microvalve in the short pulse-duration (100mSec). ANSYS simulation of the entire probe with an integrated thermopneumatic microvalve shows no perceptible temperature rise of the probe structure confirming that the designed thermopneumatic microvalve should be suitable for this research in terms of its temperature effect on the surrounding tissue

environment.

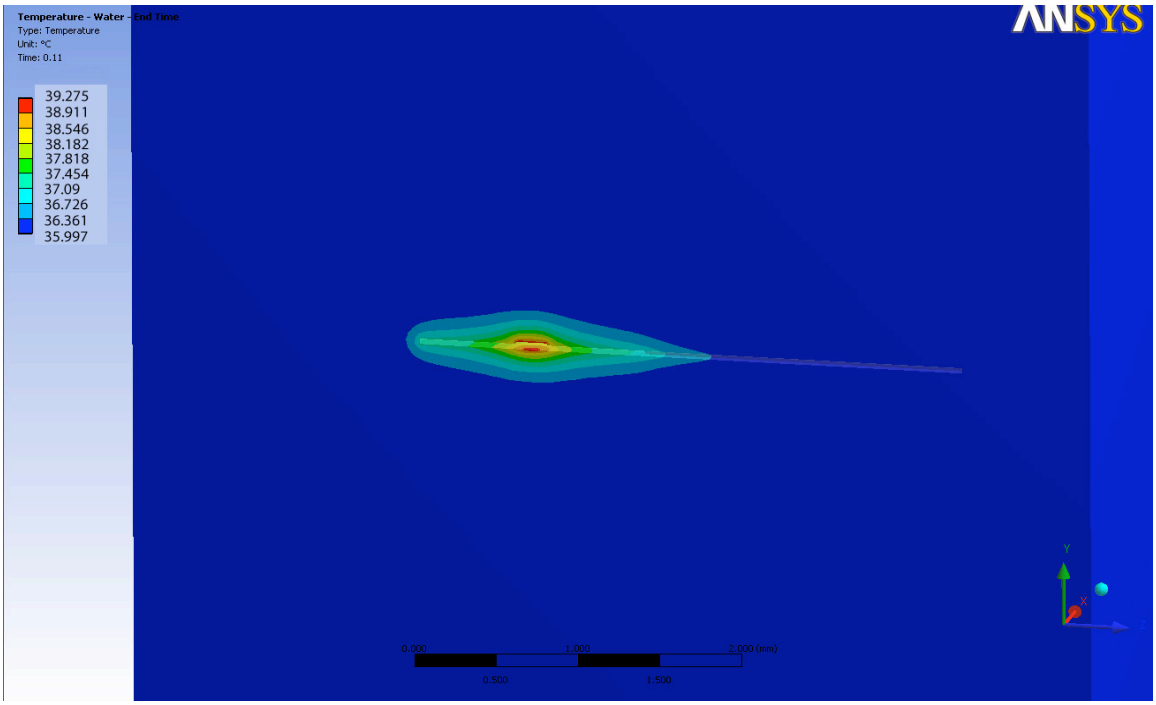

Figure 4.9: Temperature profile of the extracellular fluid along the probe shank as given by a 3-D ANSYS Simulation of the thermopneumatic microvalve.

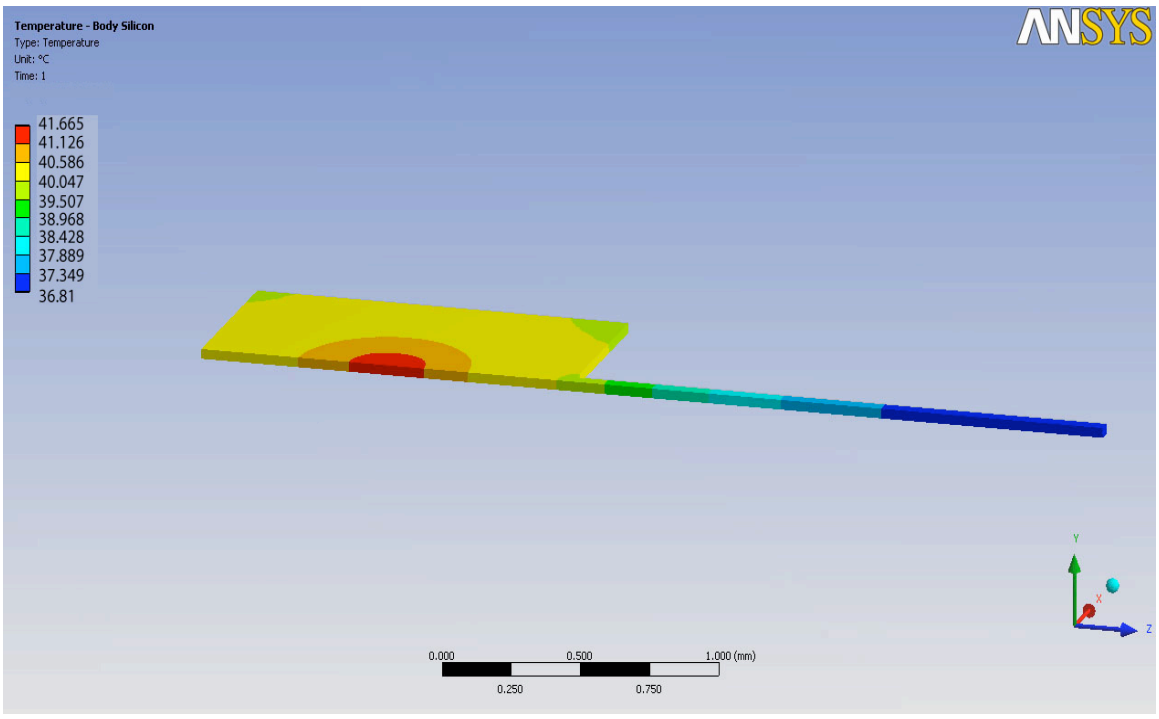

Figure 4.10: Temperature profile of the microprobe with an integrated thermopneumatic microvalve

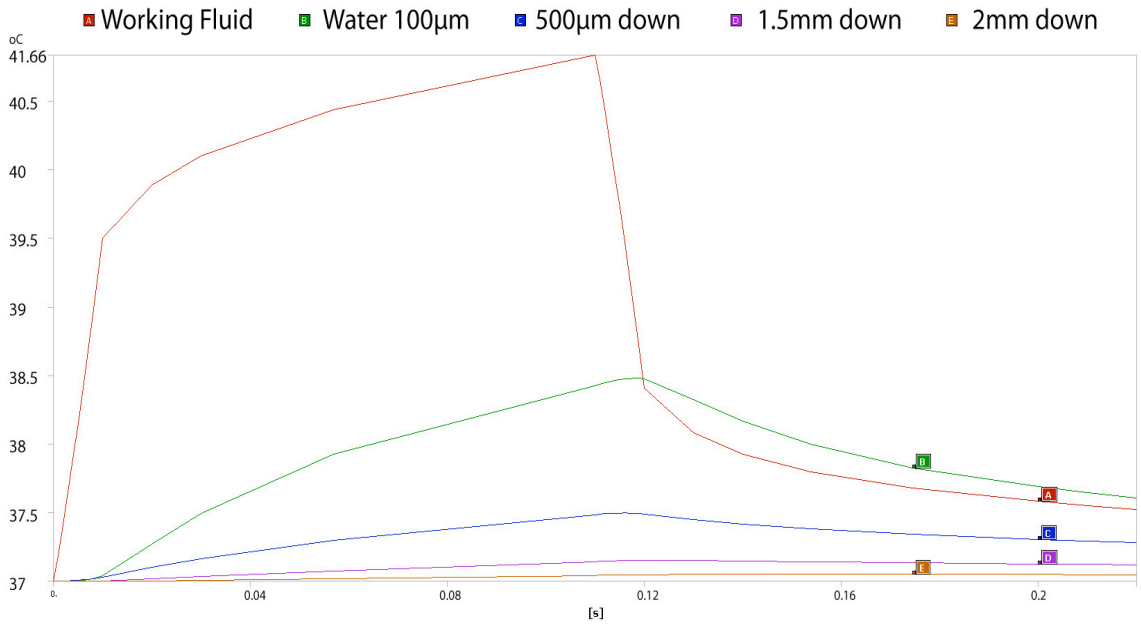

Figure 4.11: A temperature rise along the probe shank at the pulse power of 8mW and pulse duration of 100mSec. The temperature rise of the extracellular fluid 100µm away from the microvalve increases less than $2^{o}C$. The temperature rise 500µm, 1.5mm and 2mm down along the probe shank are also negligible.

CHAPTER 5

CONCLUSIONS AND SUGGESTIONS FOR FUTURE WORK

5.1 Conclusions and Contributions

This thesis has described the design of an integrated pneumatic/thermopneumatic microvalve for a chronically implantable chemical delivery system. The demonstrated microvalve is completely compatible with the existing process for recording and stimulating probes and with the use of on-chip circuitry. It requires only two masks in addition to those for the standard probe process. The results obtained in this research may be summarized as follows:

1. Two different configurations, Version I and Version II, of the process-compatible pneumatically-actuated microvalve were developed, optimized, and demonstrated. The microvalve is composed of a corrugated circular diaphragm and a normally-open dual-channel structure with the one channel passing the fluid and the other channel acting as an actuator. It uses two sacrificial polysilicon layers sandwiched between dielectric layers to form the two dual chambers of the microvalve. The feasibility of the valve designs was verified, as demonstrated by the in-vitro experiments. Both configurations of the microvalve structure were capable of having a required open flow rate (>500pL/sec) at an applied input pressure of 10kPa and meeting the design target of leak rate (<25pL/sec).

2. The ultimate performance from these structures was studied using thermal and

flow models to understand the limits and tradeoffs among power, temperature, size, pressure, and flow. The results should point the way toward improved structures and provide an understanding of this approach for other applications. Careful thermal modeling of the actuator and the probe structure was completed to understand and optimize heat flow patterns and optimize actuation. This established a framework for understanding the actuation process and for anticipating the temperature rise in surrounding tissue as a function of actuation power and structure. The actuator is capable of operating at sub-10mW levels with a response time below 20mSec and high throw. The thermal dissipation of the valve allows the surrounding tissue to remain within $2^{o}C$ of ambient. This is not only the first valve suitable for on-probe use in drug-delivery systems but as a low-voltage, low-power, structure capable of high actuation pressure and throw, it should have many other applications and extensions, e.g., to peristaltic pump.

3. The realization of probes with on-chip microvalves should provide an important step forward for microsystems capable of drug delivery and intended for applications such as seizure suppression in cases of severe epilepsy. It will add major new capability to the neural interface.

5.2 Suggestions for Future Work

The results of this research constitute a significant step forward in the challenge to develop a useful, reliable microvalve. The resulting device, although useful as a proof-of-concept, also leaves many opportunities for improvement.

1. Filling the actuation chamber is perhaps the greatest challenge to

thermopneumatic actuators. A method must be found to reliably inject a precisely metered quantity of working fluid into the actuator cavity, preferably in a batch-compatible process. Filling temperature must also be carefully controlled, both to keep air-to-fluid ratios constant, and to prevent injection and/or ejection of the epoxy seal. It may be worthwhile to investigate filling the pressure cavity with fluid in the vapor state rather than as a liquid.

2. Thermopneumatic on-probe microvalves must be fabricated with electrical recording sites. The performance and characteristics of the valve can then be evaluated in-vitro and in-vivo.

3. The demonstrated valve structure can be used to make a peristaltic pump, which may be a critical component in a chronic chemical delivery device.

4. Probe functionality must be demonstrated through in-vivo experiments. For example, experiments to determine forward masking effects from the DCN to the VCN can be performed. Masking is essentially the result of the required reset time for neurons after stimulation when they are unable to respond to further stimulation. Drug injection (e.g., GABA) can be used to repress the inhibitory cells that cause this masking to occur.

BIBLIOGRAPHY

[1] J. Csicsvari, D. A. Henze, B. Jamieson, K. D. Harris, A. Sirota, P. Bartho, K. D. Wise and G. Buzsaki, "Massively parallel recording of unit and local field potentials with silicon-based electrodes," *J. Neurophysiol.,* vol. 90, pp. 1314-1323, Aug. 2003.

[2] J. Csicsvari, B. Jamieson, K. D. Wise and G. Buzsaki, "Mechanisms of gamma oscillations in the hippocampus of the behaving rat," *Neuron,* vol. 37, pp. 311-322, Jan 23. 2003.

[3] K. D. Wise, D. J. Anderson, J. F. Hetke, D. R. Kipke and K. Najafi, "Wireless implantable microsystems: High-density electronic interfaces to the nervous system," *Proc IEEE,* vol. 92, pp. 76-97, 2004.

[4] C. Kim1 and K. D. 1. Wise, "A 64-site multishank CMOS low-profile neural stimulating probe," *IEEE J Solid State Circuits,* vol. 31, pp. 1230-8, 1996.

[5] M. D. 1. Gingerich, J. F. 1. Hetke, D. J. 1. Anderson and K. D. 1. Wise, "A 256-site 3D CMOS microelectrode array for multipoint stimulation and recording in the central nervous system," in *Proceedings of 11th International Conference on Solid State Sensors and Actuators Transducers '01/Eurosensors XV,* 2001, pp. 416-19.

[6] M. D. Gingerich, J. A. Wiler and K. D. Wise, "Use of an active microelectrode array for stimulation and recording in the central nervous system," *Annual International Conference of the IEEE Engineering in Medicine and Biology - Proceedings,* vol. 1, pp. 471, 1999.

[7] R. H. I. I. I. 1. Olsson, A. N. 1. Gulari and K. D. 1. Wise, "A fully-integrated bandpass amplifier for extracellular neural recording," in *1st International IEEE EMBS Conference on Neural Engineering 2003,* 2003, pp. 165-8.

[8] R. H. Olsson III1, D. L. Buhl, M. N. Gulari, G. Buzsaki and K. D. Wise, "A silicon microelectrode array for simultaneous recording and stimulation in the brain of behaving animals," in *Proceedings of the 25th Annual International Conference of the IEEE Engineering in Medicine and Biology Society,* 2003, pp. 1968-71.

[9] Q. Bai1, K. D. Wise and D. J. Anderson, "A high-yield microassembly structure for three-dimensional microelectrode arrays," *IEEE Transactions on Biomedical Engineering,* vol. 47, pp. 281-9, 03. 2000.

[10] Olsson III, Roy H., D. L. Buhl, A. M. Sirota, G. Buzsaki and K. D. Wise, "Band-tunable and multiplexed integrated circuits for simultaneous recording and stimulation with microelectrode arrays," *IEEE Transactions on Biomedical Engineering,* vol. 52, pp. 1303-1311, 2005.

[11] K. D. Wise, D. J. Anderson, J. F. Hetke, D. R. Kipke and K. Najafi, "Wireless implantable microsystems: High-density electronic interfaces to the nervous system," *Proc IEEE,* vol. 92, pp. 76-97, 2004.

[12] D. Papageorgiou, S. C. Bledsoe, M. Gulari, J. F. Hetke, D. J. Anderson and K. D. Wise, "A shuttered probe with in-line flowmeters for chronic in-vivo drug delivery," in *14th IEEE International Conference on Micro Electro Mechanical Systems (MEMS 2001),* 2001, pp. 212-215.

[13] Y. Li, K. Baek, M. Gulari, D. Lin and K. D. Wise, "A vacuum-isolated thermal microflowmeter for in-vivo drug delivery," in *Fourth IEEE Conference on Sensors 2005,* 2005, pp. 668-671.

[14] P. Singh and H. I. Maibach, "Iontophoresis: An alternative to the use of carriers in cutaneous drug delivery," *Adv. Drug Deliv. Rev.,* vol. 18, pp. 379-394, 1996.

[15] P. Singh and H. I. Maibach, "Applications of Iontophoresis in Dermatology: Using electrical charge to deliver compounds past the stratum corneum," *Cosmet. Toiletries,* vol. 111, pp. 55, 1996.

[16] A. K. Banga and Y. W. Chien, "Iontophoretic delivery of drugs: Fundamentals, developments and biomedical applications," *Journal of Controlled Release,* vol. 7, pp. 1-24, 4. 1988.

[17] K. D. Wise, "A Multielectrode Microprobe for Biopotential Recording," May. 1969.

[18] A. 1. Starr, K. D. 1. Wise and J. 1. Csongradi, "An evaluation of photoengraved microelectrodes for extracellular single- unit recording," *IEEE Transactions on Biomedical Engineering,* vol. BME20, pp. 291-3, 07. 1973.

[19] O. 1. Prohaska, F. 1. Olcaytug, K. 1. Womastek and H. 1. Petsche, "A multielectrode for intracortical recordings produced by thin-film technology," *Electroencephalogr. Clin. Neurophysiol.,* vol. 42, pp. 421-2, 03. 1977.

[20] P. 1. Pochay, K. D. 1. Wise, L. F. Allard and L. T. Rutledge, "A multichannel depth probe fabricated using electron-beam lithography," *IEEE Transactions on Biomedical Engineering,* vol. BME26, pp. 199-206, 04. 1979.

[21] K. L. Drake, S. L. BeMent, K. D. Wise and J. Farraye, "SILICON MULTICHANNEL MICROPROBES FOR RECORDING INTRACORTICAL SINGLE-UNIT ACTIVITY." in *Proceedings of the Ninth Annual Conference of the IEEE Engineering in Medicine and Biology Conference.* 1987, pp. 1042-1043.

[22] K. D. 1. Wise, K. 1. Najafi and K. L. 1. Drake, "A multichannel microprobe for intracortical single-unit recording," in *84CH2068-5),* 1984, pp. 87-9.

[23] K. 1. Najafi, K. D. 1. Wise and T. 1. Mochizuki, "A high-yield IC-compatible multichannel recording array [neural activity probe]," *IEEE Trans. Electron Devices,* vol. ED-32, pp. 1206-11, 07. 1985.

[24] A. 1. Bohg, "Ethylene diamine-pyrocatechol-water mixture shows etching anomaly in boron-doped silicon," *J. Electrochem. Soc.,* vol. 118, pp. 401-2, 02. 1971.

[25] K. 1. Najafi and K. D. 1. Wise, "Implantable multielectrode array with on-chip signal processing," in *86CH2263-2),* 1986, pp. 98-9.

[26] J. 1. Ji, K. 1. Najafi and K. D. 1. Wise, "A scaled electronically-configurable multichannel recording array," in *5th International Conference on Solid-State Sensors and Actuators and Eurosensors III,* 1990, pp. 589-91.

[27] S. L. 1. BeMent, K. L. 1. Drake, D. J. 1. Anderson, K. D. 1. Wise and K. 1. Najafi, "Semiconductor microprobes-recording/biocompatibility properties," in *86CH2368-9),* 1986, pp. 1622-5.

[28] S. 1. Metz, A. 1. Bertzch, D. Bertrand and P. Renaud, "Flexible polyimide probes with microelectrodes and embedded microfluidic channels for simultaneous drug delivery and multichannel monitoring of bioelectric activity," *Biosens. Bioelectron.,* vol. 19, pp. 1309-18, 05/15. 2004.

[29] D. J. Anderson, K. Najafi, S. J. Tanghe, D. A. Evans, K. L. Levy, J. F. Hetke, X. Xue, J. J. Zappia and K. D. Wise, "Batch-fabricated thin-film electrodes for stimulation of the central auditory system," *IEEE Transactions on Biomedical Engineering,* vol. 36, pp. 693-704, 1989.

[30] S. J. 1. Tanghe and K. D. 1. Wise, "A 16-channel CMOS neural stimulating array," in *92CH3128-6),* 1992, pp. 128-9.

[31] C. Kim and K. D. Wise, "64-Site multishank CMOS low-profile neural stimulating probe," *IEEE J Solid State Circuits,* vol. 31, pp. 1230-1238, 1996.

[32] M. D. Gingerich, J. A. Wiler and K. D. Wise, "Use of an active microelectrode array for stimulation and recording in the central nervous system," *Annual International Conference of the IEEE Engineering in Medicine and Biology - Proceedings,* vol. 1, pp. 471, 1999.

[33] A. C. 1. Hoogerwerf and K. D. 1. Wise, "A three-dimensional neural recording array," in *91CH2817-5),* 1991, pp. 120-3.

[34] T. E. Bell, K. D. Wise and D. J. Anderson, "Flexible micromachined electrode array for a cochlear prosthesis," in *Part 2 (of 2),* 1997, pp. 1315-1318.

[35] Q. Bai, K. D. Wise and D. J. Anderson, "High-yield microassembly structure for three-dimensional microelectrode arrays," *IEEE Transactions on Biomedical Engineering,* vol. 47, pp. 281-289, 2000.

[36] J. Chen1 and K. D. 1. Wise, "A multichannel neural probe for selective chemical delivery at the cellular level," in *Technical Digest Solid-State Sensor and Actuator Workshop,* 1994, pp. 256-9.

[37] L. Lin1 and A. P. Pisano, "Silicon-processed microneedles," *J Microelectromech Syst,* vol. 8, pp. 78-84, 03. 1999.

[38] Y. Joo, K. Dieu and C. Kim, "Fabrication of monolithic microchannels for IC chip cooling," in *Proceedings of the 1995 IEEE Micro Electro Mechanical Systems Conference,* 1995, pp. 362-367.

[39] W. Kaplan, H. Elderstig and C. Vieider, "Novel fabrication method of capillary tubes on quartz for chemical analysis applications," *Proceedings of the IEEE Micro Electro Mechanical Systems,* pp. 63-68, 1994.

[40] M. -. Gretillat, F. Paoletti, P. Thiebaud, S. Roth, M. Koudelka-Hep and N. F. de Rooij, "New fabrication method for borosilicate glass capillary tubes with lateral inlets and outlets," *Sens Actuators A Phys,* vol. 60, pp. 219-222, 1997.

[41] G. M. 1. Whitesides, "Unconventional methods and unconventional materials for microfabrication," in *Proceedings of International Solid State Sensors and Actuators Conference (Transducers '97),* 1997, pp. 23-4.

[42] S. 1. Henry, D. V. 1. McAllister, M. G. Allen and M. R. Prausnitz, "Micromachined needles for the transdermal delivery of drugs," in *Proceedings IEEE Eleventh Annual International Workshop on Micro Electro Mechanical Systems an Investigation of Micro Structures, Sensors, Actuators, Machines and Systems,* 1998, pp. 494-8.

[43] D. V. 1. McAllister, S. 1. Kaushik, P. N. 1. Patel, J. L. 1. Mayberry, M. G. Allen and M. R. Prausnitz, "Microneedles for transdermal delivery of macromolecules," in *Proceedings of the First Joint BMES/EMBS Conference,* 1999, pp. 836 vol.2.

[44] K. 1. Chun, G. 1. Hashiguchi, H. 1. Toshiyoshi, H. 1. Fujita, Y. Kikuchi, J. Ishikawa, Y. Murakami and E. Tamiya, "An array of hollow microcapillaries for the controlled injection of genetic materials into animal/plant cells," in *Proceedings of 12th International Workshop on Micro Electro Mechanical Systems - MEMS,* 1999, pp. 406-11.

[45] K. Lee, J. He, R. Clement, S. Massia and B. Kim, "Biocompatible benzocyclobutene (BCB)-based neural implants with micro-fluidic channel," *Biosensors and Bioelectronics,* vol. 20, pp. 404-407, 2004.

[46] S. 1. Metz, C. Trautmann, A. Bertsch and P. Renaud, "Polyimide microfluidic devices with integrated nanoporous filtration areas manufactured by micromachining and ion track technology," *J Micromech Microengineering,* vol. 14, pp. 324-31, 03. 2004.

[47] K. D. 1. Wise, "Silicon microsystems for neuroscience and neural prostheses," *IEEE Engineering in Medicine and Biology Magazine,* vol. 24, pp. 22-9, 2005.

[48] P. T. 1. Bhatti and K. D. 1. Wise, "A 32-site 4-channel high-density electrode array for a cochlear prosthesis," *IEEE J Solid State Circuits,* vol. 41, pp. 2965-73, 12. 2006.

[49] M. J. Lehmkuhle, S. S. Bhangoo and D. R. Kipke, "The electrocorticogram as a feedback control signal for deep brain stimulation of the subthalamic nucleus in the hemi-parkinsonian rat," in *3rd International IEEE EMBS Conference on Neural Engineering,* 2007, pp. 386-389.

[50] R. S. Fisher. (2005, Epileptic seizures and epilepsy: Definitions proposed by the international league against epilepsy (ILAE) and the international bureau for epilepsy (IBE). *Epilepsia 46(4),* pp. 470.

[51] W. H. Theodore. (2007, Brain stimulation for epilepsy. *Acta neurochirurgica. Supplementum 97(Pt 2),* pp. 261.

[52] R. S. Fisher. (2006, New routes for delivery of anti-epileptic medications. *Acta neurologica Taiwanica 15(4),* pp. 225.

[53] N. M. Graves. (2005, Neurostimulation for epilepsy, including a pilot study of anterior nucleus stimulation. *Clinical neurosurgery 52*pp. 127.

[54] W. G. Mitchell. (1999, An open-label study of repeated use of diazepam rectal gel (diastat) for episodes of acute breakthrough seizures and clusters: Safety, efficacy, and tolerance. north american diastat group. *Epilepsia 40(11),* pp. 1610.

[55] A. Okumura. (2004, A pilot study on lidocaine tape therapy for convulsions with mild gastroenteritis. *Brain development 26(8),* pp. 525.

[56] A. Okumura. (2002, A pilot study on umbilical venous level of natriuretic peptides in preterm infants and their relation to periventricular leukomalacia and antenatal complications. *Brain development 24(1),* pp. 30.

[57] D. M. Lieberman. (1995, Convection-enhanced distribution of large molecules in gray matter during interstitial drug infusion. *Journal of neurosurgery 82(6),* pp. 1021.

[58] R. J. Tamargo. (2002, The intracerebral administration of phenytoin using controlled-release polymers reduces experimental seizures in rats. *Epilepsy Research 48(3),* pp. 145.

[59] H. G. Eder. (1997, Local perfusion of diazepam attenuates interictal and ictal events in the bicuculline model of epilepsy in rats. *Epilepsia 38(5),* pp. 516.

[60] A. G. Stein. (2000, An automated drug delivery system for focal epilepsy. *Epilepsy Research 39(2),* pp. 103.

[61] M. Bialer. (2007, Progress report on new antiepileptic drugs: A summary of the eigth eilat conference (EILAT VIII). *Epilepsy Research 73(1),* pp. 1.

[62] C. Mamot. (2003, Liposome-based approaches to overcome anticancer drug resistance. *Drug resistance updates 6(5),* pp. 271.

[63] Oommen. (2005, Experimental electrical stimulation therapy for epilepsy. *Current Treatment Options in Neurology 7(4),* pp. 261.

[64] K. 1. Ikuta, K. 1. Hirowatari and T. 1. Ogata, "Three dimensional micro integrated fluid systems (MIFS) fabricated by stereo lithography," in *Proceedings IEEE Micro Electro Mechanical Systems an Investigation of Micro Structures, Sensors, Actuators, Machines and Robotic Systems,* 1994, pp. 1-6.

[65] J. Chen1, K. D. Wise, J. F. Hetke and S. C. Bledsoe Jr., "A multichannel neural probe for selective chemical delivery at the cellular level," *IEEE Transactions on Biomedical Engineering,* vol. 44, pp. 760-9, 08. 1997.

[66] R. 1. Rathnasingham, D. R. Kipke, S. C. Bledsoe Jr. and J. D. McLaren, "Characterization of implantable microfabricated fluid delivery devices," *IEEE Transactions on Biomedical Engineering,* vol. 51, pp. 138-45, 01. 2004.

[67] D. Y. 1. Sim, T. 1. Kurabayashi and M. 1. Esashi, "Bakable silicon pneumatic microvalve," in *Proceedings of the International Solid-State Sensors and Actuators Conference - TRANSDUCERS '95,* 1995, pp. 280-3.

[68] T. 1. Lisec, H. J. 1. Quenzer, M. 1. Kreutzer, S. 1. Hoerschelmann, B. 1. Wagner and W. Benecke, "Thermally driven microvalve with buckling behavior for pneumatic applications," *Sensors and Materials,* vol. 8, pp. 303-16, 1996.

[69] N. 1. Vandelli, D. 1. Wroblewski, M. 1. Velonis and T. 1. Bifano, "Development of a MEMS microvalve array for fluid flow control," *J Microelectromech Syst,* vol. 7, pp. 395-403, 12. 1998.

[70] H. Kahn. (1998, The TiNi shape-memory alloy and its applications for MEMS. *Journal of Micromechanics and Microengineering 8[3]*,pp.213.

[71] T. 1. Tadaki, K. Otsuka and K. Shimizu, "Shape memory alloys," in *Annual Review of Materials Science. Vol.18* Anonymous Annual Reviews, 1988, pp. 25-45.

[72] D. Bosch, B. Heimhofer, G. Mueck, H. Seidel, U. Thumser and W. Welser, "Silicon microvalve with combined electromagnetic/electrostatic actuation," *Sens Actuators A Phys,* vol. 37-38, pp. 684-692, 1993.

[73] J. K. Robertson and K. D. Wise, "Nested electrostatically-actuated microvalve for an integrated microflow controller," *Proceedings of the IEEE Micro Electro Mechanical Systems,* pp. 7-12, 1994.

[74] J. 1. Branebjerg and P. 1. Gravesen, "A new electrostatic actuator providing improved stroke length and force," in *92CH3093-2),* 1992, pp. 6-11.

[75] S. 1. Shoji, Van der Schoot, B., N. de Rooij and M. Esashi, "Smallest dead volume microvalves for integrated chemical analyzing systems," in *91CH2817-5),* 1991, pp. 1052-5.

[76] S. 1. Shoji and M. 1. Esashi, "Microflow devices and systems," *J Micromech Microengineering,* vol. 4, pp. 157-71, 12. 1994.

[77] C. A. 1. Rich and K. D. 1. Wise, "A high-flow thermopneumatic microvalve with improved efficiency and integrated state sensing," *J Microelectromech Syst,* vol. 12, pp. 201-8, 04. 2003.

[78] R. H. Liu, Q. Yu and D. J. Beebe, "Fabrication and characterization of hydrogel-based microvalves," *J Microelectromech Syst,* vol. 11, pp. 45-53, 2002.

[79] M. Lei1, A. 1. Baldi, T. 1. Pan, Y. Gu, R. A. Siegel and B. Ziaie, "A hydrogel-based wireless chemical sensor," in *Maastricht MEMS 2004 Technical Digest,* 2004, pp. 391-4.

[80] C. Yu, S. Mutlu, P. Selvaganapathy, C. H. Mastrangelo, F. Svec and J. M. J. Frechet, "Flow control valves for analytical microfluidic chips without mechanical parts based on thermally responsive monolithic polymers," *Anal. Chem.,* vol. 75, pp. 1958-1961, 2003.

[81] E. T. 1. Carlen and C. H. Mastrangelo, "Surface micromachined paraffin-actuated microvalve," *J Microelectromech Syst,* vol. 11, pp. 408-20, 10. 2002.

[82] P. 1. Selvaganapathy, E. T. 1. Carlen and C. H. 1. Mastrangelo, "Electrothermally actuated inline microfluidic valve," *Sensors and Actuators A (Physical),* vol. A104, pp. 275-82, 05/15. 2003.

[83] A. P. 1. Papavasiliou, A. R. 1. Pisano and D. 1. Liepmann, "High-speed and bi-stable electrolysis-bubble actuated gate valves," in *Proceedings of 11th International Conference on Solid State Sensors and Actuators Transducers '01/Eurosensors XV,* 2001, pp. 940-3.

[84] M. W. 1. Hamberg, C. 1. Neagu, J. G. E. 1. Gardeniers, D. J. 1. Ijntema and M. 1. Elwenspoek, "An electrochemical micro actuator," in *1995,* 1995, pp. 106-10.

[85] J. Lee1 and Chang-Jin Kim, "Surface-tension-driven microactuation based on continuous electrowetting," *J Microelectromech Syst,* vol. 9, pp. 171-80, 06. 2000.

[86] M. H. Sun, G. Velve Casquillas, S. S. Guo, J. Shi, H. Ji, Q. Ouyang and Y. Chen, "Characterization of microfluidic fuel cell based on multiple laminar flow," *Microelectronic Engineering,* vol. 84, pp. 1182-1185, 2007.

[87] S. RK and L. AL, "Laminar flow forced convection heat transfer and flow friction in straight and curved ducts. A summary of analytical solutions," pp. 306, 1971.

[88] R. K. Shah and A. L. London, "EFFECTS OF NONUNIFORM PASSAGES ON COMPACT HEAT EXCHANGER PERFORMANCE," *Am Soc Mech Eng Pap,* pp. 9, 1979.

[89] J. A. 1. Voorthuyzen and P. 1. Bergveld, "The influence of tensile forces on the deflection of circular diaphragms in pressure sensors," *Sensors and Actuators,* vol. 6, pp. 201-13, 11. 1984.

[90] Y. Zhang1 and K. D. 1. Wise, "Performance of nonplanar silicon diaphragms under large deflections," *J Microelectromech Syst,* vol. 3, pp. 59-68, 06. 1994.

[91] V. L. Spiering, S. Bouwstra, J. F. Burger and M. Elwenspoek, "Membranes fabricated with a deep single corrugation for package stress reduction and residual stress relief," in *Fourth European Workshop on Micromechanics (MME '93),* 1993, pp. 243-6.

[92] P. R. Scheeper, W. Olthuis and P. Bergveld, "The design, fabrication, and testing of corrugated silicon nitride diaphragms," *J Microelectromech Syst,* vol. 3, pp. 36-42, 03. 1994.

[93] P. Chen, "Floating-disk parylene microvalve for self-regulating biomedical flow controls," *Proceedings of the IEEE International Conference on Micro Electro Mechanical Systems (MEMS),* pp. 575, 2008.

[94] S. Mutlu, "A thermally responsive polymer microvalve without mechanical parts photo-patterned in a parylene channel," pp. 802, 2003.

[95] P. Chen. (2007, Surface-micromachined parylene dual valves for on-chip unpowered microflow regulation. *Journal of microelectromechanical systems 16(2),* pp. 223.

[96] C. A. Rich. (2003, A high-flow thermopneumatic microvalve with improved efficiency and integrated state sensing. *Journal of microelectromechanical systems 12(2),* pp. 201.

[97] C. A. Rich, "A thermopneumatically-actuated microvalve with improved thermal efficiency and integrated state sensing," pp. 234, 2000.

[98] C. A. Rich, "An 8-bit microflow controller using pneumatically-actuated microvalves [for automotive application]," pp. 135, 1999.